

Structural Design Analysis of the Burnelli CBY-3 Loadmaster and DC-3

A Major Qualifying Project Report

Submitted to the Faculty of the

WORCESTER POLYTECHNIC INSTITUTE

In Partial Fulfillment of the Requirements for the

Degree of Bachelor of Science

in Aerospace Engineering

By

Aaron Boyer

Aaron Boyer

Jacob Moore

Jacob Moore

Emily Raynowska

Emily Raynowska

Amaya Massari

Amaya Massari

Nicholas Paszczuk

Nicholas Paszczuk

Gabrielle Tims

Gabrielle Tims

Approved by:

John J. Blandino

John J. Blandino, Advisor
Professor, Aerospace Engineering Department
Worcester Polytechnic Institute

March 23rd, 2023

This report represents the work of one or more WPI undergraduate students submitted to the faculty as evidence of completion of a degree requirement. WPI routinely publishes these reports on the web without editorial or peer review.

Abstract

This work presents a study to investigate the structural design of the wing attachment of the 1940s era Burnelli CBY-3 Loadmaster and compare it to that of a contemporary aircraft, the Douglas DC-3. Specifically, the team calculated the equivalent stresses in the wing attachment structure for both aircraft and calculated safety factors to assess the two different designs. As part of this work, the team evaluated the efficacy of using a handheld 3D scanner to create a digital model of the components to be analyzed. The team also designed a camera stand that can be used to photographically document archival print documents. Finally, the team collected information on the aircraft restoration workflow at four museums to understand current practice, particularly with respect to use of software and 3D printing to create replicas of missing parts. The fact no digital model of the wing structural components exists posed a unique challenge as these had to be created to perform the structural analysis. A combination of archival print documents and measurements on the actual aircraft were used to create the 3D solid model. Key dimensions were checked throughout the process using measurements of accessible parts on the actual aircraft with the model adjusted accordingly. The solid model was imported into Ansys Mechanical where the stresses were evaluated under lift and drag loads representative of a typical flight condition for each aircraft. These results are summarized, and the team show that the CBY-3 wing attachment had a higher safety factor than that of the DC-3. Finally, the team summarized the findings with respect to restoration workflow and concluded with some recommendations regarding software and resources for 3D printing.

“Certain materials are included under the fair use exemption of the U.S. Copyright Law and have been prepared according to the fair use guidelines and are restricted from further use.”

Acknowledgements

This MQP team would like to give thanks to the following individuals and/or organizations that have contributed to the success of this project:

- Dr. Adriana Hera and Dr. Erica S. Stults for their teaching and guidance with Ansys Mechanical and Solidworks.
- The volunteers and staff of the New England Air Museum (NEAM) for all their support. In particular, the team would like to recognize Bob Vozzola, Carl Cruff, Doug Davis, Lou Palshaw, Wayne Dow, and Amanda Goodheart Parks for their expertise and guidance.
- Nick Orlovsky and Maria Wojciechowski, members of a corresponding Loadmaster MQP completed last year, for their assistance and knowledge.
- Lastly, the team would like to especially thank our advisor Professor John Blandino for his mentorship, direction, and support.

Table of Contents

Abstract.....	i
Acknowledgements.....	ii
Table of Contents.....	iii
List of Figures.....	v
List of Tables.....	viii
Table of Authorship.....	ix
1 Introduction.....	1
1.1 Project Goals and Objectives.....	1
1.2 Project Tasks.....	3
2 Background and Literature Review.....	5
2.1 Project Background.....	5
2.2 Brief History of Burnelli and the CBY-3 Loadmaster.....	5
2.3 Brief History of the Douglas DC-3.....	9
2.4 Competition and Eventual Dominance of the DC-3 in U.S. Commercial Aviation.....	10
2.5 Aircraft Structural Characteristics.....	12
2.5.1 Characteristics of the CBY-3 Wing Attachment.....	14
2.5.2 Characteristics of DC-3 Wing Attachment.....	20
3 Methodology of Structural Analysis Comparison.....	22
3.1 Photographic Documentation.....	22
3.1.1 Problem Description and Methodology.....	22
3.1.2 Design Construction of Camera Stand.....	24
3.2 3D Laser Scanning.....	25
3.3 CAD Model Generation.....	30
3.3.1 CBY-3 Method and Approach.....	30
3.3.2 CBY-3 Assumptions.....	37
3.3.3 DC-3 Method and Approach.....	40
3.3.4 DC-3 Assumptions.....	44
3.4 Ansys Mechanical.....	45
3.4.1 Governing Equations, Constraints, and Background of Ansys Mechanical.....	45
3.4.4 DC-3 Wing Attachment: Problem Description.....	61
3.4.5 DC-3 Methodology and Approach.....	61
4 Results of Structural Analysis Comparison.....	64

4.1 Photographic Documentation Results	64
4.2 3D Laser Scanning	65
4.3 CAD Model Generation	68
4.3.1 CBY-3 Model	68
4.3.2 DC-3 Model.....	70
4.4 Ansys Mechanical	73
4.4.1 CBY-3 Structural Analysis.....	73
4.4.2 DC-3 Structural Analysis.....	87
4.4.3 Discussion of Results.....	90
5 Methodology for Assessment of Restoration Workflow	93
5.1 Interviews	93
5.2 Project Management Software	95
5.3 Rapid Prototyping	96
6 Results and Recommendations Regarding Restoration Workflow.....	96
6.1 NEAM Interview Results	96
6.2 Museum Interview Results.....	98
6.3 Team Recommendations	106
6.3.1 Software Recommendations	106
6.3.2 3D Printing Recommendations.....	110
7 Project Conclusions and Broader Impacts	112
7.1 Conclusions	112
7.2 Broader Impacts	113
8 References.....	115
9 Appendices.....	119
9.1 Appendix A: Additional Drawings of CBY-3 Internal Wing Structure.....	119
9.2 Appendix B: Additional Results of CBY-3 Ansys Mechanical Stress Map.....	126

List of Figures

Figure 1: The Burnelli CBY-3 Loadmaster in the New England Air Museum Hanger	7
Figure 2: Rear-Right View of CBY-3 Loadmaster showing the trailing edge of the lifting body fuselage	8
Figure 3: Front-Right view of CBY-3 Loadmaster.....	8
Figure 4: Visual representation of the opening, shearing and tearing modes of deformation. [18]	13
Figure 5: The internal Structure of a wing [27]. Copyright 2023 CFI Notebook.....	14
Figure 6: Bracket Reference Letters on Wing in Storage Position.....	15
Figure 7: Bracket Reference Letters on Correct Wing Orientation	16
Figure 8: Brackets (D) and (B) respectively.....	16
Figure 9: Bracket (A).....	17
Figure 10: Bracket (C)	18
Figure 11: Metal Box Structure Encasing End of Bracket D.....	18
Figure 12: CAD Model of Bracket (B).....	19
Figure 13: Bracket (C) CBY-3 Wing Attachment	19
Figure 14: DC-3 Wing attachment lower front view	20
Figure 15: The front and isometric views of the camera rig.....	23
Figure 16: A picture depicting the laser triangulation method. Copyright 2018 Movimed	26
Figure 17: Image of the Revopoint Pop 2 3d scanner with its hardware. Copyright 1996-2023, Amazon.com, Inc. or its affiliates	27
Figure 18: Revopoint Pop2 3D scanner assembled on the tripod stand. Copyright 1996-2023, Amazon.com, Inc. or its affiliates	27
Figure 19: The user interface of Revo Scan when a scan is first initiated.....	28
Figure 20: The Revo Scan UI at the creation of a new scan.....	29
Figure 21: Image of one of the drawings used in the creation of the CAD model of each wing attachment, captured on sight at NEAM. As can be seen very few dimensions are shown in the drawing [36].....	31
Figure 22: Teslong NTS300 Dual Lens Inspection Camera [35]. Copyright 2023 Teslong	32
Figure 23: The above image was taken by the team of the internal wing structure using the NTS300 endoscope.	33
Figure 24: The above image was taken by the team of the internal wing structure, and annotations are visible to outline the dimensions of different sections.	34
Figure 25: An image of the reference scale and bolt hole portion of one of the wing attachments.	35
Figure 26: Image of a detached DC-3 wing taken by the team onsite.....	41
Figure 27: Measuring features using calipers on the detached DC-3 wing.	42
Figure 28: Image of both DC-3 wings detached during NEAM restoration process. [Personal Communication: email C. Cruff to J. Blandino, 1/16/23].....	44
Figure 29: Loads on Hinge Fittings from Approach 1[26].....	50
Figure 30: Trailing Edge Bracket Pair Material Assignment – Structural Steel View 1	51
Figure 31: Trailing Edge Bracket Pair Material Assignment – Aluminum Alloy View 1	52
Figure 32: Trailing Edge Bracket Pair Material Assignment – Aluminum Alloy View 2	52

Figure 33: Trailing Edge Bracket Pair Fixed Supports (in purple) on Upper Bracket	53
Figure 34: Trailing Edge Bracket Pair Fixed Supports (in purple) on Upper Bracket Close Up .	54
Figure 35: Trailing Edge Bracket Pair Fixed Supports (in purple) on Lower Bracket.....	54
Figure 36: Trailing Edge Bracket Pair Fixed Supports (in purple) on Lower Bracket Close Up.	55
Figure 37: Trailing Edge Bracket Pair Lift Force Distribution shown in red and with.....	56
Figure 38: Trailing Edge Bracket Pair Drag Force Distribution shown in red, with a directional red arrow.	56
Figure 39: Leading Edge Bracket Pair Material Assignment – Structural Steel View 1 highlighted in red.	57
Figure 40: Leading Edge Bracket Pair Material Assignment – Aluminum Alloy View 1 highlighted in red.	58
Figure 41: Leading Edge Bracket Pair Fixed Supports highlighted in purple.....	58
Figure 42: Leading Edge Bracket Pair Fixed Supports on Upper Bracket highlighted in purple.	59
Figure 43: Leading Edge Bracket Pair Fixed Supports on Lower Bracket highlighted in purple.	59
Figure 44: Leading Edge Bracket Pair Lift Force Distribution highlighted in red and direction shown with a red arrow.....	60
Figure 45: Leading Edge Bracket Pair Drag Force Distribution highlighted in red and direction shown with a red arrow.....	60
Figure 46: Highlighted Constrained Bolt Surfaces of the DC-3 (in blue)	62
Figure 47: Lift force applied to underside of the modeled portion of the wing (shown in red) ...	63
Figure 48: Drag force applied to leading edge of wing model (shown in red).....	63
Figure 49: Combined Lift and Drag applied to wing stringers.....	64
Figure 50: Image of the 3D scan taken of the DC-3 replica model. As can be seen the scanner did not create a full scan of the DC-3 itself and accidentally included geometry from surrounding objects.	66
Figure 51: Incomplete scan of bracket C	67
Figure 52: A CAD model drawing of bracket A (lower rear bracket of wing)	69
Figure 53: Exploded view of box structure surrounding bracket A.....	69
Figure 54: Exploded view of the trailing edge comprised of brackets A and B.....	70
Figure 55: DC-3 wing attachment as seen from the leading-edge fuselage side	71
Figure 56: DC-3 wing attachment as seen from the leading-edge wing side	71
Figure 57: DC-3 wing attachment as seen from the trailing edge fuselage side.....	72
Figure 58: DC-3 wing attachment as seen from the trailing edge wing side.....	72
Figure 59: Trailing Edge Bracket Pair Stress Map View 1	74
Figure 60: Trailing Edge Bottom Bracket Point of Interest View 1	74
Figure 61: Trailing Edge Bottom Bracket Close Up View 1 with Probe Values	75
Figure 62: Trailing Edge Bottom Bracket Close Up View 2.....	75
Figure 63: Trailing Edge Bottom Bracket Close Up View 2 with Probe Values	76
Figure 64: Trailing Edge Upper Bracket Close Up View 1.....	76
Figure 65: Trailing Edge Upper Bracket Close Up View 1 with Probe Values	77
Figure 66: Trailing Edge Upper Bracket Close Up View 2.....	77
Figure 67: Trailing Edge Upper Bracket Close Up View 2 with Probe Values	78
Figure 68: Structural Steel Properties on Trailing Edge Bracket Pair (A and B).....	79

Figure 69: Aluminum Material Properties on Trailing Edge Bracket Pair (A and B).....	80
Figure 70: Leading Edge Bracket Pair Stress Map View 1	81
Figure 71: Leading Edge Upper Bracket Close Up View 1.....	81
Figure 72: Leading Edge Upper Bracket Close Up View 1 with Probe Values	82
Figure 73: Leading Edge Upper Bracket Close Up View 2.....	82
Figure 74: Leading Edge Upper Bracket Close Up View 2 with Probe Values	83
Figure 75: Leading Edge Bottom Bracket Close Up View 1.....	83
Figure 76: Leading Edge Bottom Bracket Close Up View 1 with Probe Values	84
Figure 77: Leading Edge Bottom Bracket Close Up View 2.....	84
Figure 78: Leading Edge Bottom Bracket Close Up View 2 with Probe Values	85
Figure 79: Structural Steel Properties on Leading Edge Bracket Pair (C and D).....	86
Figure 80: Aluminum Material Properties on Leading Edge Bracket Pair (C and D).....	87
Figure 81: DC-3 wing attachment stress concentration map.....	88
Figure 82: DC-3 Stress Concentration away from the Wing Rib	88
Figure 83: DC-3 Stress Scale showing von Mises stress in units of Pa. This scale is used to interpret results in Figures 82 and 83.....	89
Figure 84: DC-3 Total Deformation	89
Figure 85: DC-3 Deformation Map at a Point of Stress Concentration.....	90
Figure 86: DC-3 Total Deformation Scale showing deformation in units of meters. This scale is used to interpret results in Figures 85 and 86	90
Figure 87: Picture of the user interface for EZ Office Inventory showing the differing ways to organize assets [32], Copyright 2006-2023, Software Advice, Inc.	107
Figure 88: Picture of the user interface for EZ Office Inventory showing an example of a list of assets [32] Copyright 2006-2023, Software Advice, Inc.....	107
Figure 89: Example of an asset tracking excel template [31], Copyright 2023, All Rights Reserved Smartsheet.....	109
Figure 90: Example project management Excel template [31], Copyright 2023, All Rights Reserved Smartsheet.....	109
Figure 91: Picture of the user interface of Jira [42], Copyright 2023 Atlassian.....	110

List of Tables

Table 1: Ansys Structural Analysis.....	3
Table 2: Restoration Workflow Recommendations.....	3
Table 3: Photographic Documentation	4
Table 4: Analysis Tasks Method and Results Sections	4
Table 5: Bracket Reference Letters.....	15
Table 6: Variables used in Camera Stand Design Analysis.....	24
Table 7: Variables for General Form of Ansys Mechanical Governing Equation	46
Table 8: Variables for Hooke’s Law.....	48
Table 9: Variables for von-Mises Stress Equation	48
Table 10: Document dimensions that fill the camera sensor (same aspect ratio) as a function of distance for the case of a Canon Rebel T7 sensor.	65
Table 11: Information Collected from Museum Interviews	99
Table 12: Summary of Structural Analysis Results.....	112

Table of Authorship

Section	Author
Abstract	Team
Acknowledgements	Team
1.1 Project Goals and Objectives	Team
1.1 Tasks	Team
2.1 Project Background	ER
2.2 Brief History of Burnelli and the CBY-3 Loadmaster	GT
2.3 Brief History of the Douglas DC-3	AM
2.4 Competition and Eventual Dominance of the DC-3 in the U.S. Commercial Aviation	GT, JM
2.5 Aircraft Structural Characteristics	AB
2.5.1 Characteristics of CBY-3 Wing Attachment	AM
2.5.2 Characteristics of DC-3 Wing Attachment	AB
3.1 Photographic Documentation	AB
3.1.1 Problem Description and Methodology	AB
3.1.2 Design Construction of Camera Stand	AB
3.2 3D Laser Scanning	GT, NP
3.3.1 CBY-3 Method and Approach	NP
3.3.2 CBY-3 Assumptions	NP
3.3.3 DC-3 Method and Approach	JM
3.3.4 DC-3 Assumptions	AB
3.4.1 Governing Equations, Constraints, and Background of Ansys Structural	AM, ER
3.4.2 CBY-3 Wing Attachment: Problem Description	AM
3.4.3 CBY-3 Methodology and Approach	AM, ER
3.4.4 DC-3 Wing Attachment: Problem Description	JM
3.4.5 DC-3 Methodology and Approach	JM
4.1 Photographic Documentation Results	AB
4.2 3D Laser Scanning	GT, NP
4.3.1 CBY-3 Model	AB
4.3.2 DC-3 Model	JM, AB
4.4.1 CBY-3 Structural Analysis	ER
4.4.2 DC-3 Structural Analysis	JM

4.4.3 Discussion of Results	AB, AM, ER, JM
5.1 Interviews	AM
5.2.1 Project Management Software	GT
5.2.2 Rapid Prototyping	AM
6.1 NEAM Interview Results	GT
6.2 Museum Interview Results	AM, GT
6.3.1 Software Recommendations of Restoration Workflow	GT, JM
6.3.2 3D Printing Recommendations	AM, NP
7 Project Conclusion and Broader Impacts	Team
9 Appendices	NP, ER

1 Introduction

1.1 Project Goals and Objectives

Goal 1: Investigate structural design features of the CBY-3 to understand the structural integrity of the four-pin wing attachment design in comparison to the safety factor of other conventional wing attachments of its time.

Objective 1: Evaluate how the CBY-3 structural design would have compared with competing aircraft such as the DC-3, built by the Douglas Aircraft Co.

Objective 2: Design and build a structure to enable photographic imaging of archival documents and drawings with minimal distortion and maximum repeatability.

To address the first objective, the team investigated the structural design characteristics of the CBY-3's four bolt wing attachment. This design feature was compared to the wing attachment used on another contemporary aircraft, the DC-3, built by the Douglas Aircraft Corporation that used an extended bracket with 328 bolts to distribute the wing load.

The second objective was addressed by designing and building a camera stand used to facilitate the photographing of archival documents with repeatable quality and minimal distortion.

Goal 2: Investigate the application of state-of-the-art rapid prototyping techniques and materials to complement the use of off-the-shelf inventory and traditionally machined, custom-made parts in the restoration process.

Objective 1: Investigate additive manufacturing options using plastics and metal to recreate damaged or missing parts.

Objective 2: Investigate 3D laser to CAD scanning options

The first objective was addressed by an extensive literature review and conducted interviews to identify current practice of using additive manufacturing in the aircraft restoration process.

The second objective was addressed by experimenting with a hand-held laser scanner to produce digitized models of solid objects that could then be imported into standard solid modeling programs such as SolidWorks. Once a solid model is generated, the parts can be exported to standard 3D printers for non-structural components that can be manufactured from plastic.

Goal 3: To work with the preservation staff at NEAM to assist in improving the software tools used by the staff to track parts, materials, scheduling, and restoration workflow.

Objective 1: Identify current workflow used by NEAM staff for restoration. This will include work organization as well as material and parts inventory control.

Objective 2: Research best practices in use by other museums, e.g., National Air and Space Museum.

Objective 3: Identify processes and software tools that could be used by the NEAM.

To address these three objectives, the team worked with the preservation staff at NEAM to assist to understand their restoration workflow, which includes tracking material and parts inventory, restoration organization, and general scheduling. The team also surveyed other museums involved in aircraft restoration to understand their processes.

Goal 4: Provide students with specialized training in and opportunity to apply software tools: MATLAB, Ansys Mechanical – Static Structural Analysis, Ansys Mechanical - Dynamic Analysis, and COMSOL

Objective 1: Train students in software: Solidworks and Ansys Structural Analysis

All students on the team underwent training in these software tools and then focused on the application of the structural analysis tools for this project.

1.2 Project Tasks

Table 1: Ansys Structural Analysis

Structural Analysis Task 1: 3D Modeling of Bracket
Problem Statement: <ul style="list-style-type: none"> - Create 3D CAD model from prototype and print documents
Solution Methodology: <ul style="list-style-type: none"> - Tools: Revopoint Pop 2 laser scanner, Solidworks, Autodesk Inventor, Revopoint software, SpaceClaim - Required Inputs: Bracket connecting the wing to the fuselage of the CBY-3 and DC-3, internal wing structure of CBY-3 and DC-3, mesh created by the laser scanner
Analysis Products: <ul style="list-style-type: none"> - Mesh created by the scanner in the Revopoint software - 3D solid model as a part in Autodesk Inventor/SolidWorks
Use of Results: <ul style="list-style-type: none"> - Autodesk Inventor/SolidWorks part of the bracket can be imported to Ansys Mechanical for a structural analysis

Structural Analysis Task 2: Perform Structural Analysis
Problem Statement: <ul style="list-style-type: none"> - Evaluate the von-Mises stress values on the wing attachment brackets of the CBY-3 and DC-3
Solution Methodology: <ul style="list-style-type: none"> - Tools: Ansys Mechanical - Required Inputs: Sum of aerodynamic wing lift and drag forces, structural forces applied to the bracket, and 3D model of CBY-3 and DC-3 wing attachment
Analysis Products: <ul style="list-style-type: none"> - Map of equivalent stress distribution - Identification of critical locations/joints
Use of Results: <ul style="list-style-type: none"> - Determination of critical stresses on wing/fuselage joint - Determination of structural integrity of wing attachment

Table 2: Restoration Workflow Recommendations

Restoration Workflow Recommendations Task 1: Document processes and software tools in current use
Problem Statement:

<ul style="list-style-type: none"> - Recommend software tools to improve processes used to track parts, materials, scheduling, and restoration workflow
Solution Methodology: <ul style="list-style-type: none"> - Collect information on restoration workflow from NEAM through interviews and/or written questionnaire. - Collect information on restoration workflow from other museums through interviews and/or written questionnaire
Analysis Products: <ul style="list-style-type: none"> - Documentation of restoration workflow, software used, and incorporation of 3D printing from multiple museums
Use of Results: <ul style="list-style-type: none"> - Findings used to formulate recommendations

Table 3: Photographic Documentation

Photographic Documentation Task 1: Camera Rig Creation
Problem Statement: <ul style="list-style-type: none"> - Create a camera rig to take accurate top-down pictures of engineering drawings and blueprints
Solution Methodology: <ul style="list-style-type: none"> - Tools: Personal Camera, Parts from previous MQPs and ordered from McMaster-Carr, Acrylic sheets - Required Inputs: Engineering Drawings and blueprints in order to digitize
Analysis Products: <ul style="list-style-type: none"> - Blueprint line tracings in Solidworks to correct digital 3D model dimensions
Use of Results: <ul style="list-style-type: none"> - Blueprint dimensions will help to ensure the accuracy of the digital 3D model dimensions, Pictures of engineering calculations and papers will help to inform structural analysis and museum workflow improvement.

Table 4: Analysis Tasks Method and Results Sections

	Methodology Section	Results Section
Ansys Structural Analysis		
3D Scanning of Bracket	3.2	4.2
CAD Model Generation of Wing Attachments	3.3	4.3
Performance of Ansys Mechanical Analysis	3.4	4.4
Restoration Workflow Recommendations		
Document processes and software tools in current use	5.1, 5.2	6.1, 6.2, 6.3

Photographic Documentation		
Photo Rig Creation	3.1	4.1

2 Background and Literature Review

2.1 Project Background

Worcester Polytechnic Institute’s Aerospace Department and the New England Air Museum (NEAM) have partnered to investigate some structural design aspects of the CBY-3 Loadmaster in comparison with the Douglas DC-3, a contemporary aircraft. Specifically, the NEAM staff was particularly interested in a structural analysis of the CBY-3’s unique wing attachment, compared to the approach used on the DC-3. In order to perform a comparison, a structural analysis of the DC-3’s wing attachment had to be completed as well. These structural analyses provided a measurement of the safety factor in the form of maximum stress compared to the material’s ultimate tensile strength.

This report will address the structural analysis of the wing attachment of each plane discussed above. Some qualitative and numerical aerodynamic data in this report is supported by a fellow student team’s aerodynamic analysis of the CBY-3 [23]. These student teams worked as two separate sub teams within this collaborative WPI – NEAM project.

2.2 Brief History of Burnelli and the CBY-3 Loadmaster

Vincent Justus Burnelli was born in Temple, Texas in 1895 and his family moved to New York in 1908. From a young age aviation piqued his interests and at just 20 years old, he formed his own aircraft company in 1915 titled the Burnelli Aircraft Company. He first developed the Burnelli-Carassi Bi-Plane during WW1 for the United States Military, who unfortunately did not

purchase the plane. Shortly afterward in 1917, Burnelli joined the Continental Aircraft Company as chief engineer and superintendent but did not stay for long, as in 1918 he joined the Lawson Airplane Company. There Burnelli designed America's first twin engine airliner, the Lawson C-2. However, it wasn't until he joined T.T. Remington to form the Airliner Engineering Company in 1920 when he developed his first aircraft with a lifting-body design, a key feature of the CBY-3 Loadmaster. The first lifting body design was created in 1917 by Roy Scroggs and continued to be developed by Scroggs and other aircraft designers like Vincent Burnelli [25].

The CBY-3 Loadmaster was an original design by Vincent Burnelli, but it was not his first design to incorporate a lifting fuselage. Burnelli had six previous prototypes utilizing the lifting fuselage before designing the CBY-3 Loadmaster. The first of these was the RB-1. Built in 1920, the RB-1 used two sets of wings, classifying it as a biplane. This plane could transport up to 35 passengers, however it suffered from a lack of control. In his next design, the RB-2, improvements focused mainly on performance and lifting capabilities. Built in 1923, the RB-2 was able to transport 6000lbs, plus a 3-person crew, which was proven during a test flight when the plane transported two cars. However, this design also suffered from inadequate control [1].

In 1928, Burnelli drafted a new design specifically to improve the control problems with the RB-1 and RB-2. The CB-16 featured a twin-boom tail that corrected some of the stability problems of the RB-1 and RB-2 and incorporated a retractable landing gear. His next design, while not offering many changes from the CB-16, featured variable wing camber and could take off and land in just 300 ft. His next two designs, the UB-20 and UB-14 built in 1930 and 1934 respectively, included modern features such as smooth, flat metal stress-skin instead of fabric. These designs also featured structural improvements to make the planes less vulnerable to the aerodynamic forces experienced during flight, as well as to improve lifting capabilities [1].

After additional performance improvements, Burnelli completed the construction of the CBY-3 Loadmaster in 1944. As with most of Burnelli's previous designs, only one prototype of the aircraft was ever built. The CBY-3 Loadmaster incorporated all that Burnelli had learned since first designing the RB-1. For numerous reasons, that will be mentioned in Section 2.4, the plane was not purchased by any customers, however the prototype saw roughly fifteen years of service in both Canada and even in South America before being left to sit in Friendship Airfield in Baltimore, Maryland in 1964 [22]. After a decade of neglect and exposure to the elements, the aircraft was finally retired to the New England Air Museum in 1972, where it would eventually undergo extensive restoration and is now currently on display [22].



Figure 1: The Burnelli CBY-3 Loadmaster in the New England Air Museum Hangar



Figure 2: Rear-Right View of CBY-3 Loadmaster showing the trailing edge of the lifting body fuselage



Figure 3: Front-Right view of CBY-3 Loadmaster

2.3 Brief History of the Douglas DC-3

Around the time of the CBY-3's creation, there was another aircraft that had already changed the landscape of commercial aviation. This was the DC-3, which unlike the CBY-3 quickly gained traction as a popular aircraft for both civilian and military applications. The DC-3, built by the Douglas Aircraft Company, is widely considered to be the catalyst for the birth of modern commercial flight. The aircraft was originally designed in 1934 as a commercial flight vehicle for American Airlines in two variations: one that accommodated for overnight flights and one that contained more seating than the DC-2 14 passenger model [14]. In June of 1936 American Airline purchased the first DC-3, the Douglas Sleeper Transport, that contained seating that could be converted into beds at night, allowing for more comfortable nighttime flying; two months later the airline company purchased the standard model without overnight seating [7 and 13]. Its all-metal exterior and cylindrical fuselage gave it a prominent look that made it one of the most well recognized aircraft of the mid-20th century, and it was the first airliner to, “fly profitably without government subsidy” [19]. The DC-3’s structure is the inspiration behind most commercial airliners in flight today [20]. The aircraft reduced the flight time between the west and east coasts of America in half, from a grueling 30 hours to 15 hours, with only three stops for refueling. Its body style was safe and accommodated 21 passengers comfortably, while also giving pilots the luxury of “stability, ease of handling, and excellent single engine performance” [19]. After the purchases by American Airlines, the DC-3 quickly saw a successful start in commercial flight. The new airliner’s success in the civilian world would quickly draw attention from military suppliers, where its massive success would only continue with the onset of the Second World War.

While the DC-3 was originally made to be a commercial airliner, the urgent need to transport troops and military cargo, beginning with World War II, led the way for the DC-3 to be

adopted for military use. The modified aircraft, classified as the C-47, swapped comfortable seating for soldier sleeping arrangements and cargo storage so that it could be used as a transport aircraft. Gliders could also be attached to the underside of the C-47 after production to carry extra supplies. Five hundred C-47s dropped paratroopers into Normandy for the D-Day invasion in 1944, and the C-47 continued to serve in the Berlin airlift (1948 – 1949), and later in the Korean War (1950 – 1953) and Vietnam (1963 -1975) [8]. Named the “Gooney Bird” by the Airforce, the C-47 was considered very reliable, and, as retired Air Force Lt. Col. James J. Krajicek stated, “It was an airplane that might forgive you if you made a mistake” [8].

2.4 Competition and Eventual Dominance of the DC-3 in U.S. Commercial Aviation

Although Burnelli’s design could have seen widespread use within the aerospace industry, unfortunately, that is not what occurred. There were many reasons why the CBY-3 was never a serious contender in the commercial aviation market, but the main reasons were bad business tactics, unfortunate political connections on the part of its creator, and market conditions that did not allow for a new transport and cargo aircraft to easily find a market. These market conditions were driven by a postwar surplus of the DC-3. Burnelli was considered an outsider in the industry and was described to be a talented engineer but not a very savvy businessman. He patented all the details of the aircraft to protect his design concepts and refused to allow the U.S government to buy the rights to these patents, keeping manufacturers from making “Burnelli-style” airplanes. Burnelli also did not join the Aviation Manufacturers Association or choose to work for any other large manufacturing companies. Chalmers Goodlin stated that Burnelli “did not appreciate how dishonest big businesses could be” [3].

In 1949, Burnelli met Goodlin, a former test pilot for Bell Aircraft, and the two quickly bonded, in part due to their status as “outsiders” in the industry. Goodlin later became a stockholder in the Burnelli Company as he grew to love the lifting-fuselage concept as well as working with Burnelli. Goodlin argued that the military-industrial complex was to blame for Burnelli’s lack of success, and he presented some interesting narratives that support his argument. One notable example was from 1940 when Burnelli was invited to the White House to have President Franklin Roosevelt sign a production contract for one of his other designs that had won an Army Corps competition. Before Roosevelt signed, he asked Burnelli who his backer was, Burnelli’s response was Arthur Pew, a supporter of Roosevelt’s political opponent. According to David Noland [3], Roosevelt “exploded with anger” and Burnelli never got the contract, or any other contract. Other examples illustrate the fact that some aerospace companies avoided working with Burnelli. Goodlin believed Boeing was the “kingpin in the anti-Burnelli conspiracy” as the Burnelli concept was pitched to them and promptly ignored. However, a decade later, the 754 Husky was developed with a lifting fuselage design very similar to the CBY-3 design. Goodlin demanded Boeing pay the Burnelli Company royalties, but Boeing refused, and eventually needed to abandon the 754. Similar instances occurred with other companies, but to a lesser extent. After many rejections and failures, Burnelli never built another aircraft.

A final reason that the CBY-3, and other Burnelli aircraft never saw widespread adoption was the near total saturation of the transport aircraft market by the DC-3. With more than 13,000 DC-3's and C-47's, being produced by 1945. The DC-3 was also nearly a decade old, with the first DC-3's having been produced and put into service in 1936. Additionally, in 1945, as the Second World War ended, thousands of C-47s were repurposed and sold, reducing the price of the aircraft [19]. The CBY-3 was not able to achieve widespread popularity at least in part because there was

simply no existing market to sell it in. The DC-3 was a very well known, reliable, and cheap alternative that existed in vast quantities, while the CBY-3 was new, comparatively untested, and would likely have been more expensive than the vast surplus of DC-3's. The DC-3 was one of the most successful aircraft in history and Burnelli could not find a market that would be profitable for the CBY-3 [8].

2.5 Aircraft Structural Characteristics

The structural design of an aircraft is equally as important as the aerodynamic design to achieve the desired performance and safety. The individual parts and assemblies that comprise the airframe experience many different forces, so it is important to note the correct terminology used to describe the behavior of these structural elements when subjected to different loads. First, and perhaps most important, is stress concentration. Stress concentration is a location in or on an object where the stress is significantly greater than in the surrounding region. This typically occurs in a component when there is an irregularity that interrupts the flow of stress, such as an irregularity in the material or geometry, which can be caused by its design or by accidental nicks and scratches. The degree of stress concentration can be described by the *stress concentration factor* K_t which is the dimensionless quantity that quantifies how concentrated the stress is in a part [17].

Stress concentrations are the main cause of deformation, which is the change in size or shape of an object after a load or force acts on it. It is crucial to understand how an object or component may deform and how likely it is to return to its original state after undergoing a load in order to understand the stability and strength of a structure. There are two main terms that describe the deformation of objects. First is *elastic deformation*, this refers to a change in shape of an object that is self-reversing after the load has been removed. *Plastic deformation* refers to the permanent change in shape of an object that is not self-reversing even after the load has been

removed [17]. It is possible for an object to experience both elastic and plastic deformation from the application of one load.

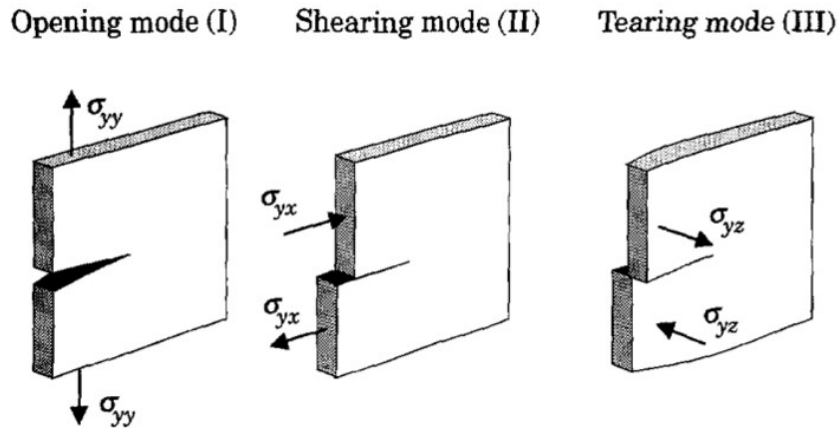


Figure 4: Visual representation of the opening, shearing and tearing modes of deformation. [18]

Once a load has caused significant deformation to an object, there is a high likelihood that the object will fail or break. The failure of an object can be described in two different ways. First is *brittle failure*, which occurs when an object experience little to no plastic deformation, meaning that there is a very small amount of permanent deformation before the object suddenly fails. Alternatively, *ductile failure* occurs when there is a large amount of plastic deformation that occurs before the object fails, meaning that it can be largely deformed or distorted in a permanent way before failing or fracturing [17].

For aircraft to withstand the numerous forces and loads that are placed on it, such as lift and drag, aircraft designers often use various types of members to construct the structural framework of both the fuselage and the wings. *Skin stringers* are responsible for transferring the aerodynamic loads placed on the surface of an aircraft, as well as the bending loads faced by the

wings onto the frames and ribs that make up most of its structure. It is important not to confuse a stringer with a *longeron*, which tends to make up the structure of the fuselage, carry heavier loads than, and are much longer in relation to stringers [18]. Figure 5 provides an illustration of the different structures comprising the structure of a wing.

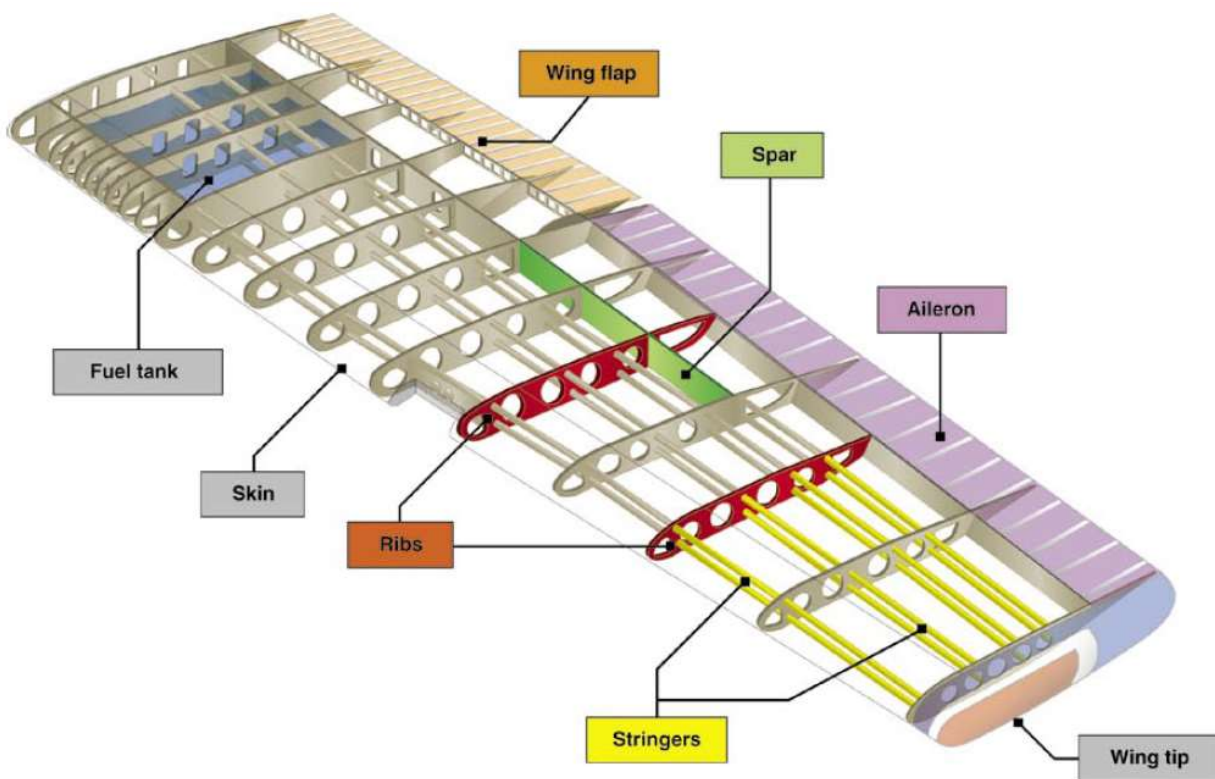


Figure 5: The internal Structure of a wing [27]. Copyright 2023 CFI Notebook

2.5.1 Characteristics of the CBY-3 Wing Attachment

The CBY-3 wing attachment differs greatly from that of the DC-3. The CBY-3's wing attachment configuration consists of four brackets with corresponding one-inch steel pins that

attach the wing to the fuselage. This configuration allows the wing to be removed and reattached with relative ease. The brackets are identified in at least one of the archival documents [26] as being part of the upper part of the wing or the lower and then denoted as being located on the “front” side of the wing closest to the nose of the plane or the “back” side, closer to the tail of the plane. To limit confusion, in this report the brackets will be referenced as letters. Table 5 lists the bracket reference letters and Figure 6 shows a picture of the wing with the brackets labeled with their corresponding reference letters.

Table 5: Bracket Reference Letters

Brackets	Reference Letters
Lower Rear	A
Upper Rear	B
Lower Front	C
Upper Front	D

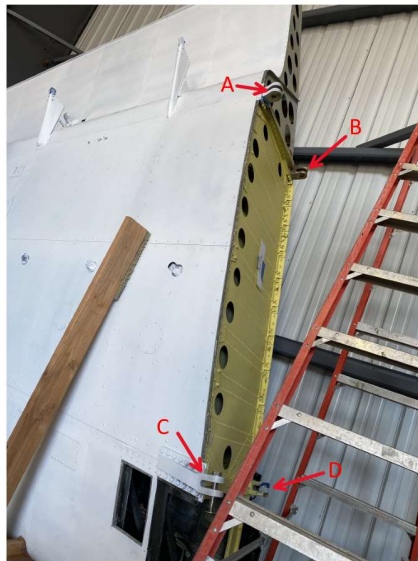


Figure 6: Bracket Reference Letters on Wing in Storage Position



Figure 7: Bracket Reference Letters on Correct Wing Orientation

While all the brackets have a similar general shape there are differences between them that are important to identify. Both upper brackets (B) and (D) are slanted at an angle of 7 degrees, but bracket (D) is slanted downward towards the bottom of the plane while bracket (B) slants upward towards the top of the aircraft.

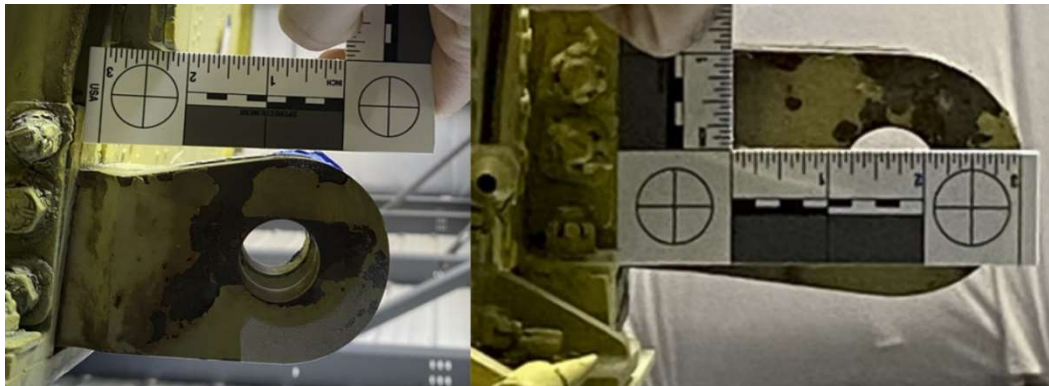


Figure 8: Brackets (D) and (B) respectively

Similarly, bracket (A) is slanted 23 degrees towards the bottom of the aircraft.

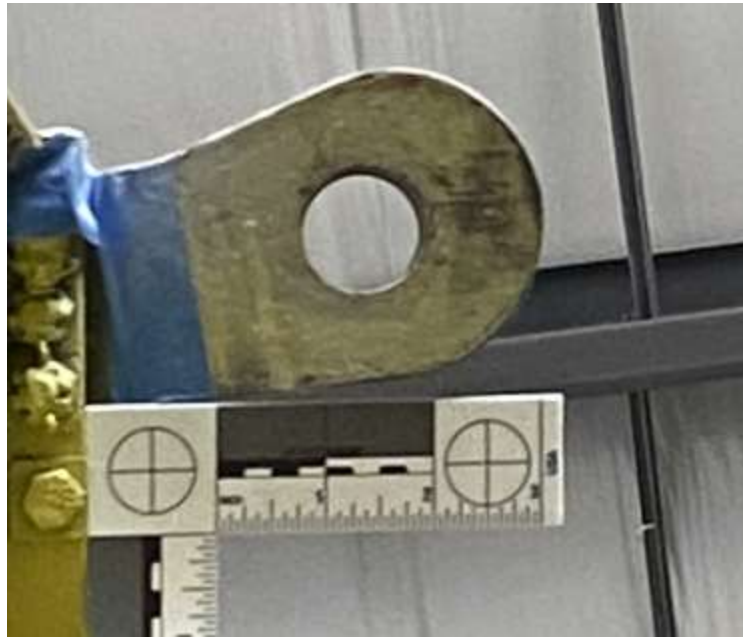


Figure 9: Bracket (A)

Bracket (C) is slanted 8 degrees towards the bottom of the aircraft as well. To avoid confusion in the discussion to follow, we will refer to the “bolt-end” and the “wing-end” of each bracket. The bolt-end refers to the portion of the bracket with the dual loops that are inserted into the fuselage and through which the attachment pin is placed. The wing-end of the bracket refers to the portion of the bracket that is attached to the wing.

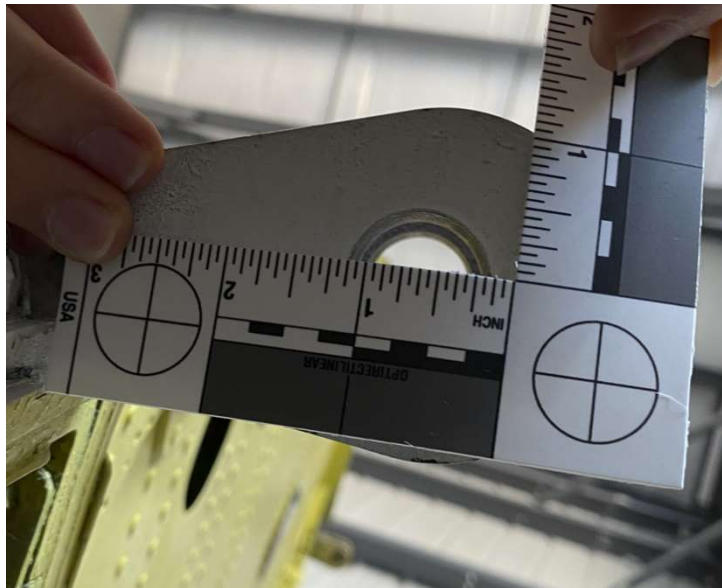


Figure 10: Bracket (C)

Brackets (A), (B), and (D) are attached to the inner structure of the wing with most of their structure enclosed in a metal box that is bolted into the wing's inner structure.



Figure 11: Metal Box Structure Encasing End of Bracket D

All three of these brackets' wing ends are perpendicular to the outer structure of the wing.

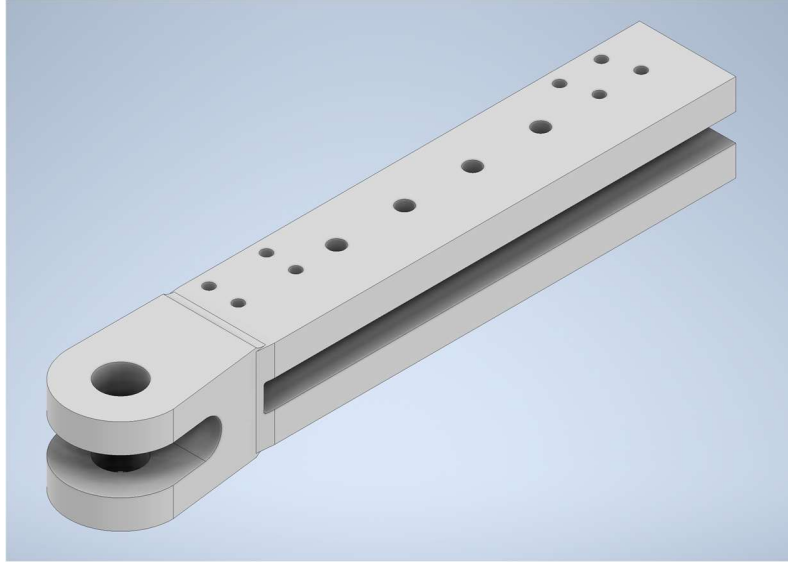


Figure 12: CAD Model of Bracket (B)

Bracket (C)'s trailing edge is bolted into a metal plate on the outside of the wing. Its trailing edge is parallel to the outside structure of the wing unlike the other three brackets. Figure 13 is a picture showing the orientation of the end of bracket (C).

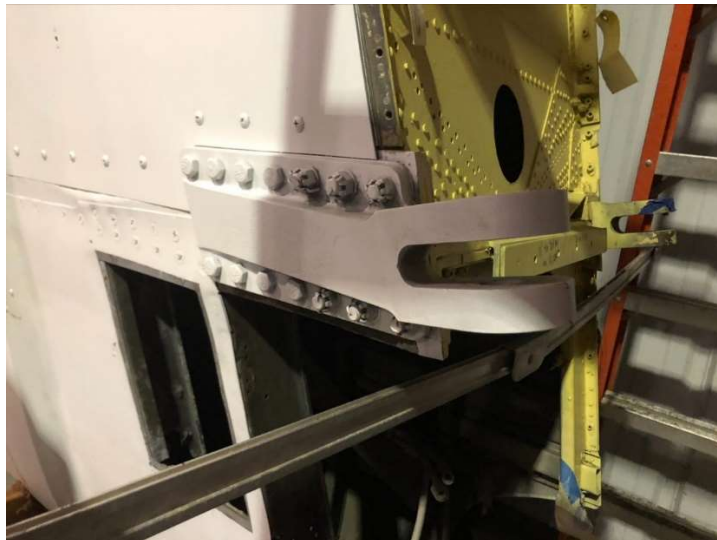


Figure 13: Bracket (C) CBY-3 Wing Attachment

2.5.2 Characteristics of DC-3 Wing Attachment

Most of the DC-3 wing's span lies beyond the point where it is attached to the fuselage of the aircraft, just beyond the engine nacelles. In contrast to the CBY-3, this attachment is achieved through the use of 328 individual bolts [41] along a flange that runs along both sides of the connection point. This double-sided flange runs along the perimeter of the ring in a chordwise direction. Each side of the flange is riveted to the wing surface and the two flanges are clamped together with the string of bolts. This flange is shown for the portside wing of the DC-3 in Figure 14.



Figure 14: DC-3 Wing attachment lower front view

These bolts are not evenly spaced along the flange, with closer spacing near the leading edge, and immediately below it. Each bolt is approximately 0.25 inches in diameter, and the flange is approximately 0.3 inches wide, shown in Figure 14. Again, in contrast to the CBY-3, the DC-3 wing attachment distributes any stress from the wing over the length of the bracket held together by a large number of bolts and attached to the wing with an even larger number of rivets.

2.6 Use of Rapid Prototyping in Aircraft Restoration

Rapid prototyping is found in many industries today that require the most efficient fabrication of a physical element or part. *Rapid Prototyping* refers to a variety of techniques used to quickly fabricate a part using computer aided design (CAD) [29]. Two main techniques of rapid prototyping are *Additive Manufacturing* and *3D Printing*. Additive manufacturing is the creation of objects or parts through the addition of new material whereas 3D printing involves the creation of an object one layer at a time. This means that 3D printing is a method to conduct additive manufacturing, but additive manufacturing is a more general term used to describe many more processes than just 3D printing [30].

Rapid prototyping utilizes additive manufacturing to fabricate components quickly and efficiently. Additive manufacturing has become a key part of overhaul and restoration, as it allows for the repair of worn or damaged parts, as compared to scrapping and rebuilding which can be wasteful and expensive. Additive manufacturing is typically used to perform geometric and structural repairs. Geometric repairs focus on surface level wear and damage on frequently used parts. A notable example of this is the repair of the C-130J landing gear shelf bracket, a part that frequently experiences corrosion. With additive manufacturing, the corrosion on this part was repaired to new condition with material that gave it increased corrosion resistance [34]. Structural repairs involve parts with more significant damage than those requiring geometric repairs. This

means the material deposited during the additive manufacturing is needed to restore the static and fatigue strength margin as well as the component's geometry. This method was used with the AerMet 100 Bar, where damage from electro-discharge was repaired and the static and fatigue strength of the part was restored as well.

Rapid Prototyping / Additive Manufacturing is also being used in museum restoration, specifically for historical aircraft. One example of where this technique has been used is the Air Mobility Command Museum at Dover Air Force Base. This museum was able to use Dover Air Force Base's 3D printing lab to manufacture parts for both a C-17 Globemaster III and a KB-50J Superfortress. These parts were generally small and cosmetic in function but could not be easily procured by traditional means. This methodology, if not exact procedure, could be useful for NEAM. While NEAM does not currently have an onsite additive manufacturing lab, the concept of using additive manufacturing to replace smaller cosmetic parts of historical aircraft that could not be easily or cheaply acquired through other means such as outsourcing may work well.

3 Methodology of Structural Analysis Comparison

3.1 Photographic Documentation

3.1.1 Problem Description and Methodology

During the initial stages of the 3D modeling design process for the aerodynamic analysis of the CBY-3 and the DC-3 the intended method to collect dimensions was to rely heavily on the blueprints available at NEAM. The intent was to take top-down photographs of each of the blueprints and use SolidWorks to recreate the blueprints, giving accurate outlines of each of the parts. These outlines could then be extruded into parts which could be assembled into the final

model of the aircraft. To support this effort, a photography rig, or stand, was designed to enable consistency in photographic documentation.

The first step was to determine the height at which a camera would need to be mounted in order to fill the entirety of the picture with each sized blueprint. With this information a camera rig was designed to be able to position the camera at each of the heights to take pictures of the documents. Figure 15 shows the 3D model of the camera rig that was designed for the project.

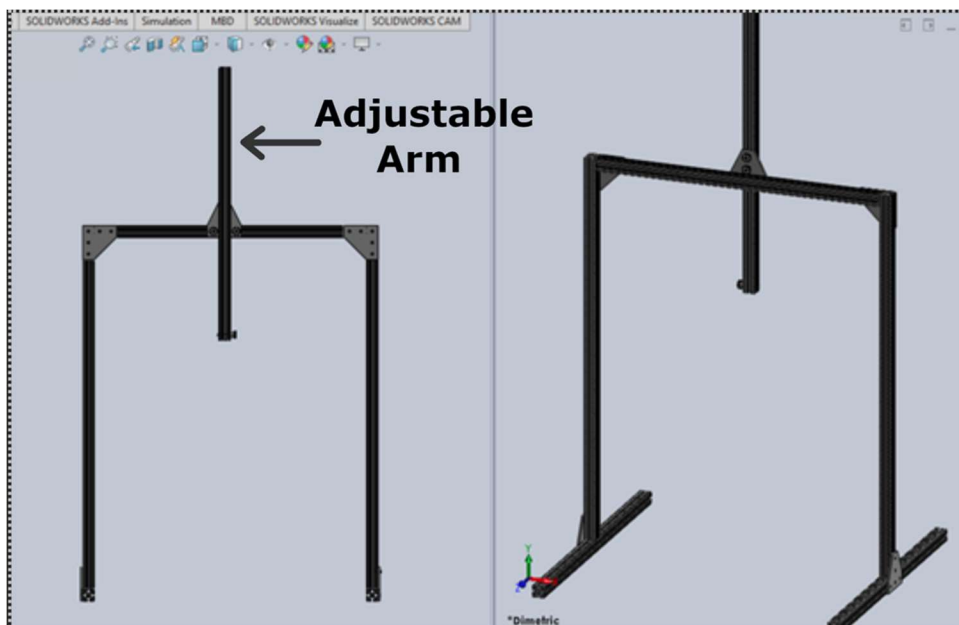


Figure 15: The front and isometric views of the camera rig

This design allows for the blueprint to be laid in between the legs of the rig perpendicular to the front of the camera. The camera is mounted on a 1/4 - 20 UNC threaded fastener at the bottom of the adjustable arm. Each of the beams comprising this camera rig are one-inch solid aluminum x-channels, with steel corner brackets to hold them together. The arm is attached with two hex bolts that allow the camera a maximum height of 42 inches and a minimum height of 18 inches. This allows perfectly framed pictures of documents between the range of a US letter paper

to a 32 x 52-inch blueprint. These papers are sandwiched between two layers of 1/4-inch-thick clear acrylic to ensure that they lie flat while being photographed.

Due to the long wait time for the parts to be ordered and shipped, for the work presented in this report the team took pictures with a camera held by hand to capture the needed images. This means that while the camera rig was not used for this project, it will be available to future teams to digitally archive documents. Another objective of the project is to work with NEAM to determine methods to improve workflow during restoration. This camera rig will allow the effective digitization of documents which can be explored as a part of improving workflow. Having documents digitized, indexed, and readily available allows for much quicker access to information than finding physical documents in boxes.

3.1.2 Design Construction of Camera Stand

In order to determine the maximum and minimum height required for the adjustable arm, Equation 1 was used to determine camera field of view at a given distance between the document and the camera focal plane.

Table 6: Variables used in Camera Stand Design Analysis

Value	Variable	Units
Sensor Width	S_W	mm
Sensor Height	S_H	mm
Focal Length	F	mm
Document Width	D_W	in
Document Height	D_H	in

Distance to object	L	in
--------------------	-----	----

$$FOV = 2 \cdot \arctan\left(\frac{S_W}{2 \cdot F}\right) \quad (1)$$

Given the FOV angle for a particular camera sensor width and lens focal length, the next step is to determine the camera mount height necessary for that FOV to encompass the entirety of the document being photographed. The height of the camera focal plane above the document will always be proportional to the camera sensor height-to-width ratio. This means that both Equations work regardless of solving for the FOV along the document's vertical or horizontal axis.

$$\arctan\left(\frac{D_H \cdot L}{2}\right) = \frac{FOV}{2} \quad (2)$$

Equation 2 was derived from the angular relationship between D_H and L , where they make a right-angle triangle to allow the use of trigonometry functions to determine FOV. This provides a relation between L and the FOV determined by S_W and F in Equation 1. The camera lens must be at a certain distance, L , for the document in the image to fill its entirety. It is important to note that the height calculated using Equation (1) is precisely at the focal plane mark of the camera and not necessarily the front of the camera lens. This means that for each size camera there will be an offset from this calculated distance to the document in order to fill the entirety of the photo. This must be determined by hand for each camera used.

3.2 3D Laser Scanning

3D laser scanning technology is a tool that can scan virtually any object with high precision and turn it into a computer-generated solid model. This technique uses the laser's light to capture the shape of the 3D object and turn it into a "point cloud", i.e., a set of data points with a fixed

coordinate system [21]. The infrared light from the laser scanner is reflected into a camera sensor, using the principle of triangulation to measure distance, allowing it to map out the objects' shape. This means that the sensor measures the angle of the returning laser light from the object, using trigonometry to calculate the distance to, and hence the characteristics of surface features [33].

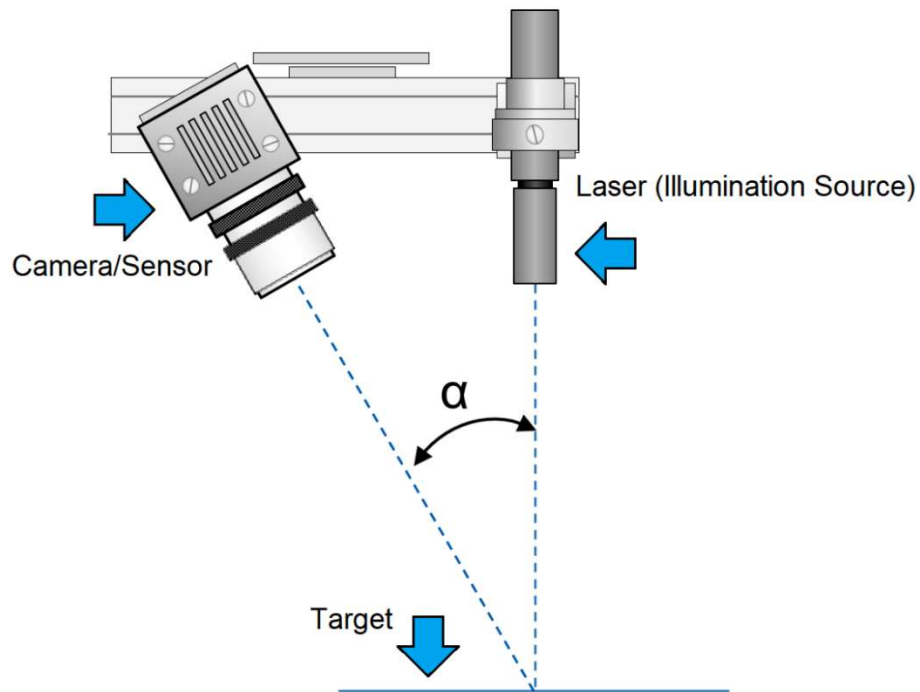


Figure 16: A picture depicting the laser triangulation method. Copyright 2018 MoviMED

The point cloud for the object created from the scan and triangulation calculations can then be meshed into the object's geometry, which can be converted into a computer-generated solid model. This technology was investigated for this project because the team could use it to create parts that can either be 3D printed or modeled for analysis from physical parts. Software SolidWorks for example, performs this task well by allowing the mesh files created by the 3D scanner to be easily downloaded and turned into a solid model through the click of a button.

The scanner selected for this project is the “Revopoint Pop 2” manufactured by Revopoint, which comes with a laser-camera unit, a tripod, a cable to hook it up to a computer and cables that include USB A and C converters (See Figure 17).



Figure 17: Image of the Revopoint Pop 2 3d scanner with its hardware. Copyright 1996-2023, Amazon.com, Inc. or its affiliates



Figure 18: Revopoint Pop2 3D scanner assembled on the tripod stand. Copyright 1996-2023, Amazon.com, Inc. or its affiliates

The “RevoPoint Pop 2” uses a dual camera with infrared structured light, which is a projected pattern of light mapped onto surfaces, and a Class 1 infrared laser as its light source [28

and 39]. A Class 1 infrared laser is completely safe to the eye and has a 0.7milliwatt power output [40]. The companion software called “Revo Scan”, is used to display the scans taken by the device, which is compatible with Windows versions 8 and up, MacOS, Android, and iOS. When the scanner is connected to the computer and *Revo Scan* is open, the scanner can be turned on to create virtual point clouds and meshes. These meshes can be saved as PLY, OBJ or STL files. These files, while not common, are mesh file types, which are very useful for creating CAD models, and especially for 3D scanning because of their ability to store color and texture information accurately. The numerous capabilities outlined above, and reasonable price (\$700) made this scanner the optimal choice for the team.

The Revo Scan software is very user-friendly, allowing the user to create numerous high-quality scans quickly. The interface shown in Figure 19 shows the RevoPoint home screen when the scanner is plugged into the user’s computer. At this screen the operator can see a preview of the RGB (red, green, and blue color model) and depth views, which both show the object currently being seen by the scanner. The *Preview* tab was useful to get a view of what the scanner currently sees, so that adjustments to the brightness of the scan or position of the object could be made.

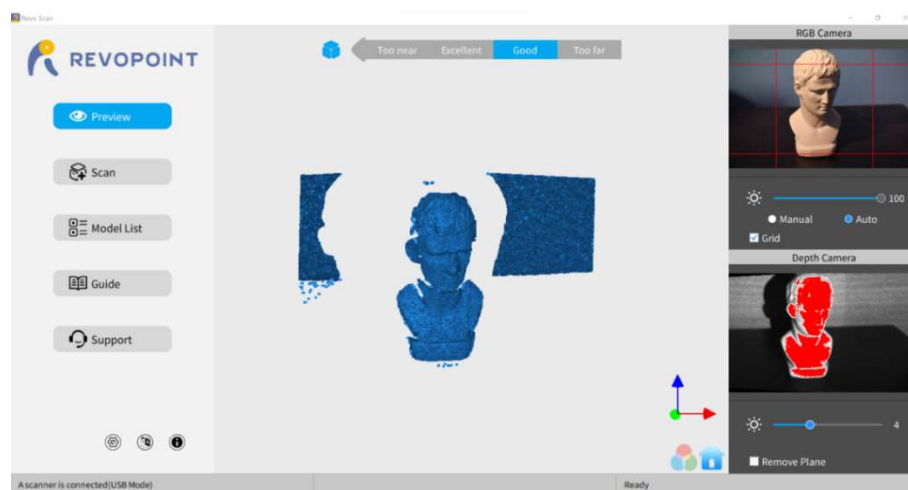


Figure 19: The user interface of Revo Scan when a scan is first initiated

From the preview window, the user can navigate to the *Scan* tab to begin a new scan.

Figure 20 shows the *New Project* screen that appears at the beginning of a scan.

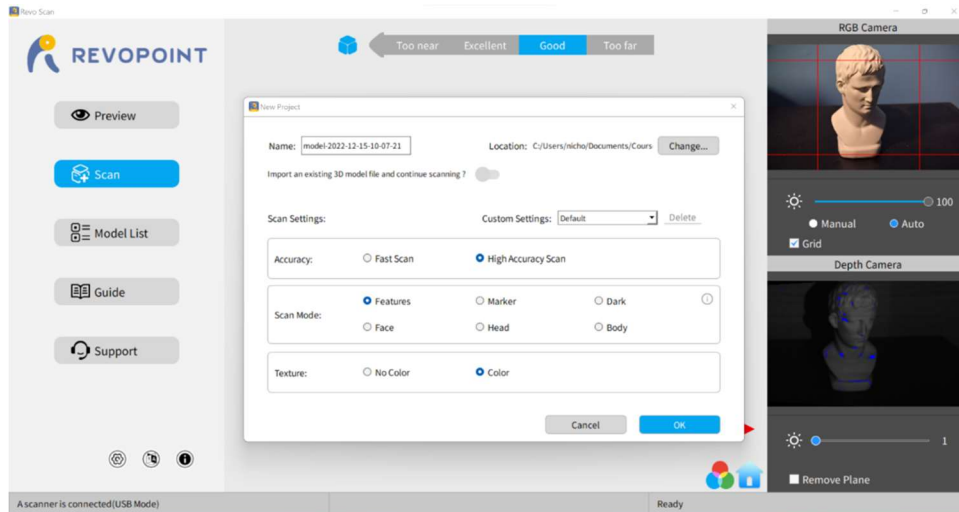


Figure 20: The Revo Scan UI at the creation of a new scan

Once a new project has been initiated; the operator can select the custom setting that would best capture the object of choice. For most of the scans in this project, the *High Accuracy Scan*, *Features*, and *Color* options were selected, because the team wanted to capture as much detail as possible. After initiating the scan, it was clear when an error occurred or because the command window displays a red color on geometry that has not been accurately recorded. However, after the successful completion of a scan the operator simply completes the scan and can save it to the computer in any one of the file types mentioned above, allowing the user to utilize the scan as a CAD part for further use in other applications such as an Ansys Mechanical.

3.3 CAD Model Generation

3.3.1 CBY-3 Method and Approach

The team followed a trial-and-error approach to create the CAD model of the wing attachment for the CBY-3. This meant trying multiple different methods to obtain and record the dimensions of each attachment until a full and complete CAD model could be created. When first deciding to create a CAD model of each of the four wing attachments of the CBY-3, the team's initial instinct was to utilize the Revopoint Pop 2 3D scanner to quickly create these models. However, the team was unable to use the 3D scanner to create a working solid model of the wing attachment brackets for reasons discussed in Section 4.2.

Because creating a CAD model of each bracket using the 3D scanner was no longer an option, the team began creating these models from scratch. This required a combination of approaches because of the many unknown dimensions of each bracket. The team first started by gathering all dimensions possible from the drawings and blueprints available at NEAM. This meant going through numerous boxes of historical files to find drawings that were specifically relevant to the dimensions of each of the four wing attachments. While difficult to locate at first, the team was able to find a few drawings that provided some base dimensions on one of the wing attachments. However, these drawings lacked the dimensions necessary to create a complete CAD model of each attachment. One of the drawings from the archival material used in the creation of this CAD model can be seen in Figure 21.

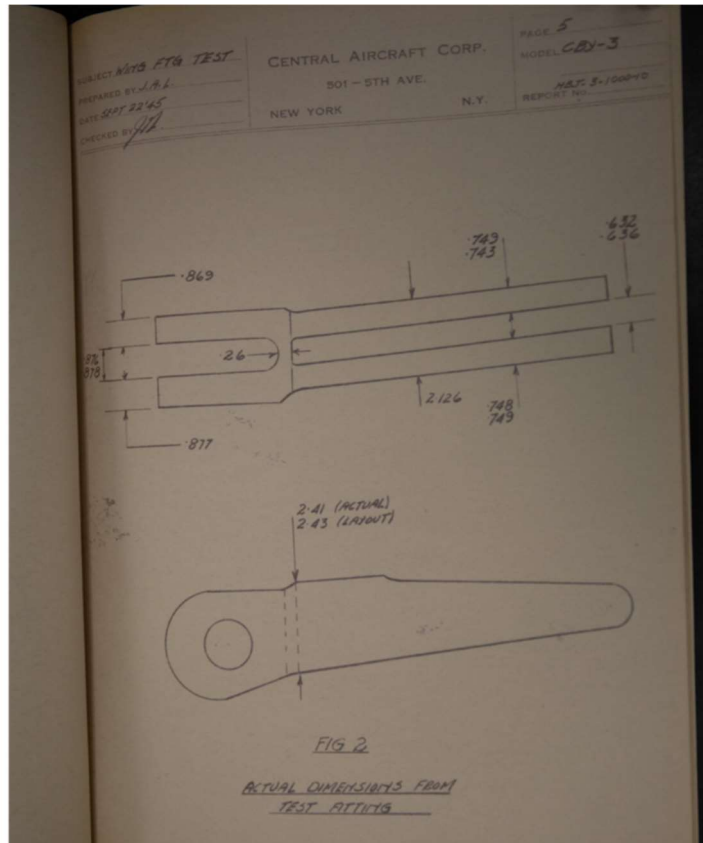


Figure 21: Image of one of the drawings used in the creation of the CAD model of each wing attachment, captured on sight at NEAM. As can be seen very few dimensions are shown in the drawing [36].

Since few dimensions were available from the drawings alone, these needed to be supplemented by physical measurements of the attachments themselves. The team tried a few different tools and methods to measure all necessary dimensions. The first was simply using calipers to measure different thicknesses and bolt hole diameters. While taking measurements, the team was careful to gently tighten or extend the calipers to the length of the desired object, to avoid inaccurate measurements, in addition to taking measurements at least twice to make sure the values were correct.

As previously stated, all sides of a given bracket installed on the wing were not visually accessible to the team. To address this the team decided to use an endoscope (an inspection camera with narrow and flexible camera shaft) to view the inner structure of the wing and inaccessible sections of the brackets. The endoscope selected for use during this project is the NTS300 Pro Inspection Camera with 5-inch HD screen, manufactured by Teslong. This endoscope has a 10ft long cable with two different cameras, a frontward facing and side facing (perpendicular to front) camera. This endoscope also includes a bright LED light so that it can be used in dark environments such as a pipe, or in this case an aircraft wing. The endoscope interface also allows the user to capture images, video and even sound. An image of this endoscope from the manufacturer's website can be seen in Figure 22.



Figure 22: Teslong NTS300 Dual Lens Inspection Camera [35]. Copyright 2023 Teslong

Using the endoscope, the team was able to view the inner structure of the wing, which revealed another challenge. It wasn't possible to hold an actual measurement device within the wing so the team decided to use a reference object, or an object with known dimensions, that could be used to determine the exact dimensions of another object by using this reference as a basis for comparison. Using the reference object, the exact dimensions of the hidden portion of the bracket could be determined, as well as the necessary dimensions of the internal wing structure. An image taken within the CBY-3 wing using the endoscope can be seen in Figure 23.



Figure 23: The above image was taken by the team of the internal wing structure using the NTS300 endoscope.



Figure 24: The above image was taken by the team of the internal wing structure, and annotations are visible to outline the dimensions of different sections.

The method of using a reference object to determine different dimensions was also applied to accessible features on the outside of the wing as well. This was especially helpful to determine the exact geometry of each bracket. Since the drawings/blueprints did not provide any information about the angle the bolt hole of each bracket turned with respect to the portion that is held within the wing, the team also had to measure this. As shown in Figure 25, a reference scale or “evidence ruler” was used to determine this exact angle so that an accurate CAD model could be created.

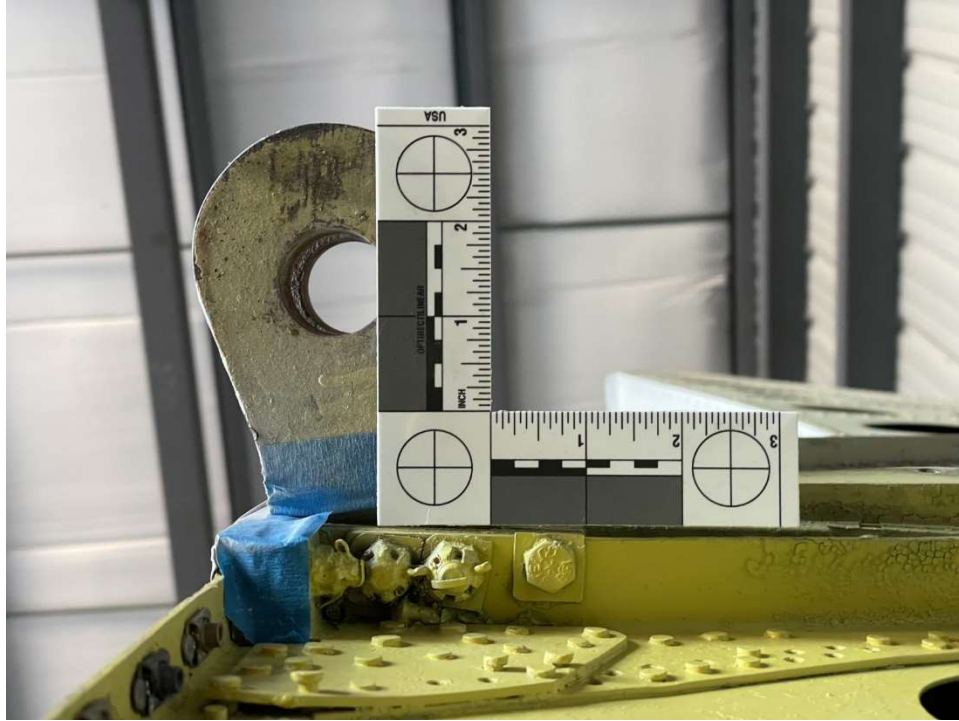


Figure 25: An image of the reference scale and bolt hole portion of one of the wing attachments.

Once most of the dimensions were known, the team could start to create CAD models of each wing attachment bracket, as well as the internal wing structure, so that this could be used in Ansys Mechanical. To make sure the models eventually used in Ansys Mechanical were manageable in size, the team decided to create two assemblies, each of which would include two brackets and a limited portion of the internal wing structure. The internal structure surrounding the two brackets would allow half of the total wing loading to be applied to each of the two assemblies so that the induced stresses in the brackets and surround structure could be evaluated.

To create solid models for the brackets and wing sections, the team selected Autodesk Inventor Professional [37] for this process because many members were familiar with this tool. The team used the dimensions collected from the drawings and field measurements to create the CAD models. The team started by creating each of the four-wing attachment brackets (in no

particular order), which were each completed following the same process. First, a general sketch of the sideview of each bracket was created so that the extrude feature within Inventor could give this sketch depth and turn it into a 3D object. Next, additional sketches were created and the extrude cut feature used to add sections to the bracket where it would attach to the wing structure or where a bolt would be placed. Once the bracket was created including all of its features, the geometry of the part needed to be finalized. Again, utilizing the sketch feature, the angle of the attachment bolt hole was added to finalize each bracket. The methodology of using sketches and extrusions was used in the creation of all four brackets as well as each section of the internal structure of the wing.

After all the individual parts were created, the Assembly function within Inventor was used to create the two assemblies, one for the two brackets and surrounding structure near the leading edge of the wing, the second for the two brackets closest to the trailing edge. Using the Assembly function would allow the team to mate each of the individual parts to one another so that a final assembly resembling the entire inner wing structure could be created. The team broke down this final assembly into six different smaller assemblies. The overall wing structure was divided into two smaller assemblies as previously described, the wing structure near the trailing edge of the wing, and the wing structure near the leading edge. These were further divided into three smaller assemblies again, both following the same method. These three smaller assemblies consisted of the “box” like structure around each bracket (one assembly for each) and the structure that joins these two “boxes”.

Using this approach, the team was able to create a CAD model of the internal structure, by starting small and working up to large assemblies. First, the “box” structures around each bracket were created and saved as individual assemblies (total of four assemblies). Next, the internal wing

structure between the two brackets near the leading and trailing edge was created (total of six assemblies). After these six smaller assemblies were finalized, two final assemblies were created utilizing these. One that joined the corresponding assemblies to create the internal structure of the trailing edge of the wing, and one that created the internal structure of the leading edge. For further clarification, exploded views of each assembly can be found in Section 4.3.1.

Breaking up the overall assembly like this allowed the team to make more accurate “mates” that is, joining individual parts to one another in a more accurate way. Additionally, this meant that if a mistake was made when creating the “box” structure around one of the brackets, this mistake could be addressed and the smaller assembly updated, allowing for small changes to be made easily. If this approach was not followed, and two large assemblies consisting of all individual parts were created, a small mistake could trickle down and be nearly impossible to address without having to recreate the entire final assembly.

3.3.2 CBY-3 Assumptions

It is important to note that the team prioritized using drawings to gather as many dimensions as possible, unless a part on the actual aircraft indicated otherwise, in which case measurements from the aircraft were prioritized. However, despite the numerous resources available to the team and the number of measurements taken from the wing itself, there were still unknowns that needed to be addressed. These unknowns were usually a result of some internal structure not being readily accessible for measurement, even with the endoscope. Because of this, the team needed to make several assumptions about the internal structure of the wing and wing attachment brackets to create a full model for the Ansys Mechanical Structural Analysis.

To start, in the creation of the wing attachment bracket, the team had to make three major assumptions. The first is the bolt hole size in each bracket so that the bracket could be attached to the surrounding wing structure. None of the drawings the team reviewed included the size of each of these holes and unfortunately because the bracket was attached to the internal wing structure already, the bolts could not be removed to measure the diameter of each bolt. This led the team to assume the size of the bolt based on the size of the bolt head. The team researched typical bolts and their corresponding bolt head dimensions, as well as understanding the realistic size of each bolt to infer their dimensions. Figure 53 in Section 4.3.1, shows the bolt hole dimensions on bracket A, which is the same throughout brackets B and D.

Next, was the physical shape of each bracket, as shown by the drawing in Figure 21. The original design showed that the bracket was designed to have a rounded shape on the end that sits within the wing. However, upon inspection of the aircraft, each bracket had a rectangular edge shape which did not correspond to the drawing. Following its approach of prioritizing the measurement made on the actual aircraft, the team measured the rectangular shape of the bracket present on the wing and utilized these dimensions in the CAD model. Additionally, for bracket C specifically, the surrounding area of the main bolt hole portion that attaches the wing to the fuselage was assumed to be $\frac{3}{4}$ of an inch longer than the rest of the brackets. To clarify, the main bolt hole itself was still the same dimensions as the other brackets, however the surrounding area was stretched to ensure the bolt holes would align flush to the fuselage. The team made this assumption due to the fact that brackets A and B were aligned with each other to provide a better fit with the fuselage. Examining the fuselage, it was clear that brackets C and D would have to be aligned in order to accomplish the same tolerance as A and B. because it made intuitive sense for the design of the aircraft. Performing this allowed the main bolt hole of bracket C to rest parallel

to that of bracket D, meaning that the wing would attach flush to the fuselage, if this assumption had not been made, the wing would not rest flush, and a gap would be present between the wing and fuselage.

The next set of assumptions made by the team involved the assemblies that make up the internal wing structure. Starting with the “skin” that goes on the outside of the entire wing, the team decided not to include “skin” in the CAD model because the main purpose of the skin is to distribute the aerodynamic loads experienced by the wing into its internal wing structure, meaning that adding skin would only overcomplicate the model. Because the purpose of this project is to investigate the internal structure of the wing, the “skin” was not added to the model. Similarly, the CAD model only included the internal structure of the wing up until the first rib. Meaning that the internal structure past the first rib and the fuselage side of the attachment were not included. Because this project was focused on the structural analysis of the attachment joint, the entire wing and fuselage structure was not included. Limiting the analysis to the two assemblies that capture stresses surrounding all four attachment brackets allowed the team to perform the required stress analysis while keeping the problem computationally manageable.

The actual aircraft relies on hundreds of rivets to attach individual parts and assemblies to one another so that they are conjoined almost permanently. The team assumed that including the numerous rivets in this model would not serve any purpose other than significantly increasing the computing resources needed. The entire purpose of riveting is to attach two parts together with the strongest and lightest joint possible, so that stresses can “flow” between connected structures. In addition to the computing resources already noted, the actual number of rivets would be nearly impossible to include in the model because of the time required to model them. For these reasons, any riveted section of the internal structure was treated as one piece instead of multiple layers.

The final assumption in the creation of this CAD model was that dividing the bracket pairs near the leading edge and trailing edge into separate assemblies would still allow an accurate assessment of stresses near each bracket. There are two main reasons behind this decision: the added complexity that would have been created with a single model, and the time constraints of this project. Having one model comprising both the leading and trailing edge of the bracket pairs would require the addition of other smaller objects to the model such as the wing's internal fuel tank. Adding additional components to the final model would make it much more complex which can and likely would cause meshing and other unforeseen errors in the Ansys Mechanical Structural Analysis. This added complexity would likely not add any additional meaningful results. All of the wing loads are ultimately transferred to the fuselage through the four attachment brackets, so the largest stresses will exist and can be investigated in the surrounding structure.

3.3.3 DC-3 Method and Approach

The team used both images taken at NEAM by the team, or by NEAM staff, of the DC-3 wing attachment to create a 3D model of the part. Over several visits to NEAM, on November 10th, 2022, December 12th, 2022, and January 1st, 2023, the team gathered data on the dimensions of the wing attachment and were sent images of a completed wing in the process of being attached during the restoration of a DC-3 at the museum. [Personal Communication: email C. Cruff to J. Blandino, 1/16/23]. These images are shown in figures 26 through 28. This provided a general understanding of the wing attachment geometry and dimensions, which could then be used to create the model.

In order to create an accurate 3D model of the DC-3 wing attachment the team took images of an exposed DC-3 wing stored in an outside field at NEAM, as well as used images taken by NEAM staff during restoration. Over several visits to NEAM, on November 10th and December 12th, 2022, and January 17th, 2023, the team gathered data on the dimensions of the wing attachment. Camera images were used to determine wing features size in relation to other features, while calipers were used for precise measurements of wing components. The team was also provided pictures of a completed wing in the process of being attached during the restoration of a DC-3 at the museum. This provided a specific understanding of the wing attachment geometry and dimensions, which could then be used to create the model.



Figure 26: Image of a detached DC-3 wing taken by the team onsite



Figure 27: Measuring features using calipers on the detached DC-3 wing.

During review of historical documents of the DC-3 wing the team determined that from the root of the wing to the wing attachment joint it is a NACA 2215 airfoil, with a linear taper from that point on to a NACA 2206 at the tip. The NACA airfoil is a standardized measurement of the shape of an airfoil, the first number represents the camber as a percentage of the chord, the second number is the percentage distance to maximum camber measured in tenths of a chord length, the last two digits describe the maximum thickness as a percentage of chord. This information was used in XFLR5 airfoil analysis software [38] to find the coordinates of the wing root airfoil outline, which is conveniently the same point along the span that the wing attachment joint is at. The data from XFLR5 could then be exported as a point cloud into Autodesk Inventor to complete the 3D modeling. The airfoil outline was then compared to images of the DC-3 wing attachment to determine the internal structure of the wing. Figure 27 shows the leading edge of the detached DC-3 wing which the team used to find dimensions for the wing ribs, stringers, and thicknesses of the different structural components. Figure 28 shows both detached wings during the DC-3 restoration

process, which were used to determine the complete geometry of the wing connection point. This was required as the detached wing the team was able to measure at NEAM was damaged. The resulting 3D model is of a wing section that includes the structure along the complete chord length and a half meter of depth along the span. The distributed nature of the DC-3 wing attachment required the model to include an entire section (or “slice”) of the wing. This was different for the CBY-3 that has four separate attachment points. Having this section of the wing modeled allowed for an analysis of how the wing connection and surrounding structure were affected by the lift and drag forces applied to them during cruise conditions.

Ansys Mechanical only allows for the importing of models in specific file formats, because of this the team had to export the model from Autodesk Inventor to a step file. This allowed for the transfer of the file between Autodesk Inventor and Ansys Mechanical but also resulted in errors occurring in the model geometry during transfer. These errors were serious enough to stop the model from being meshed in Ansys Mechanical. To prevent this the team developed an iterative process of importing the model into Ansys Mechanical, identifying any error prone areas in Ansys Mechanical, then returning to Autodesk Inventor to correct the geometry in those areas before repeating the process. Through this process the team identified multiple areas with high likelihood of failure and corrected the geometry iteratively. Eventually the model was successfully exported into Ansys Mechanical without any errors, and this is what was the final 3D model.



Figure 28: Image of both DC-3 wings detached during NEAM restoration process. [Personal Communication: email C. Cruff to J. Blandino, 1/16/23]

3.3.4 DC-3 Assumptions

Due to the unique geometry of the DC-3 wing attachment the team decided that the most effective method of modeling would be to complete it as a single part. This decision was made since very few of the components that make up the wing assembly are flat so they can be mated tangential to each other. The level of precision required to make the required number of curved faces would be both too time consuming and computationally involved. A consequence of this

assumption is that the forces acting on the wing section are transferred uniformly through the structural members instead of concentrating in places where the sheets would be riveted together. This corresponded to a similar assumption made by the team when modeling the CBY-3 wing attachment, that plates of metal, when riveted together could be treated as a single and solid piece. The team determined this was a simplification that could be made without compromising the results of the analysis due to the focus of the analysis being on the attachment bolt holes and not the overall structure.

Due to the number of bolt holes, 328 [41], required to hold the wing to the fuselage of the DC-3, the team decided that it would be infeasible to measure the exact position of each along the perimeter of the wing attachment bracket. Instead, the team followed the fact that the bolts were sectioned into groups along the perimeter of the wing attachment with each group having roughly the same distance between all the bolts off the same group. This meant that for each group of bolts along the chord they were distanced from each other a set amount that was measured with calipers from the detached wing at NEAM. This resulted in all 328 bolts being present in the model with an anticipated variance from their actual position of less than a quarter of an inch.

3.4 Ansys Mechanical

3.4.1 Governing Equations, Constraints, and Background of Ansys Mechanical

Ansys Mechanical is a structural analysis software, made available to students by WPI licensing. The team utilized this software tool to complete the structural analysis of the CBY-3 and DC-3 wing attachments. Ansys Mechanical uses finite element analysis (FEA) to analyze how different loading and condition affect complex geometries.

The main governing equation that Ansys Mechanical uses is given by Equation (3) where the variables are defined in Table 7.

$$[M]\{a\} + [C]\{v\} + [K]\{u\} = \{f(t)\} \quad (3)$$

Table 7: Variables for General Form of Ansys Mechanical Governing Equation

Value	Variable	Units
Mass	M	kg
Acceleration	a	kg/m ²
Damping	C	~
Velocity	v	~
Stiffness	K	kg/m
Displacement	u	
Load	$F(t)$	N

The form of this equation implemented is adjusted based on the type of analysis that is being conducted. The three most general types of analysis are: static, modal, and dynamic. Static analysis is used to evaluate stress and deflection of parts subject to loads that are applied when the parts are not in motion and the governing equation simplifies to

$$[K]\{u\} = \{f(t)\} \quad (4)$$

A static structural analysis was carried out on the wing attachment of both aircraft, using Ansys Mechanical. The process of how this analysis will be conducted is described in methodology Section 3.4.2.

In order to perform stress analysis in Ansys Mechanical, constraints on the system being modeled are defined in the program. Constraints in Ansys Mechanical are characteristics of the problem such as where an object is being held fixed to prevent rigid body motion. They also can be defined as forces acting upon the object in question. Fixed supports will hold selected bodies in place within the 3D space and is utilized to lower the degrees of freedom of the assembly. The location of the fixed support application is crucial for structural analysis as it can dramatically affect results. However, the user must be careful to not over constrain the model. Over constraint occurs when the object is held so fixed that there is no room for motion whatsoever, and that can lead to errors that do not allow for a solution. Examples of where a model would be over-constrained are when adjacent or touching edges are both fixed and thus causing contradictory instructions for the program's method [9]. The constraint used for this analysis is described in Section 3.4.2 for the CBY-3 Loadmaster wing attachment and Section 3.4.5 for the DC-3 wing attachment.

The parameter calculated in this analysis that was used to compare the two wing attachments was the von-Mises stress. The von-Mises stress maps for each type of wing showed how the loads were dispersed along the wing attachment structure. The von-Mises stress indicates if a material, typically a metal, will yield or fracture under a given loading. The von-Mises stress equation is derived from Hooke's Law and converts the strain tensor calculated from Hooke's law into a scalar value that can then be compared against the material's yield and ultimate tensile stress. Hooke's law and the definition of the von-Mises stress are given in Equations (5) and (6) respectively.

$$\epsilon_{ij} = \frac{(1 + \nu)\sigma_{ij} - \nu\delta_{ij}\sigma_{kk}}{E} \quad (5)$$

Table 8: Variables for Hooke's Law

Value	Variable	Units
Strain Tensor	ϵ_{ij}	~
Poisson's Ratio	ν	~
Stress Tensor	σ_{ij}	Pa
Identity Matrix	δ_{ij}	~
Principle Stress	σ_{kk}	Pa
Young's Modulus	E	Pa

$$\sigma_v = \sqrt{\frac{1}{2}[(\sigma_{11} - \sigma_{22})^2 + (\sigma_{22} - \sigma_{33})^2 + (\sigma_{33} - \sigma_{11})^2]} \quad (6)$$

Table 9: Variables for von-Mises Stress Equation

Value	Variable(s)	Units
von-Mises Stress	σ_v	Pa
Principle Stresses	$\sigma_{11}, \sigma_{22}, \sigma_{33}$	Pa
Off-Axis Stresses	$\sigma_{12}, \sigma_{23}, \sigma_{13}$	Pa

3.4.2 CBY-3 Wing Attachment: Problem Description

The CBY-3 utilizes a four-bracket wing attachment that allows the wing to be easily installed and removed. While this provides convenience for manufacturer and maintenance personnel, the true structural integrity of this wing attachment is not known. To investigate one aspect of the wing's structural integrity a FEA of the CBY-3 wing attachment was conducted in Ansys Mechanical. This allowed areas of stress concentration to be identified and compared with the material limits.

3.4.3 CBY-3 Methodology and Approach

The aircraft was analyzed using a static structural analysis assuming flight condition loading for simplification. The team first approached the problem by attempting to use loads applied to the four individual brackets, found in a 1945 report on the wing's hinge fittings located during our visit to NEAM on November 11, 2022 [26]. After further investigation of the loads listed in this report, it was concluded that the loads were calculated under some critical or extreme condition due to the magnitudes reported, which did not correspond to a cruising condition. For example, a single component of a force on a single bracket was listed as 116,650 lbf in magnitude! In addition, to apply the loads at the locations indicated in the report, the fixed support would have not been on the bracket and fuselage side, but rather on the outer edge of the wing attachment. The team agreed that if it used the load values and points of application shown in the report, they would be solving for a stress distribution in areas other than the brackets that were not the main area of interest. The loads from the archival report are shown in Figure 29 [26].

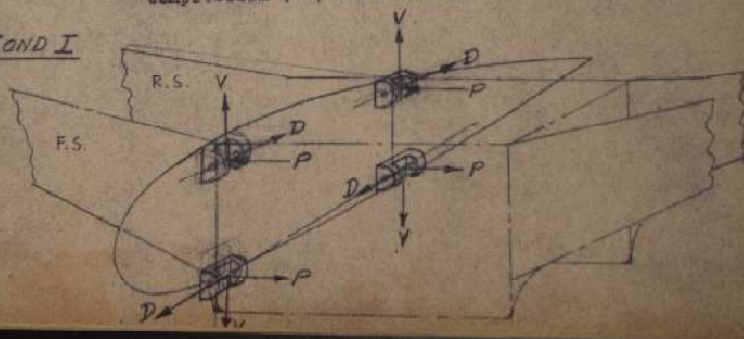
TABLE 1

LOADS ON HINGE FITTINGS

CONL	Item	Load	F (side)	V (vertical)	D (drag)
I	a Upper Front	-	115,630	+ 8,900	+ 25,480
	d Lower Front	+	115,910	- 14,280	- 25,320
	b Upper Rear	-	173,770	+ 590	+ 14,930
	c Lower Rear	+	222,730	- 28,250	- 19,130
II	a Upper Front	+	21,420	- 1,630	- 4,680
	d Lower Front	-	47,560	+ 5,860	+ 10,390
	b Upper Rear	+	43,820	- 140	- 3,770
	c Lower Rear	-	70,460	+ 8,940	+ 5,050

- NOTES: 1) Figures are taken from Table 50, page 149 of ER 3-1004 for critical conditions I and II. Signs of V and D are reversed.
- 2) Sign convention:
Tension + ; up + ; aft + .
- 3) All loads include a fitting factor of 1.20
- 4) Tension (+) is inboard
Compression (-) is outboard.

COND I



MICHAEL GREGOR & ASSOCIATES

Figure 29: Loads on Hinge Fittings from Approach 1[26]

The second approach to this problem was to apply the wing's lift and drag, corresponding to a specific flight condition, to the respective faces of the attachment and to fix the inner faces of the bracket holes in the 3D space. This would simulate the modelled wing attachment being fixed to the fuselage (assumed stationary in inertial space). The forces acting on the wing in cruise condition were then applied to respective faces on the wing attachment. The team worked in partnership with another student team who had completed a full aerodynamic analysis on the CBY-3 [23], thereby providing a set of lift and drag data that could be used in the present analysis.

The analyses simulated a stationary fuselage with the section of the wing attachment that is modeled free to move. To run the simulation, the team imported the solid model we generated into Ansys Mechanical, then assigned specific materials to the different components in the model. The brackets were assigned to be structural steel. All components, besides the brackets themselves, were assigned as an aluminum alloy (Personal communication, Email from Doug Davis to John Blandino, March 2, 2023). In Figure 30, the components with a material assignment of structural steel are shown highlighted in red.

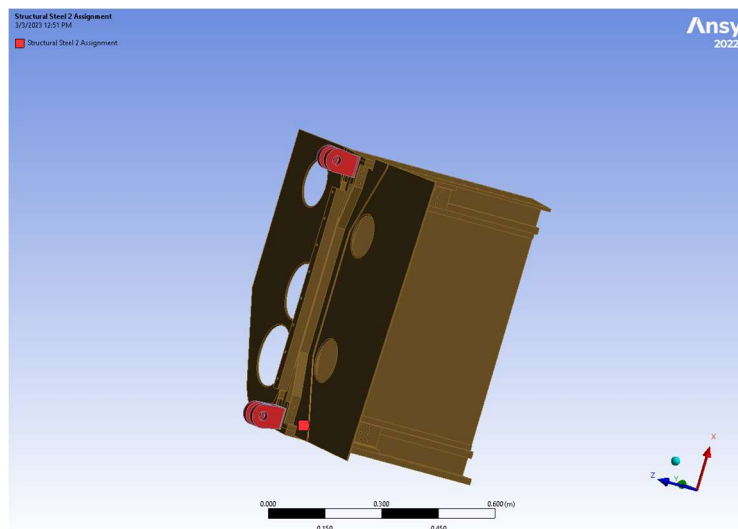


Figure 30: Trailing Edge Bracket Pair Material Assignment – Structural Steel View 1

Figures 31 and 32 show the components from the trailing edge bracket that have been given a material assignment of aluminum alloy highlighted in red.

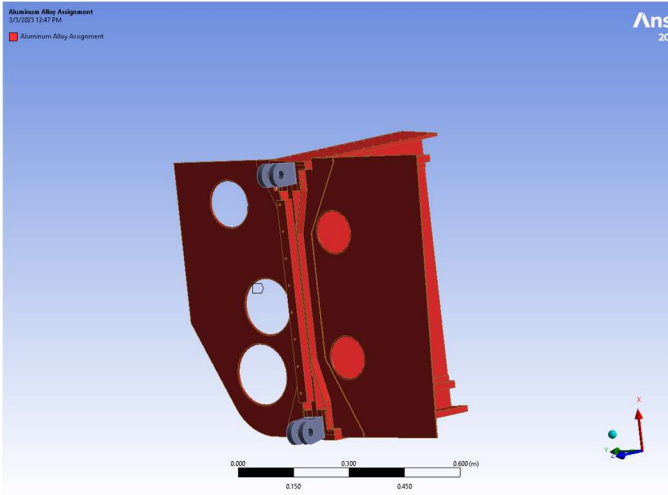


Figure 31: Trailing Edge Bracket Pair Material Assignment – Aluminum Alloy View 1

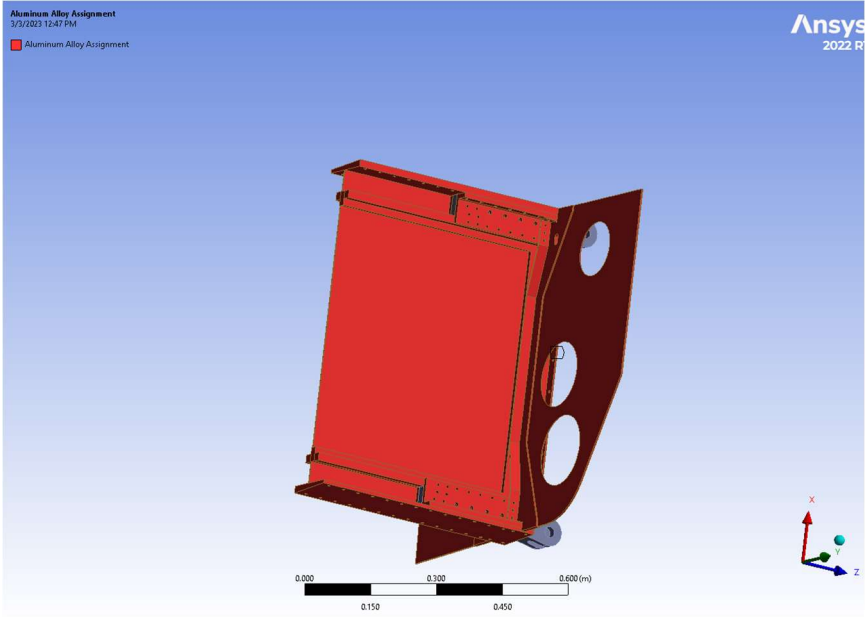


Figure 32: Trailing Edge Bracket Pair Material Assignment – Aluminum Alloy View 2

Once the geometry was imported and assigned material specifications, a mesh is generated to split the model up into small domains over which the governing equations are solved as part of the analysis. The mesh was sized with a minimum dimension of 67.248 mm, so that it would capture the intricacies of the assembly without being too small for Ansys Mechanical to handle. After the mesh is generated, the surfaces corresponding to fixed supports are identified, and the loads are applied. The CBY-3 was fixed at the bolt holes in each of the four brackets. These are shown in Figures 33-36 highlighted in purple. These constraints simulate the wing being attached to the fuselage at those four brackets. In real life, there is a bolt going through each of the holes.

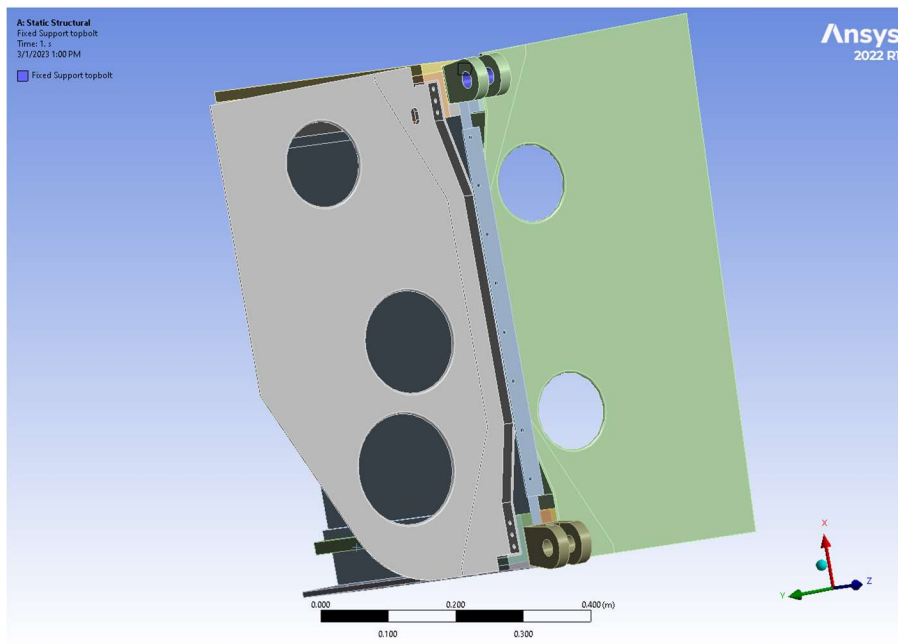


Figure 33: Trailing Edge Bracket Pair Fixed Supports (in purple) on Upper Bracket

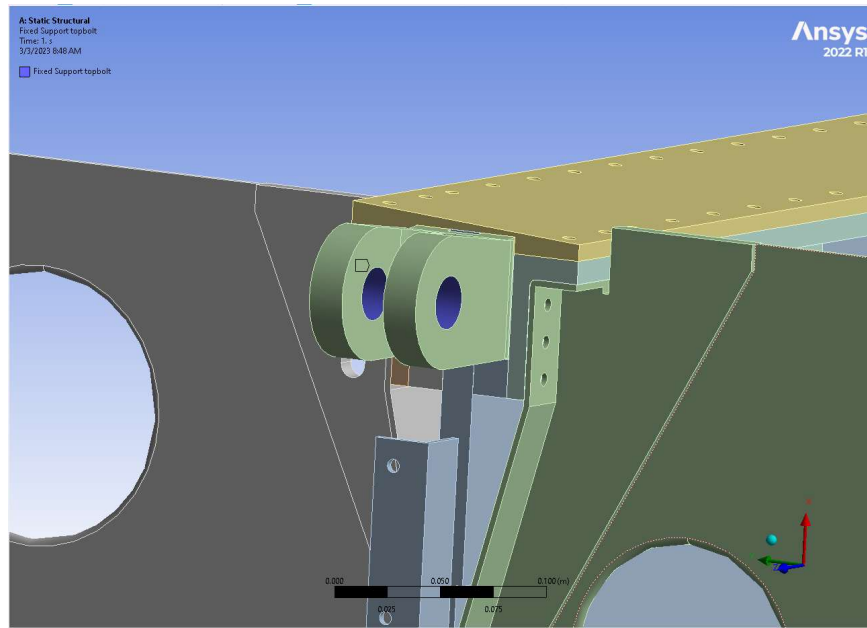


Figure 34: Trailing Edge Bracket Pair Fixed Supports (in purple) on Upper Bracket Close Up

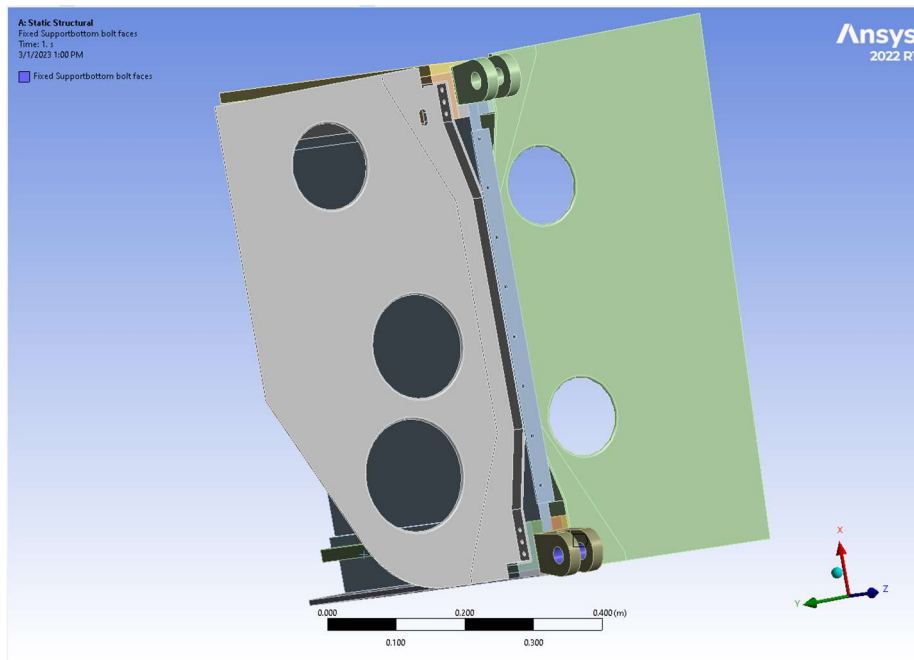


Figure 35: Trailing Edge Bracket Pair Fixed Supports (in purple) on Lower Bracket

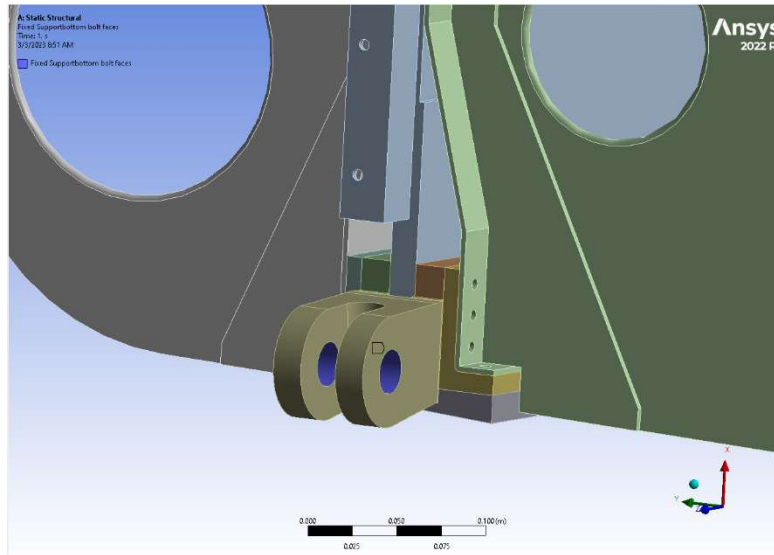


Figure 36: Trailing Edge Bracket Pair Fixed Supports (in purple) on Lower Bracket Close Up

The forces were then applied to faces of the solid model to simulate the motion of the wing relative to a stationary fuselage. The direction of the lift force is shown in Figure 37 as a red arrow, with the face that the force was applied to, highlighted in red. The face that is selected was chosen to be the point of contact for lift since it directly experiences it on the skin of the wing. Similarly, the drag force was applied to the immediately impacted on the skin of the aircraft. The drag force is applied in the direction of the red arrow and distributed over the highlighted faces in red as shown in Figure 38.

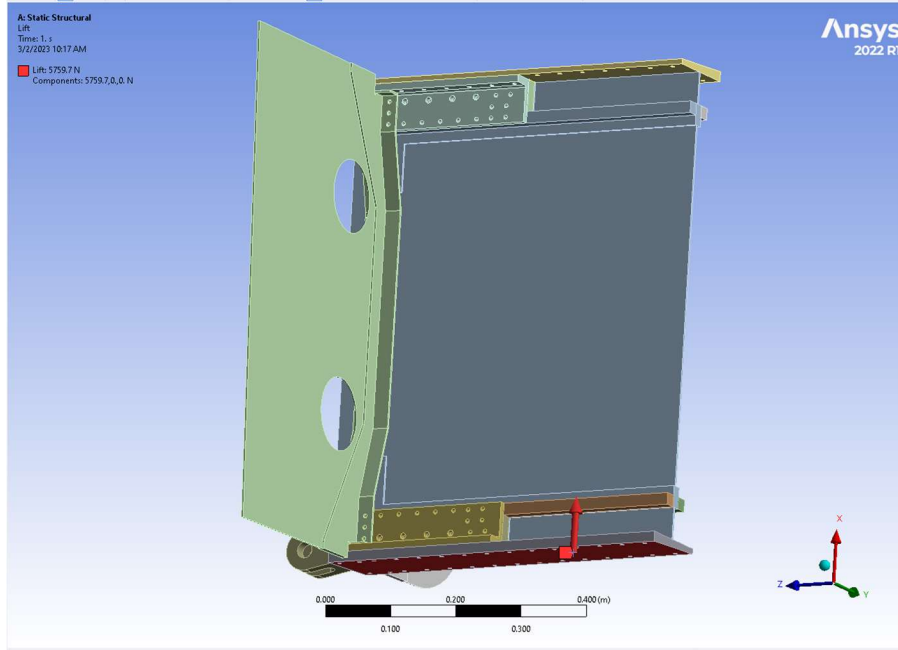


Figure 37: Trailing Edge Bracket Pair Lift Force Distribution shown in red and with a directional red arrow.

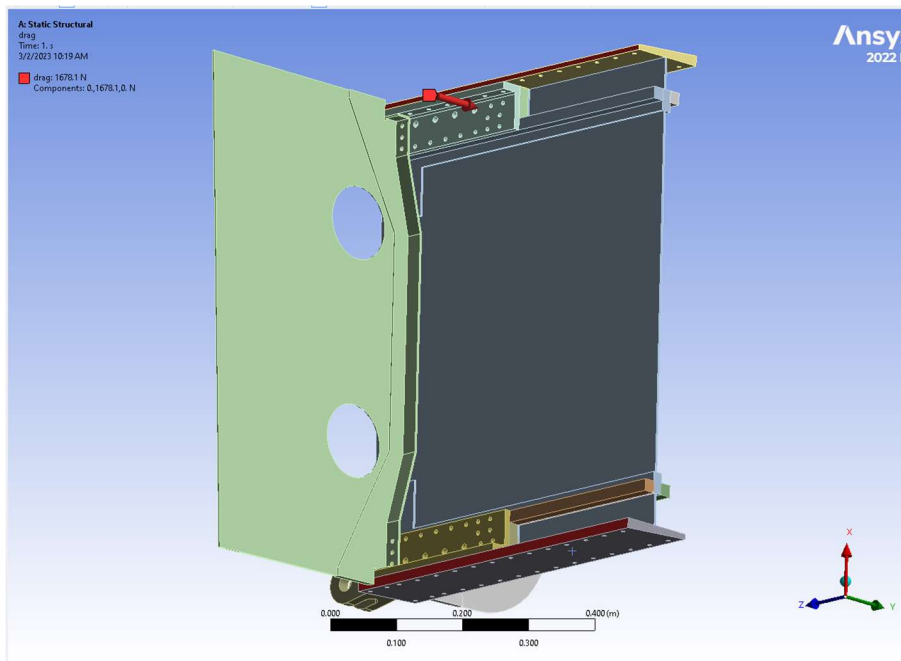


Figure 38: Trailing Edge Bracket Pair Drag Force Distribution shown in red, with a directional red arrow.

The lift and drag force values were obtained from a previous MQP project [23] that identified the coefficients of lift and drag in cruise conditions, as mentioned above. The team assumed that the lift and drag forces were equally distributed between the front and rear bracket pairs. The team determined the lift force per wing from Ref. 23 to be 5.76 kN, and the drag force per wing to be 1.68 kN at sea level [23]. These lift and drag values were calculated per wing by the partner student team at an angle of attack of 2.5 degrees, and the forces used are for one wing. These values correspond to the steady state cruising conditions of the aircraft with a cruising speed of 193 mph at sea level.

Ansys Mechanical was then instructed to solve for total equivalent stress (Von-Mises) to see how the loads were distributed among the four brackets. The same methodology was applied to the front bracket pair as for the rear bracket pair just described. The material assignment constrained (fixed) surfaces, and surfaces over which lift and drag forces are applied for the front bracket pairs are shown in Figures 39-45.

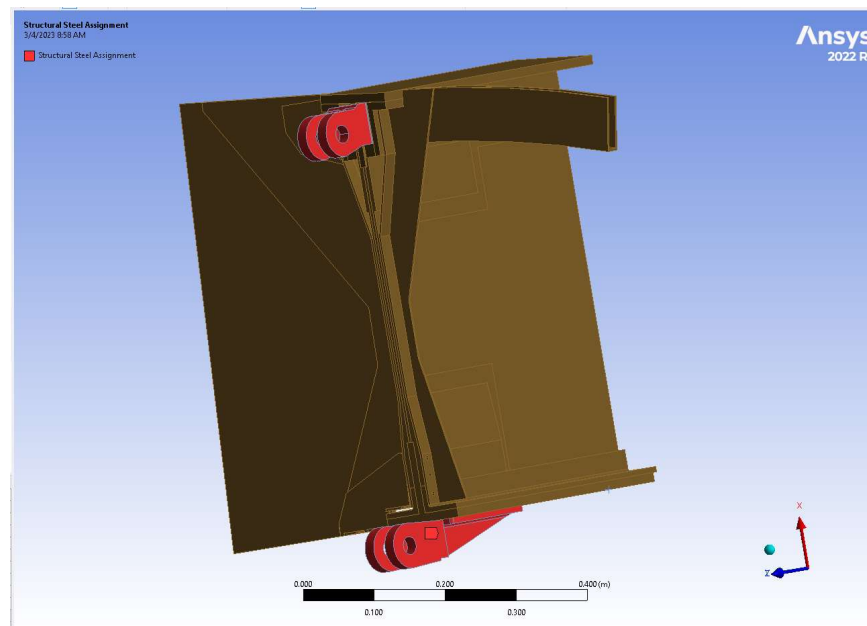


Figure 39: Leading Edge Bracket Pair Material Assignment – Structural Steel View 1 highlighted in red.

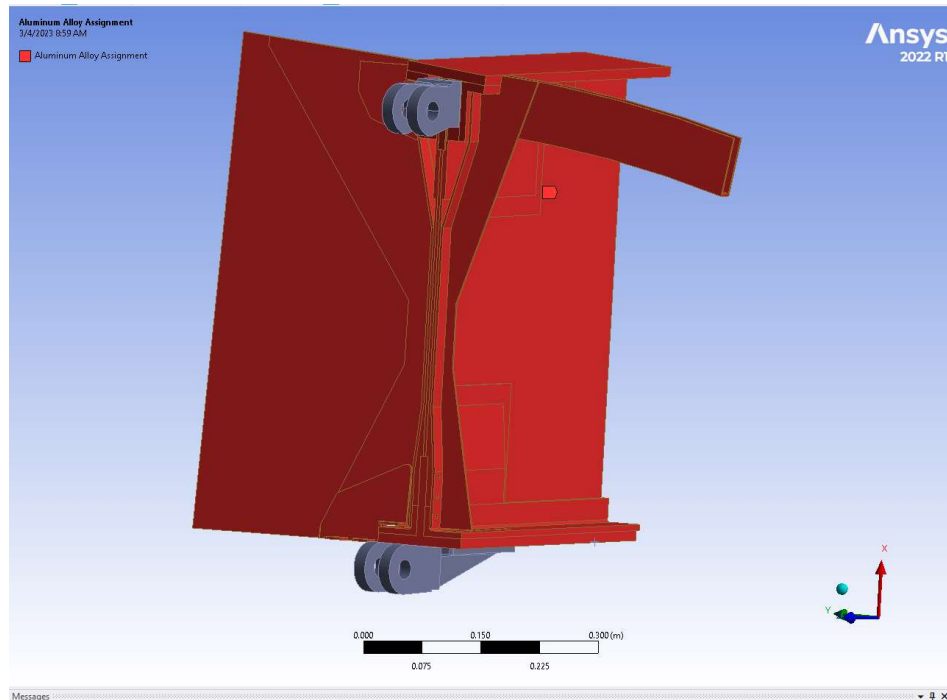


Figure 40: Leading Edge Bracket Pair Material Assignment – Aluminum Alloy View 1 highlighted in red.

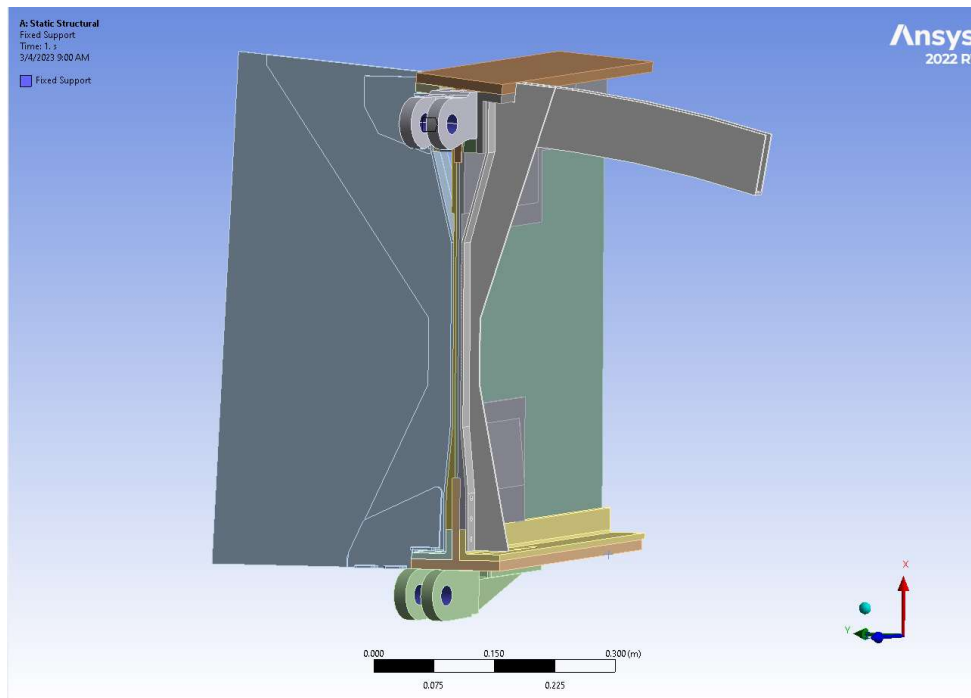


Figure 41: Leading Edge Bracket Pair Fixed Supports highlighted in purple.

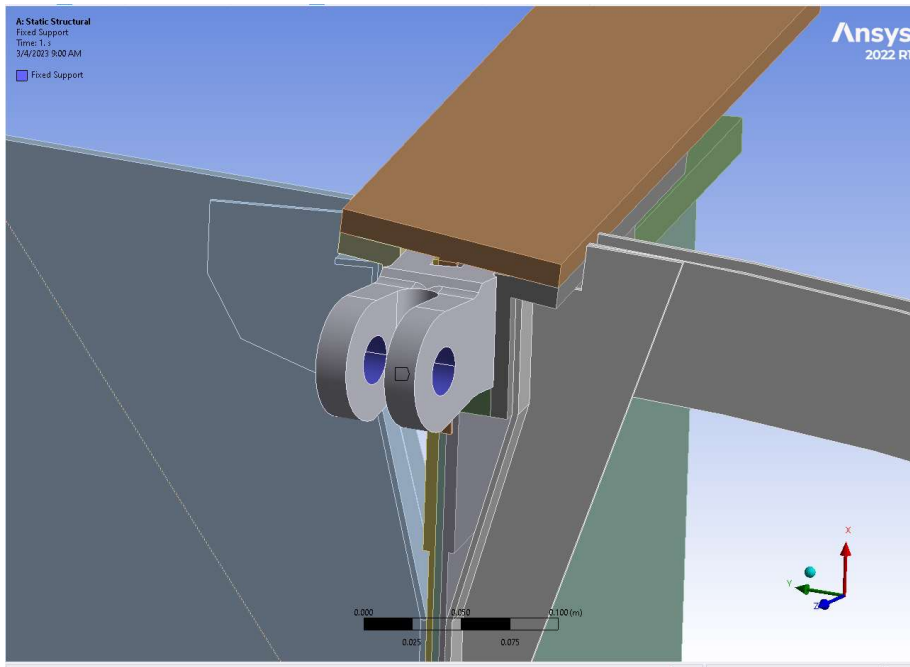


Figure 42: Leading Edge Bracket Pair Fixed Supports on Upper Bracket highlighted in purple.

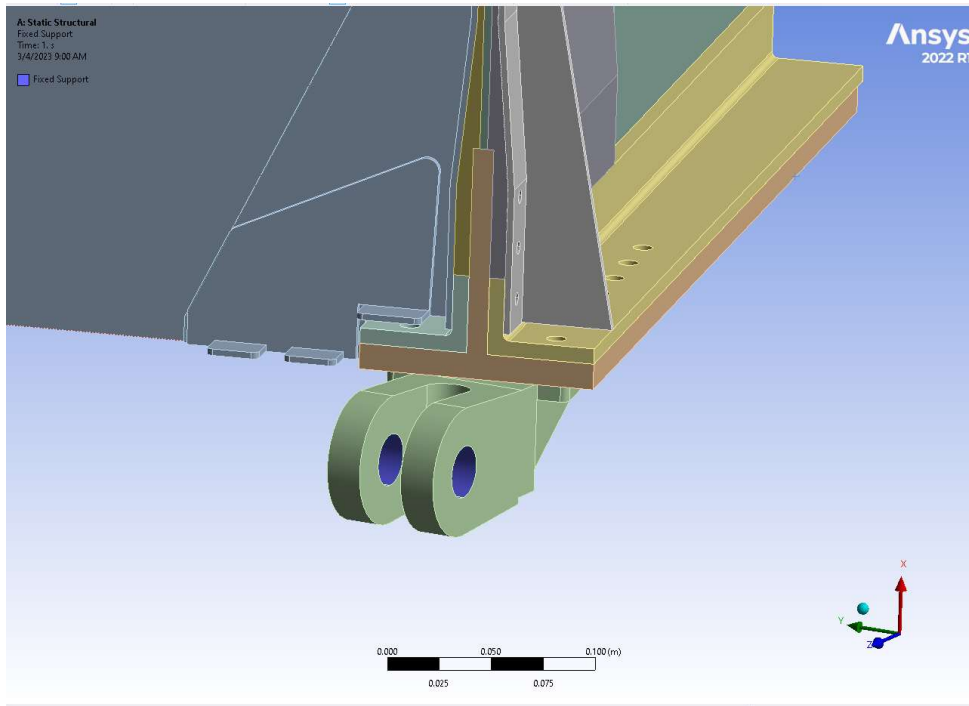


Figure 43: Leading Edge Bracket Pair Fixed Supports on Lower Bracket highlighted in purple.

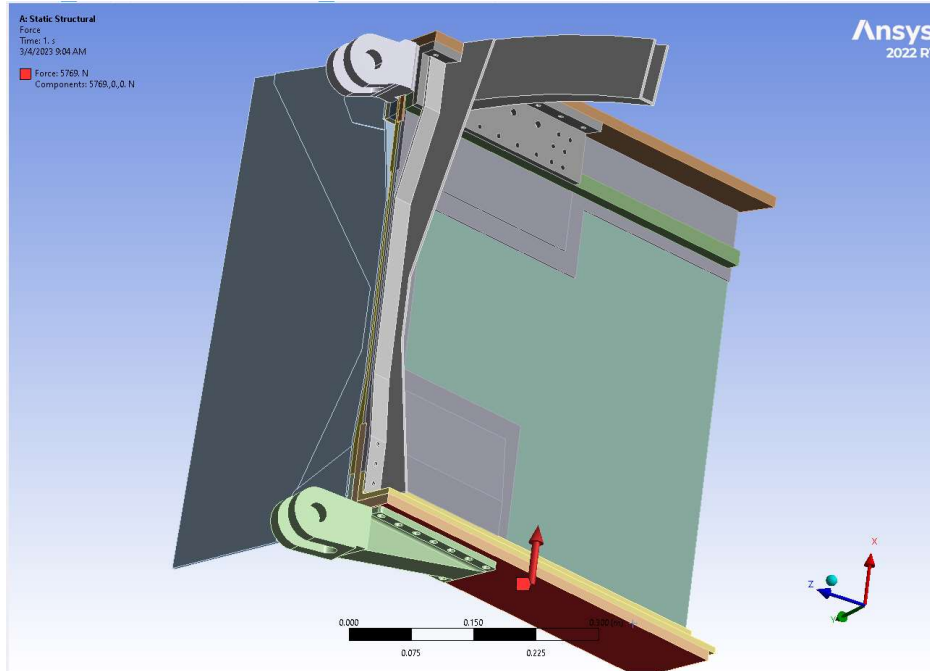


Figure 44: Leading Edge Bracket Pair Lift Force Distribution highlighted in red and direction shown with a red arrow.

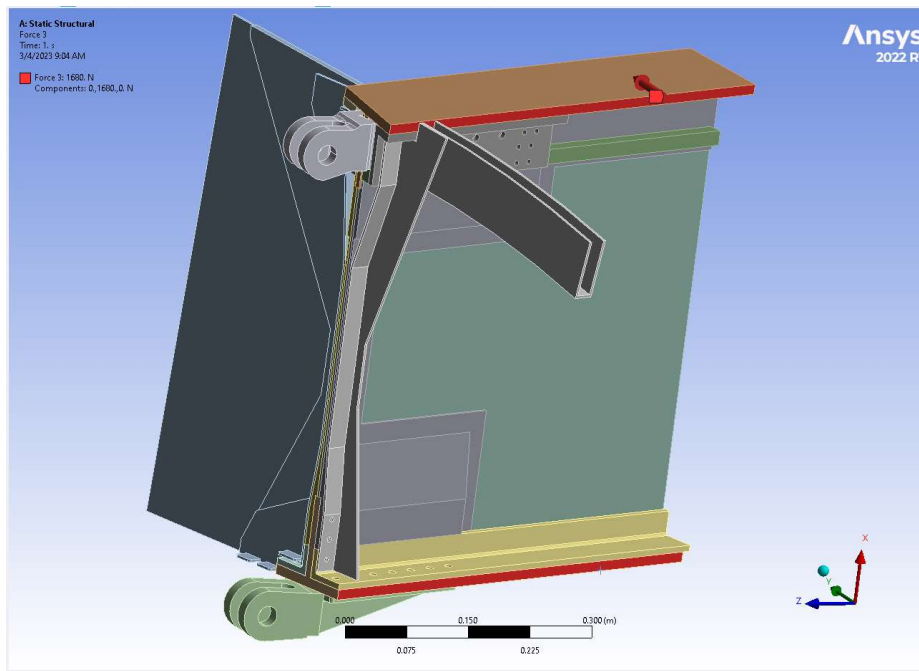


Figure 45: Leading Edge Bracket Pair Drag Force Distribution highlighted in red and direction shown with a red arrow.

3.4.4 DC-3 Wing Attachment: Problem Description

The DC-3 wing attachment is achieved by an arrangement of 328 bolts around the outer edge of the airfoil. The wing and fuselage come together at a flange connected by the bolts to create a seam around the circumference of the airfoil. These bolts carry all of the load on the wing, and keep the wing attached to the fuselage during flight. In order to determine the effectiveness of this attachment in distributing the load of the wing, along with the attachment's structural integrity, a FEA of the DC-3 wing attachment was conducted in Ansys Mechanical. This allowed areas of stress concentration to be identified and compared with the material limits.

3.4.5 DC-3 Methodology and Approach

The DC-3 wing attachment was analyzed using a static structural analysis tool in Ansys Mechanical. The team decided that the most effective method of analysis was to model and analyze both the wing attachment point and a surrounding section of wing to accurately model effects of applied loads on both the attachment and surrounding structure. The team agreed that, to simplify the problem, only the equivalent cruising condition lift and drag forces on the wing would be considered. The team initially thought that portion of the model closer to the wing tip should be fixed, and that the forces should be applied to the attachment face (i.e., closest to the fuselage) itself, however the opposite was eventually used. This is because most of the force on the wing would be acting on the rest of the wingspan, rather than directly on the wing attachment. Additionally, we identified the bolt holes along the flange face as constrained (fixed) surfaces in order to determine the stress concentration and deformation along the wing attachment face. This approach mirrors that used for the CBY-3 analysis. Figure 46 shows the bolt holes that were constrained highlighted in blue.

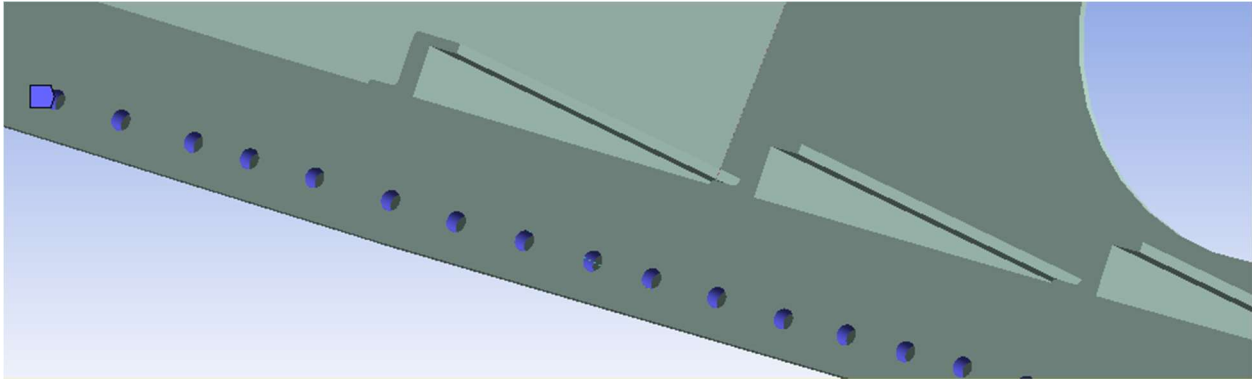


Figure 46: Highlighted Constrained Bolt Surfaces of the DC-3 (in blue)

The lift and drag forces on the wing of a DC-3 at cruise conditions and a 2.5-degree angle of attack were found from analysis presented in the MQP report from the same student team that calculated the CBY-3 flight loads [23]. Their paper yielded lift and drag values of 77434.24 N and 4621.51 N respectively for each wing corresponding to flight at 207 mph and at sea level [23]. Because the 3D model consisted of only a half meter span section of a wing that has an overall wingspan of 10.75 meters, the lift and drag values were split into two parts, one part that would represent the forces generated by the 10.25 meter section not modelled, and the other the forces on the half meter section that was modeled. The component of the lift and drag that would act on the section of the wing modeled were applied to the undersurface and leading edge of the wing skin respectively. This is displayed in Figures 47 and 48. The arrows show the direction in which the lift and drag force are applied and the surfaces over which the loads are distributed are highlighted in red.

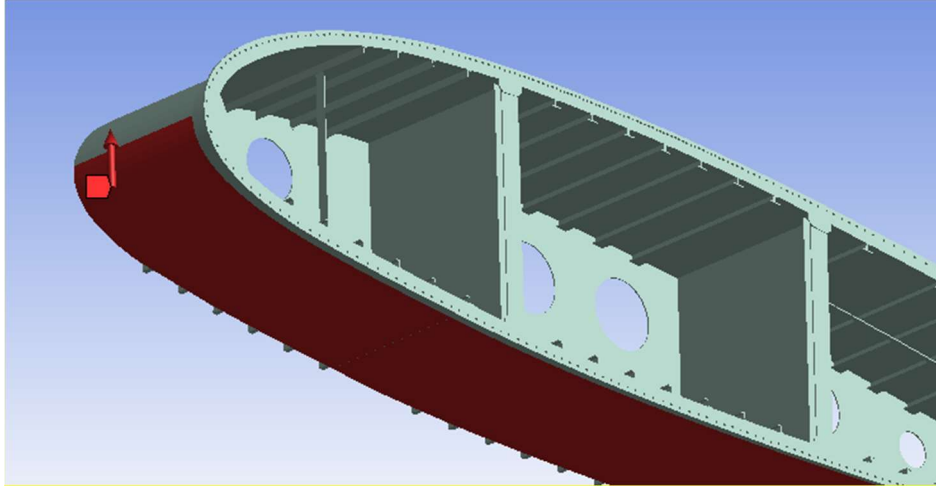


Figure 47: Lift force applied to underside of the modeled portion of the wing (shown in red)

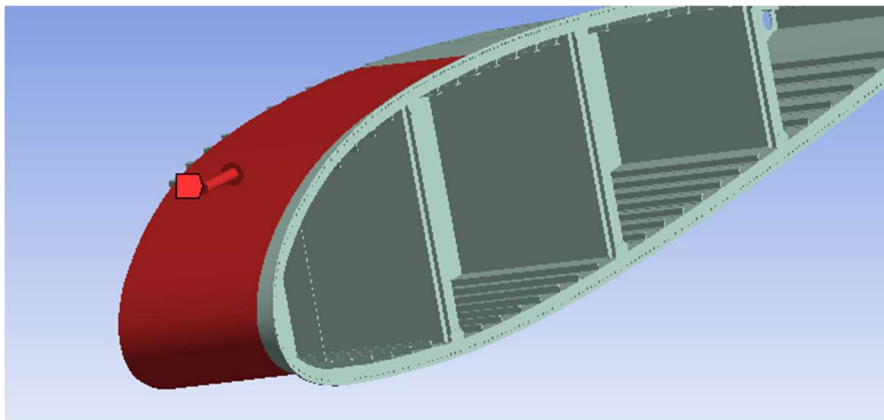


Figure 48: Drag force applied to leading edge of wing model (shown in red)

The component of lift and drag produced by the rest of the wing was applied to the stringers of the 3D model as these were the structural members intended to carry this load from the rest of the wing to the wing attachment point. This meant that the lift and drag were applied to the same face on these stringers as two separate directional components. This is shown in Figure 49.

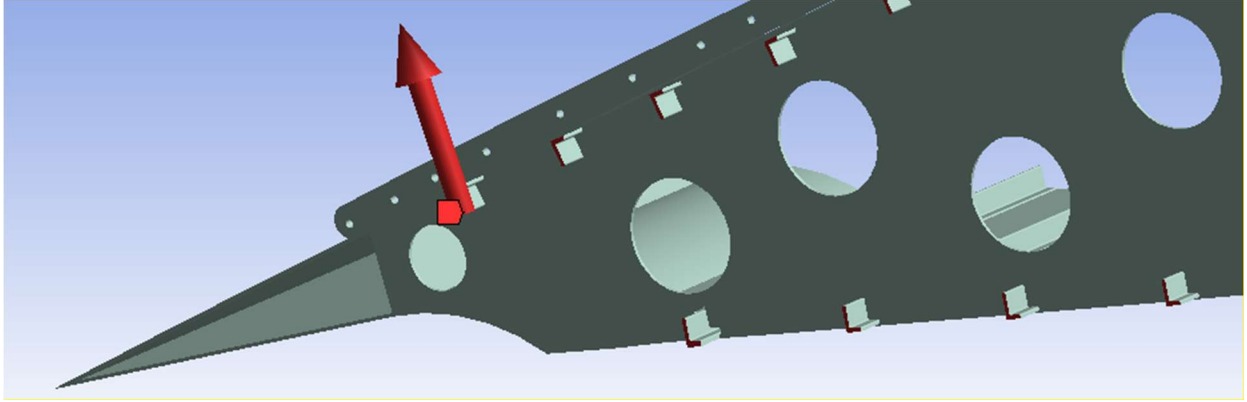


Figure 49: Combined Lift and Drag applied to wing stringers

From historical documentation [13] the material of the attachment and all surrounding structure was identified as aluminum alloy with uniform properties. The team chose to use the aluminum alloy properties built into ANSYS Mechanical. This information was specified in the Ansys Mechanical model and was used to compare the applied loads and resultant stresses to the yield and ultimate strengths of the material. Finally with these materials specified for the model in Ansys Mechanical the team performed a static structural analysis to determine the von-Mises stress and total deformation on the model. These results are presented in Section 4.4.3.

4 Results of Structural Analysis Comparison

4.1 Photographic Documentation Results

With the equations derived in Section 3.1 for the FOV and distance to document necessary to take a “perfectly cropped” (i.e., same aspect ratio as the camera sensor) image, the team was able to create a table with values for the dimensions of the viewing angle given common distances for the camera that was used in the project. The team had access to a Canon Rebel T7 camera through one of the members, with a sensor size of 22.3 by 14.9 mm (APS-C) and a minimum lens

focal length of 18mm. Assuming this sensor, Table 10 lists the document width and height that would fill the sensor frame (in both dimensions) as a function of height above the document. For documents or archival drawings with a different aspect ratio than the camera sensor, the equations from Section 3.1 can be used to calculate the required camera height to make sure the largest dimension can be captured in the image.

Table 10: Document dimensions that fill the camera sensor (same aspect ratio) as a function of distance for the case of a Canon Rebel T7 sensor.

Distance to Document (inches)	Document Width in View (inches)	Document Height in View (inches)
1	14.88	9.36
18	22.32	14.04
24	29.76	18.6
36	44.64	28
42	52.08	32.64

4.2 3D Laser Scanning

While the user interface of the *RevoScan* software was very user friendly, unfortunately generating a scan with the scanner itself was not as simple. There were two main problems that frequently occurred during scanner operation. First, was the stability of the scanner. It is imperative that the operator handles the scanner very gently while a scan is in process. Any sudden bumps or jostles would often cause the scanner to lose focus and lose its place on the object being imaged. This often caused many errors, which resulted in the need for a scan to be repeated multiple times. Moving the scanner at a slow and steady pace resulted in the most complete version of a scan.

Another solution to this problem was to place the object of choice on a revolving turntable, while the scanner remained stationary.

An unexpected problem experienced with the scanner was the effect of colored surfaces on the quality of a scan. When scanning different colored objects, the team found that the scanner experiences difficulties capturing the geometry of dark colored surfaces. One example of this was evident when attempting to create a 3D model of the CBY-3 Loadmaster wind tunnel model and a DC-3 replica model. The DC-3 model was generated in its entirety by the scanner, with all geometries defined, whereas the CBY-3 Loadmaster scan was completely unsuccessful. After further scanning attempts, the team determined that the dark green skin of the CBY-3 Loadmaster model was the cause of the failed scan. The DC-3 scan was successful for two reasons. First, the main color of the model is solid white, allowing the infrared laser light to reflect well. Second, the DC-3 model was much smaller than that of the CBY-3, meaning that there were less errors due to operator handling of the scanner and the improved capability of the scanner to recognize the full geometry of the smaller model. This demonstrated to the team that the scanner has difficulty creating scans of large models that are dark colored. Therefore, no scan of the CBY-3 wind tunnel model was created.



Figure 50: Image of the 3D scan taken of the DC-3 replica model. As can be seen the scanner did not create a full scan of the DC-3 itself and accidentally included geometry from surrounding objects.

After gaining experience with the Revopoint Pop 2 scanner, the team attempted to create a full scan of each wing attachment bracket. Initial success with this process was found because of the bright white surface of each bracket, allowing the scanner to capture its geometry easily. However, there was a problem here because most of the structure comprising each bracket was hidden within the wing itself, meaning that the scanner could not view the entire bracket making a full scan impossible. The team attempted to edit the incomplete scanner generated CAD model, however found no success because of the scan's complex geometry. The faces between the scanner generated and user generated portions of the model could not be edited together. Figure 52 demonstrates the complex geometry generated by the scan of bracket C.



Figure 51: Incomplete scan of bracket C

While the scanner was able to form a solid model based on the incomplete geometry of the bracket, the difficulties described above prevented the creation of a model containing all details of the bracket. For future use of the scanner, it may be beneficial to change the color of dark surfaces before scanning them. One way the team thought to do this would be to dust baby powder or

another similar lightly colored powder onto the object, so that the dark surface becomes more easily visible. This method would allow the user to temporarily change the surface color of an object in a manner that could be easily removed. Another recommendation would be to invest in a large, stable turntable for the object to be placed on to increase the stability of the scanning process.

4.3 CAD Model Generation

4.3.1 CBY-3 Model

The CAD models created for this project are a complex assembly comprised of numerous parts. After their completion, the team created exploded views of each assembly, as well as drawings of each wing attachment bracket so that each bracket's dimensions could be documented. As discussed in Section 3.3.1 complete dimensions were difficult to find from blueprints alone, and even after extensive measurements, assumptions about each bracket still needed to be made. Online drawings and models of these brackets created as a part of this project should serve as a record of each bracket's dimensions for future use.

The drawing created of bracket A is shown in Figure 53. One can see three different views of the bracket and all the dimensions needed to recreate the part in the future. In Figures 54 and 55, exploded views of the “box” like structure surrounding bracket A are shown, as well as the full trailing edge assembly that was used within the Ansys Mechanical analysis. Additional drawings of each bracket and the corresponding exploded views of each assembly can be found in the Appendix.

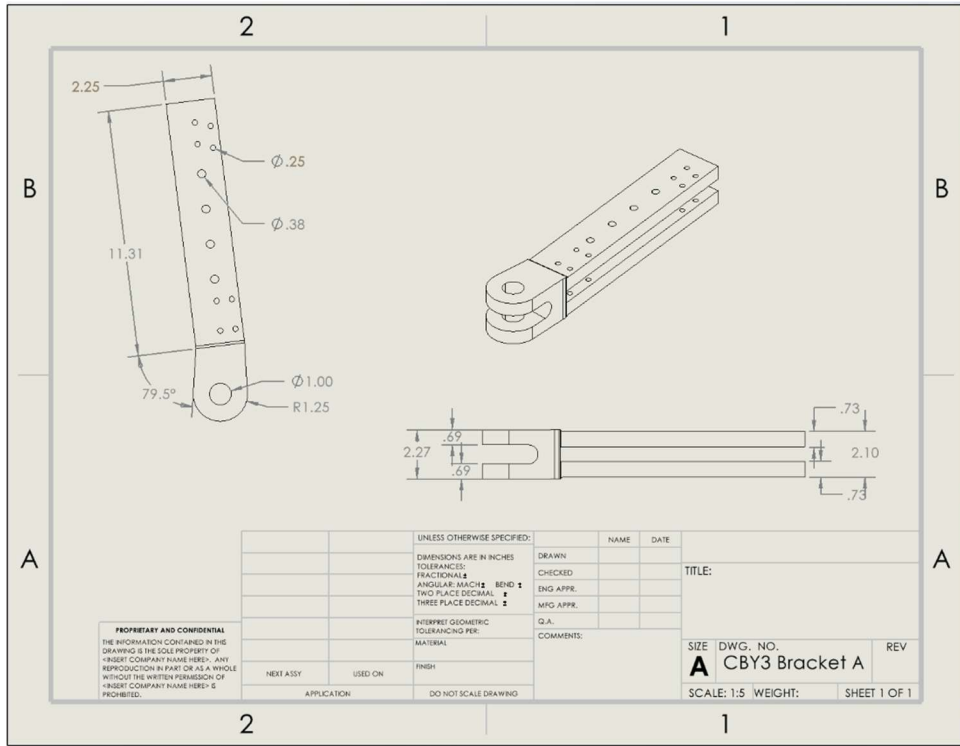


Figure 52: A CAD model drawing of bracket A (lower rear bracket of wing)

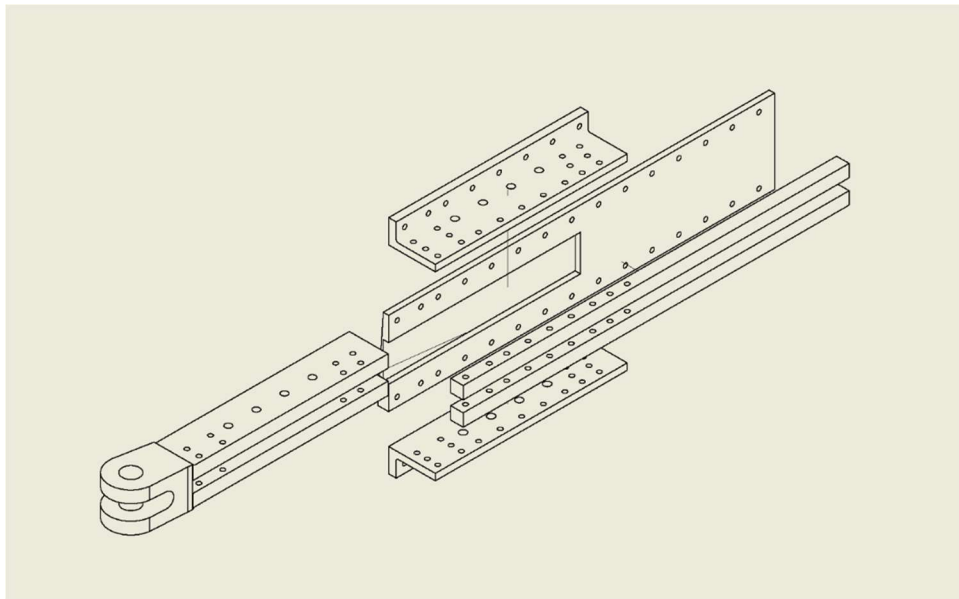


Figure 53: Exploded view of box structure surrounding bracket A

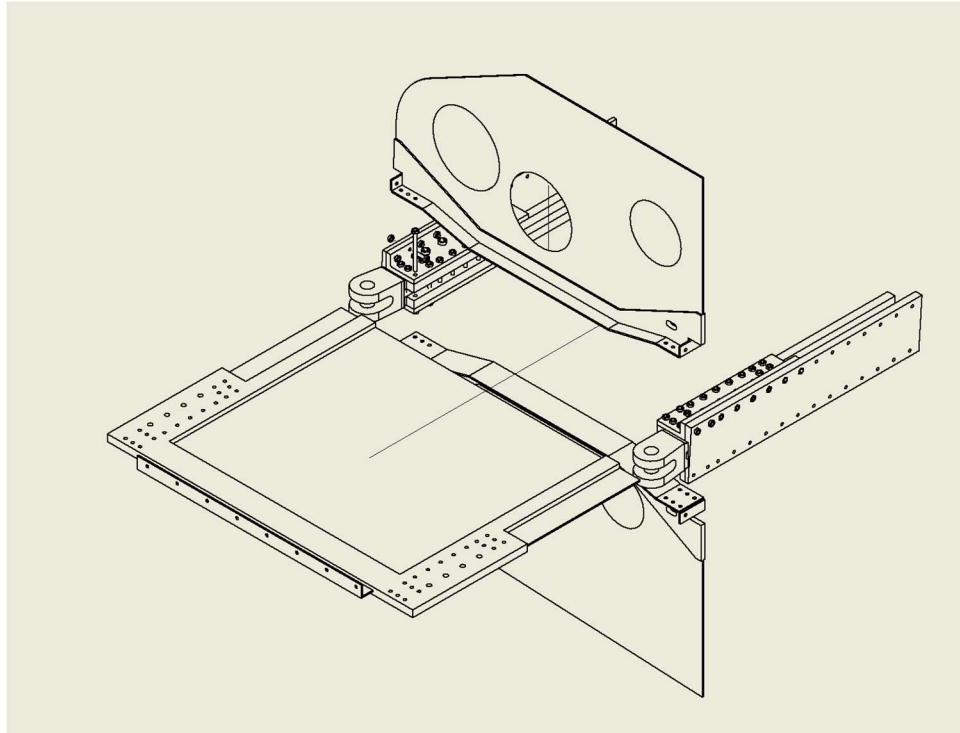


Figure 54: Exploded view of the trailing edge comprised of brackets A and B

4.3.2 DC-3 Model

The CAD model of the DC-3 wing attachment that resulted from the process described in Section 4.3.2 resulted in a single part encompassing the entirety of the wing attachment. This included the wing attachment itself including bolt holes, the wing skin, the ribs, and the stringers that stiffen the internal structure of the wing section. The model included 0.5 meters of the wing's length from the attachment point outward in the direction of the wing tip. Below in Figures 56 through 59. These images show the wing attachment from both the leading edge and trailing edge, as well as the two sides facing the fuselage and the rest of the wing respectively.

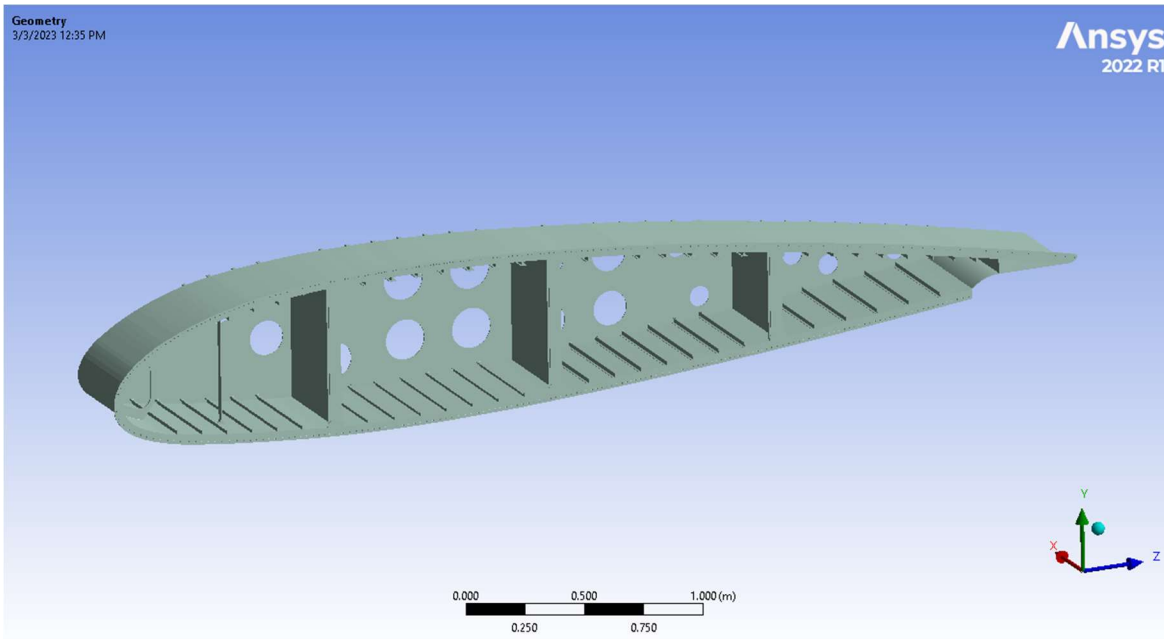


Figure 55: DC-3 wing attachment as seen from the leading-edge fuselage side

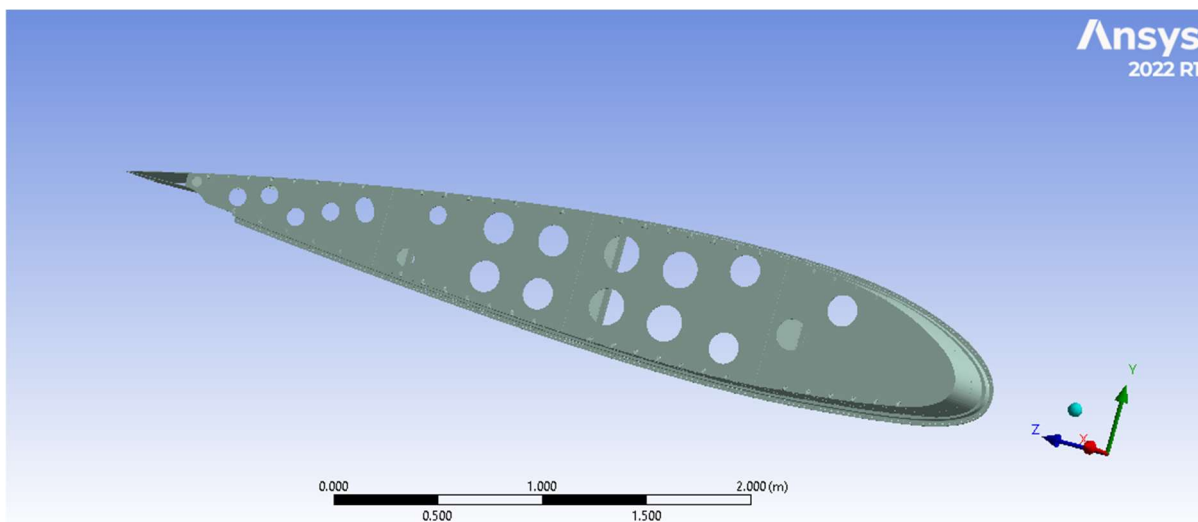


Figure 56: DC-3 wing attachment as seen from the leading-edge wing side

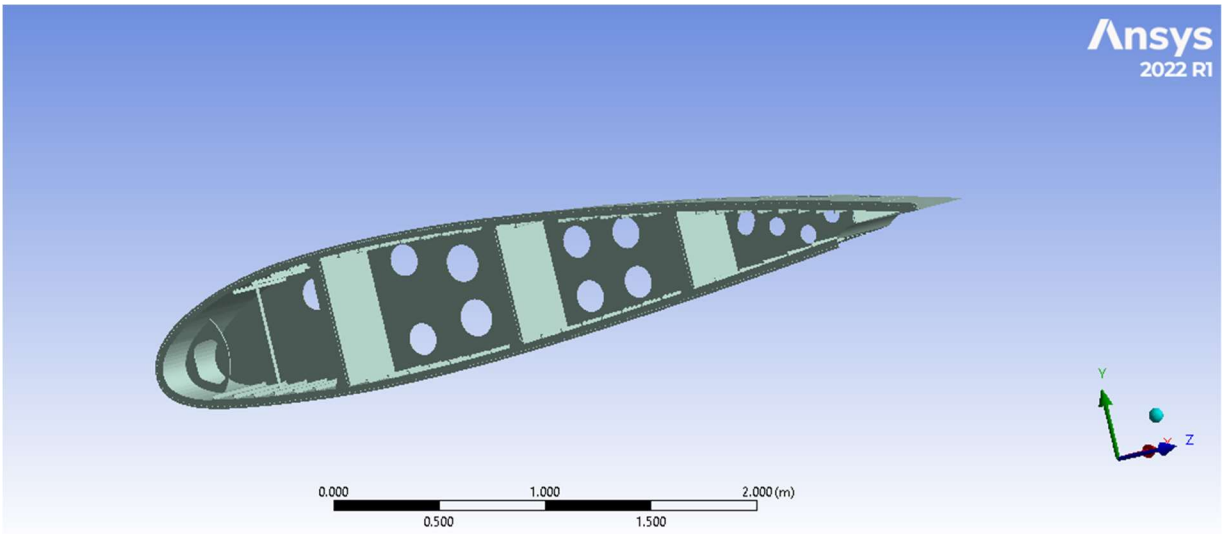


Figure 57: DC-3 wing attachment as seen from the trailing edge fuselage side

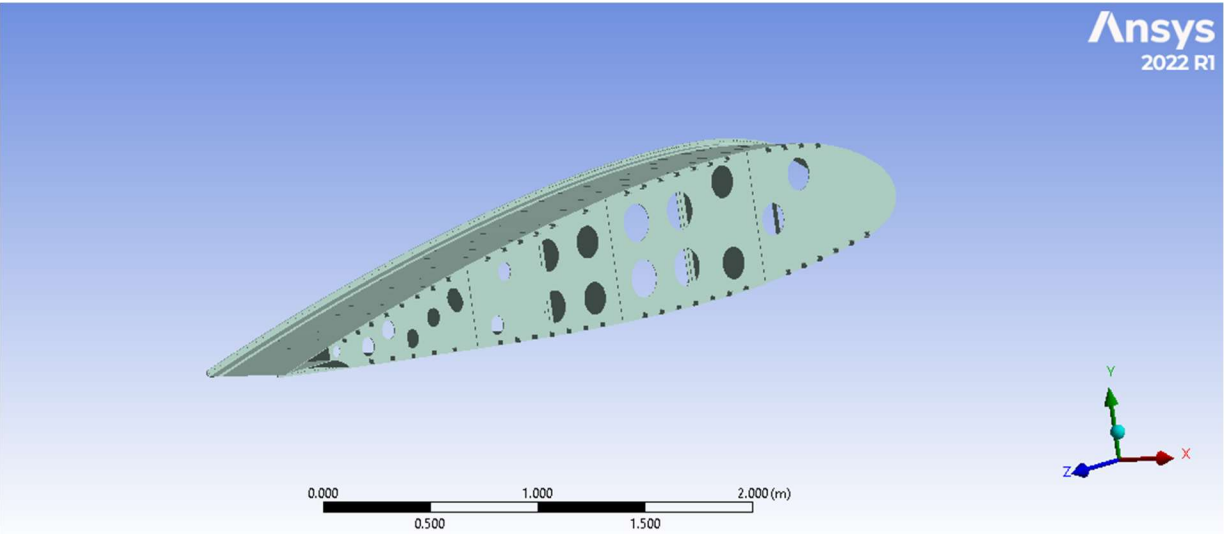


Figure 58: DC-3 wing attachment as seen from the trailing edge wing side

4.4 Ansys Mechanical

4.4.1 CBY-3 Structural Analysis

Ansys Mechanical formulates a stress map by solving the governing equations within the cells defined by the mesh created for the analysis. The team had an option to solve for deformation as well but decided to not utilize this solution because the team was interested in the ultimate tensile strength rather than seeing a distorted model. Results are displayed through color mapping, where the deep blue color identifies minimum stress relative to the overall stresses, and where the warmer and red colors identify stresses close to the maximum stresses in the solution. For the rear brackets, the key in Ansys Mechanical shows an absolute minimum equivalent stress of 1322 Pa, and an absolute maximum of 25.9 MPa.

To present the stress map, each bracket pair was modeled, and its results shown separately. Included are closeup views at points of interest with only the stress mapping, and then again with probe values (i.e. values at specific points identified). Results are presented in this manner to allow the reader to view the full span of the stress map without the probe value tags being in the way. More views of the stress map can be found in Appendix B. Figures 60-68 show the stress map of the trailing edge bracket pair. The maximum stress was located at the red tag in Figure 61 with a corresponding stress value of 26.5 MPa.

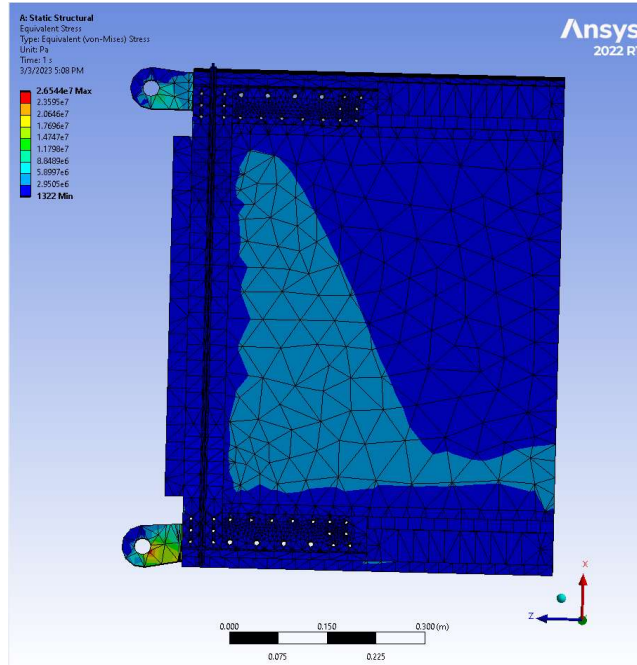


Figure 59: Trailing Edge Bracket Pair Stress Map View 1

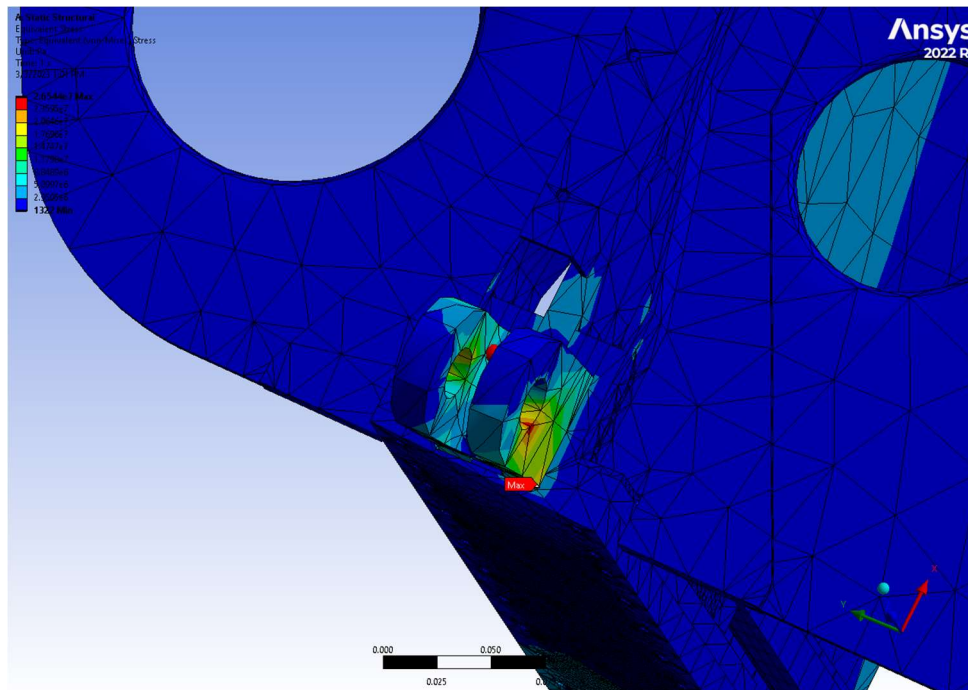


Figure 60: Trailing Edge Bottom Bracket Point of Interest View 1

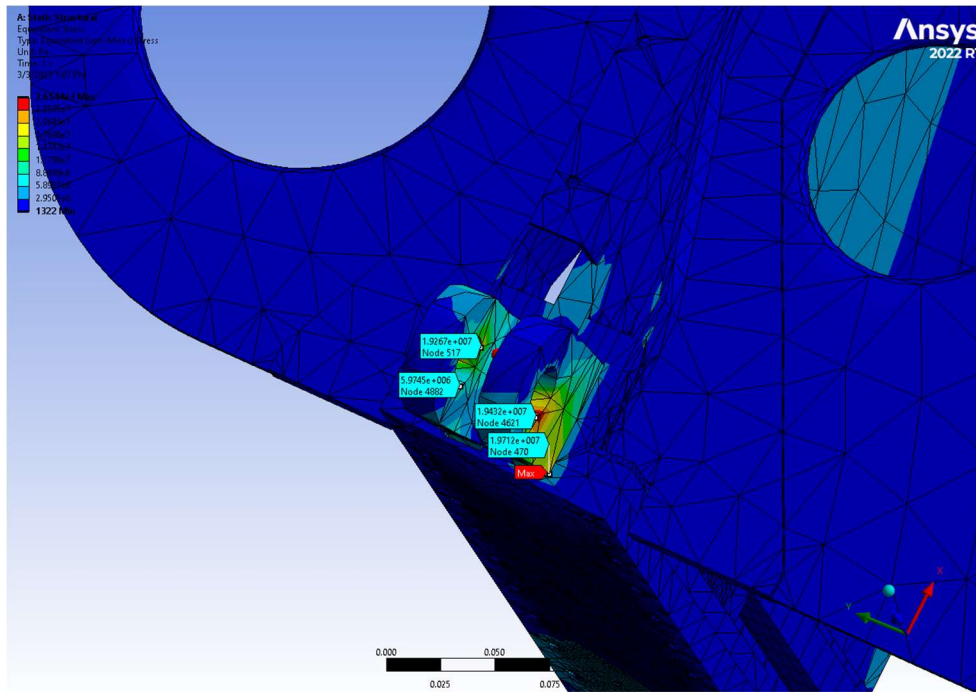


Figure 61: Trailing Edge Bottom Bracket Close Up View 1 with Probe Values

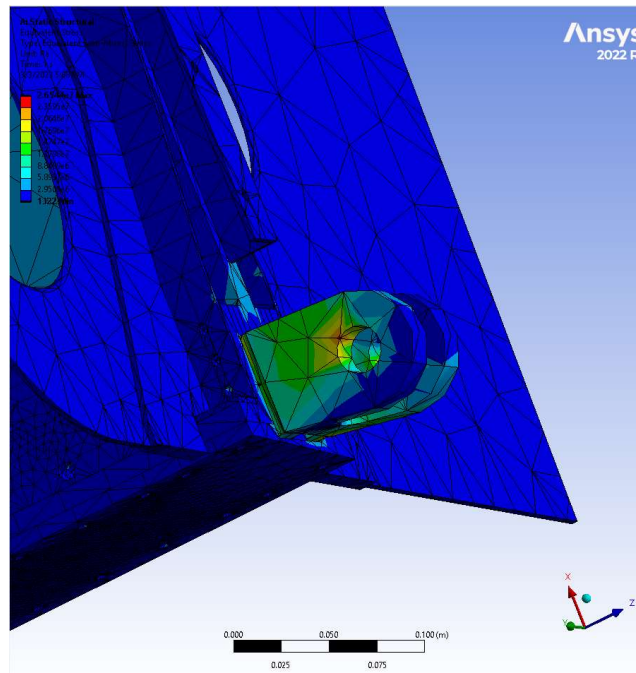


Figure 62: Trailing Edge Bottom Bracket Close Up View 2

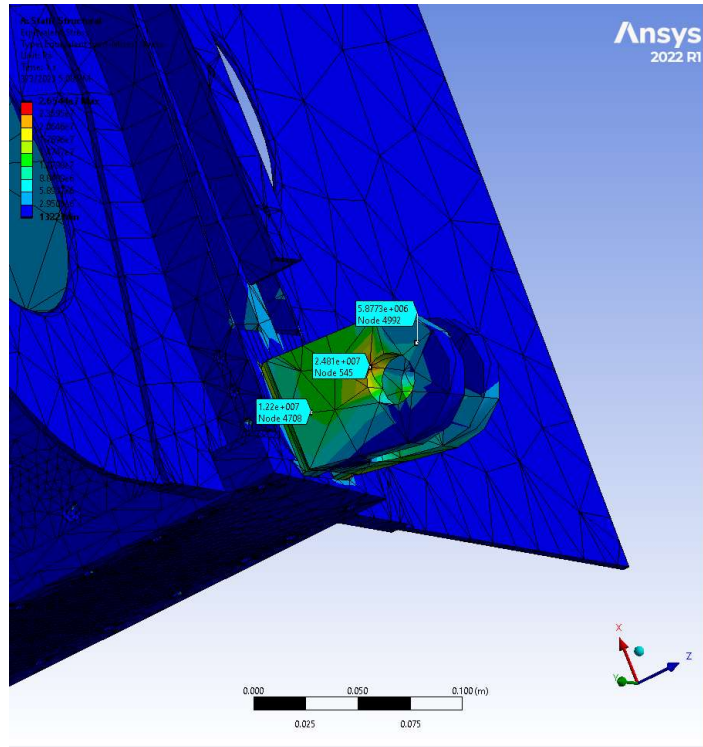


Figure 63: Trailing Edge Bottom Bracket Close Up View 2 with Probe Values

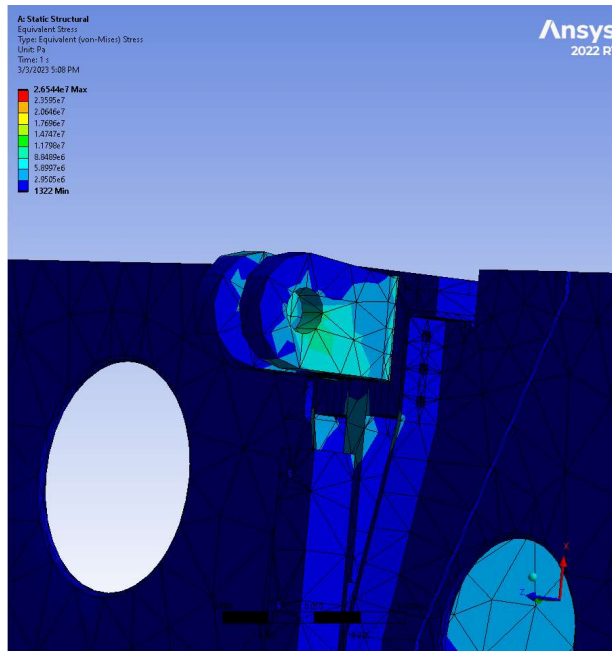


Figure 64: Trailing Edge Upper Bracket Close Up View 1

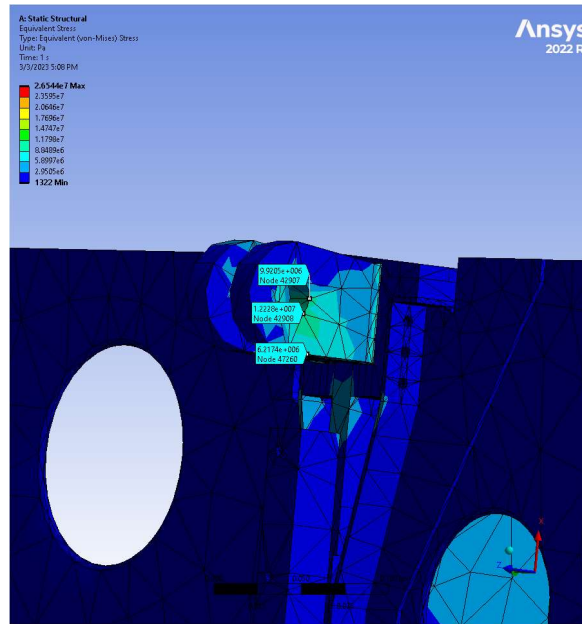


Figure 65: Trailing Edge Upper Bracket Close Up View 1 with Probe Values

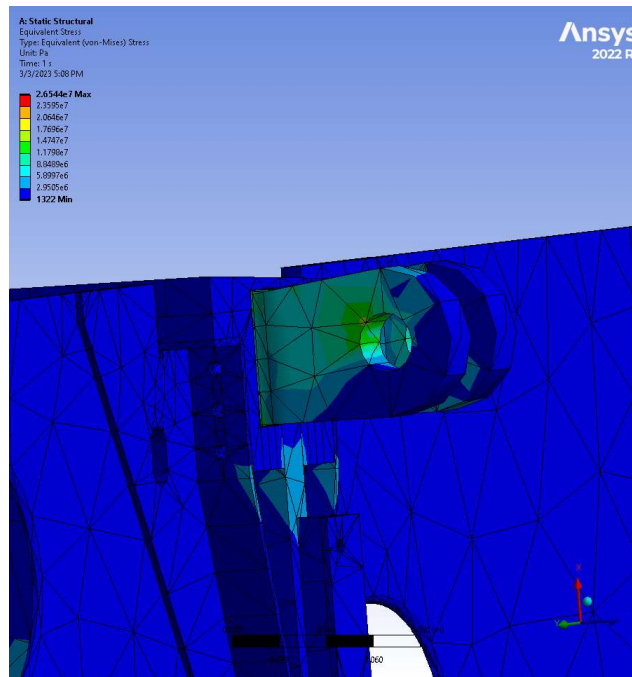


Figure 66: Trailing Edge Upper Bracket Close Up View 2

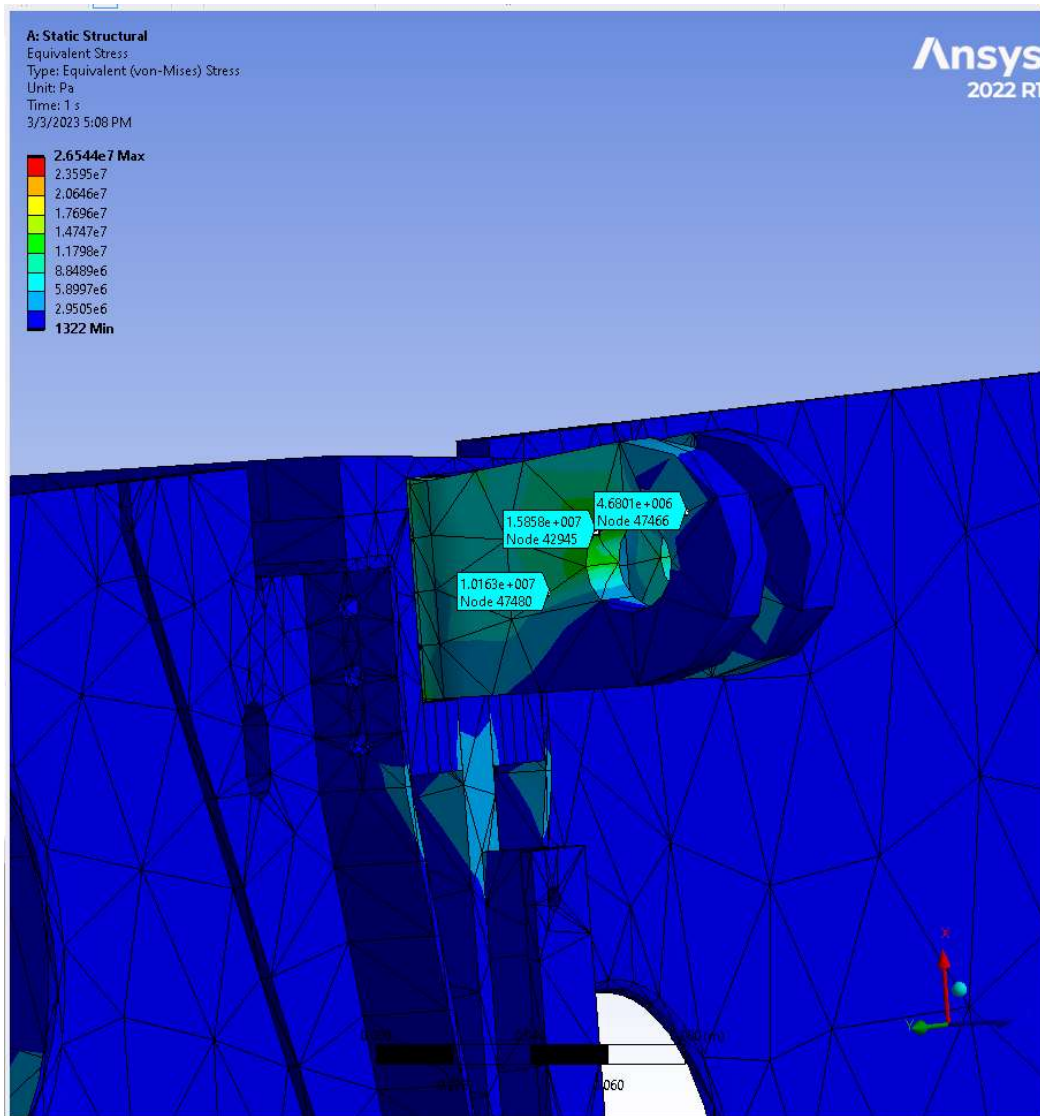


Figure 67: Trailing Edge Upper Bracket Close Up View 2 with Probe Values

Figures 69 and 70 are tables from Ansys Mechanical that show the material properties of the structural steel and aluminum alloy in the rear bracket analysis. From these tables, the team utilized the tensile ultimate strength in our results discussion. These numbers were used in a comparison of the von-mises stress from the simulation.



Structural Steel 2



Fatigue Data at zero mean stress comes from 1998 ASME BPV Code, Section 8, Div 2, Table 5-110.1

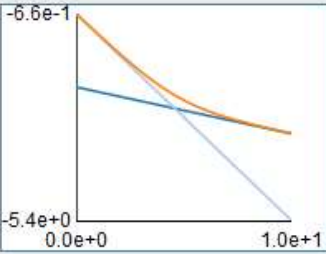
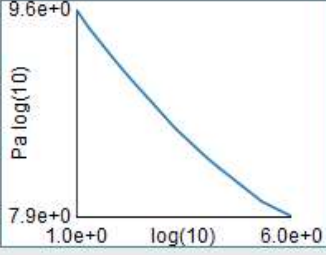
Density	7850 kg/m ³
Structural	
▼ Isotropic Elasticity	
Derive from	Young's Modulus and Poisson's Ratio
Young's Modulus	2e+11 Pa
Poisson's Ratio	0.3
Bulk Modulus	1.6667e+11 Pa
Shear Modulus	7.6923e+10 Pa
Isotropic Secant Coefficient of Thermal Expansion	1.2e-05 1/°C
Compressive Ultimate Strength	0 Pa
Compressive Yield Strength	2.5e+08 Pa
Strain-Life Parameters	
S-N Curve	
Tensile Ultimate Strength	4.6e+08 Pa
Tensile Yield Strength	2.5e+08 Pa

Figure 68: Structural Steel Properties on Trailing Edge Bracket Pair (A and B)



Aluminum Alloy



General aluminum alloy. Fatigue properties come from MIL-HDBK-5H, page 3-277.

Density	2770 kg/m ³
Structural	
▼ Isotropic Elasticity	
Derive from	Young's Modulus and Poisson's Ratio
Young's Modulus	7.1e+10 Pa
Poisson's Ratio	0.33
Bulk Modulus	6.9608e+10 Pa
Shear Modulus	2.6692e+10 Pa
Isotropic Secant Coefficient of Thermal Expansion	2.3e-05 1/°C
Compressive Ultimate Strength	0 Pa
Compressive Yield Strength	2.8e+08 Pa
S-N Curve	
Tensile Ultimate Strength	3.1e+08 Pa
Tensile Yield Strength	2.8e+08 Pa

Figure 69: Aluminum Material Properties on Trailing Edge Bracket Pair (A and B)

Similar to the solutions for the trailing edge pair, the leading-edge bracket pair also was solved to generate a map of equivalent stress, shown in Figures 71-81. More views of the stress map can be found in Appendix B. For the leading-edge bracket pair, the maximum stress was located at a point of the bottom bracket shown with a maximum probe tag, at a value of 51.07 MPa.

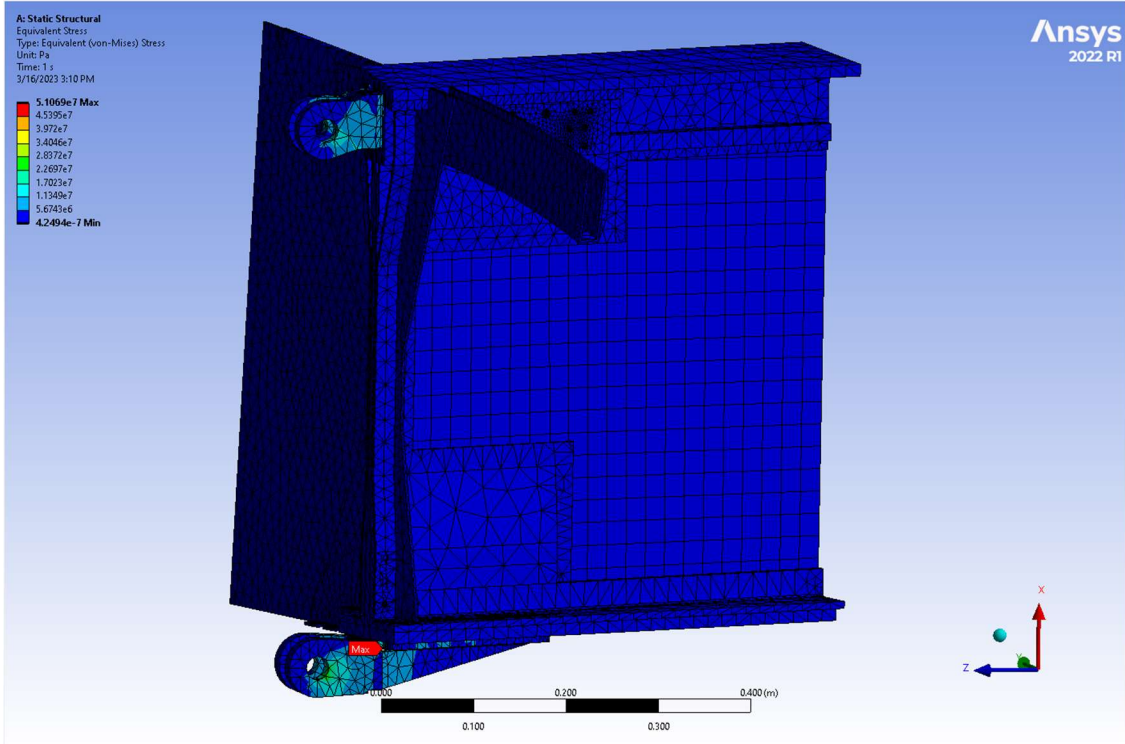


Figure 70: Leading Edge Bracket Pair Stress Map View 1

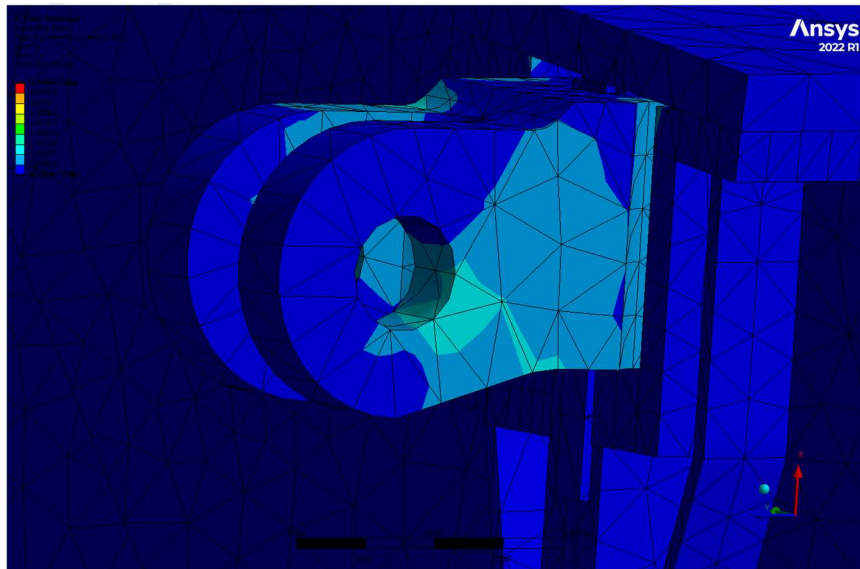


Figure 71: Leading Edge Upper Bracket Close Up View 1

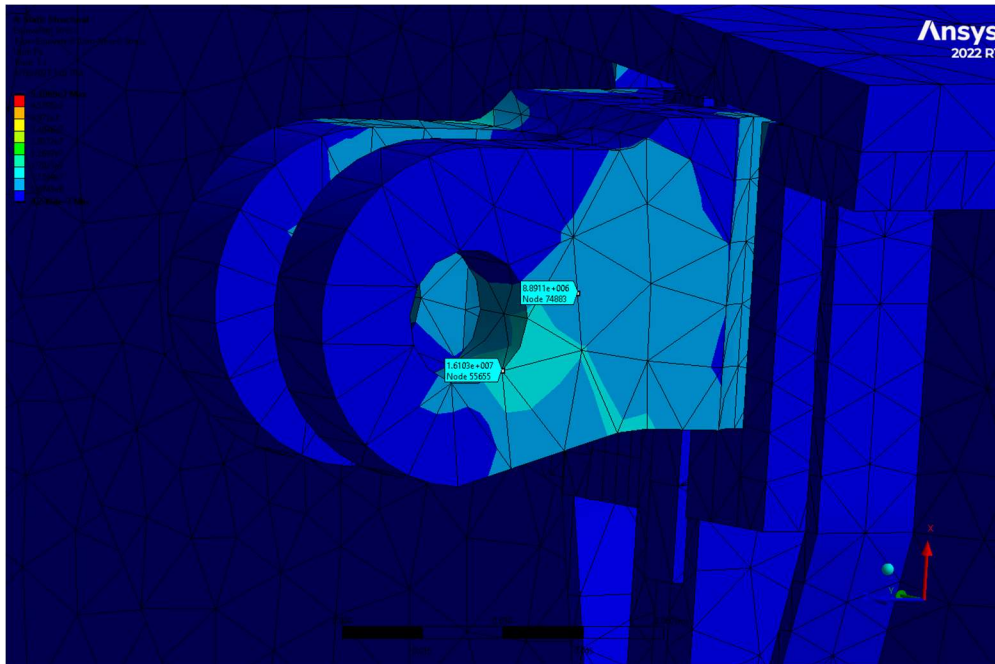


Figure 72: Leading Edge Upper Bracket Close Up View 1 with Probe Values

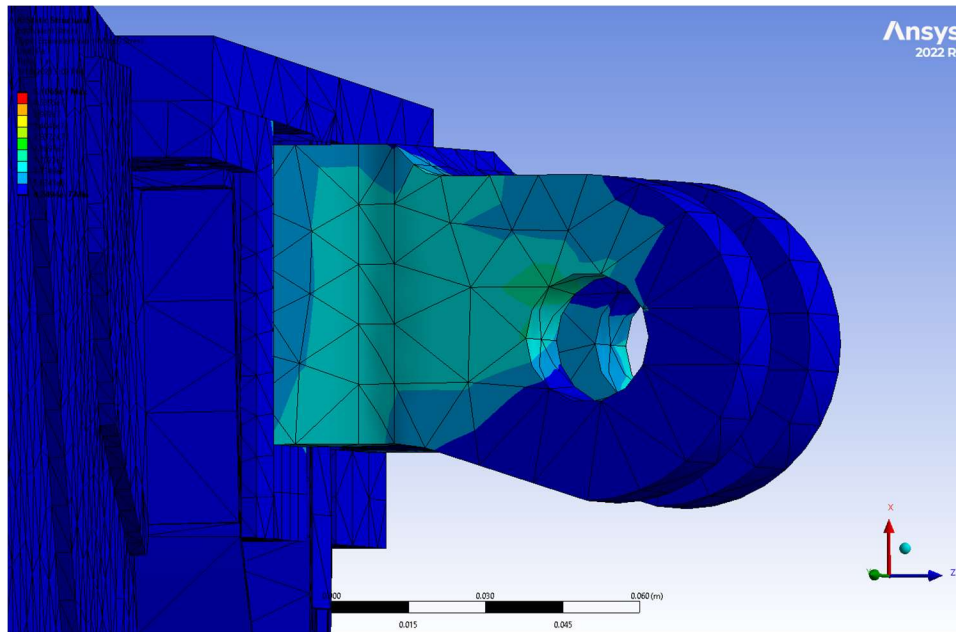


Figure 73: Leading Edge Upper Bracket Close Up View 2

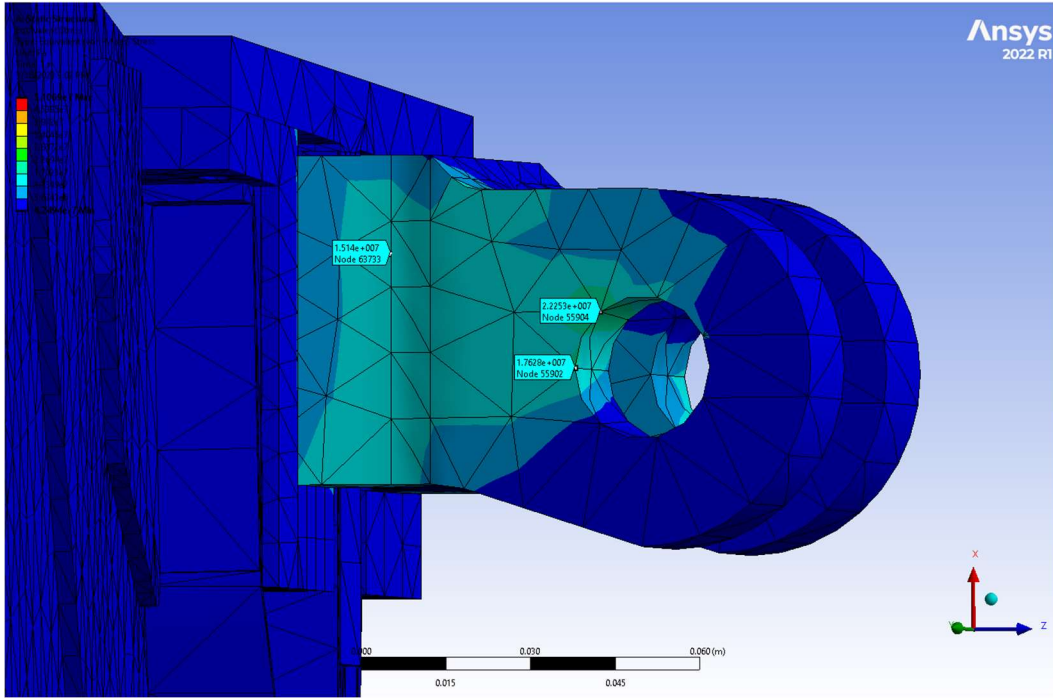


Figure 74: Leading Edge Upper Bracket Close Up View 2 with Probe Values

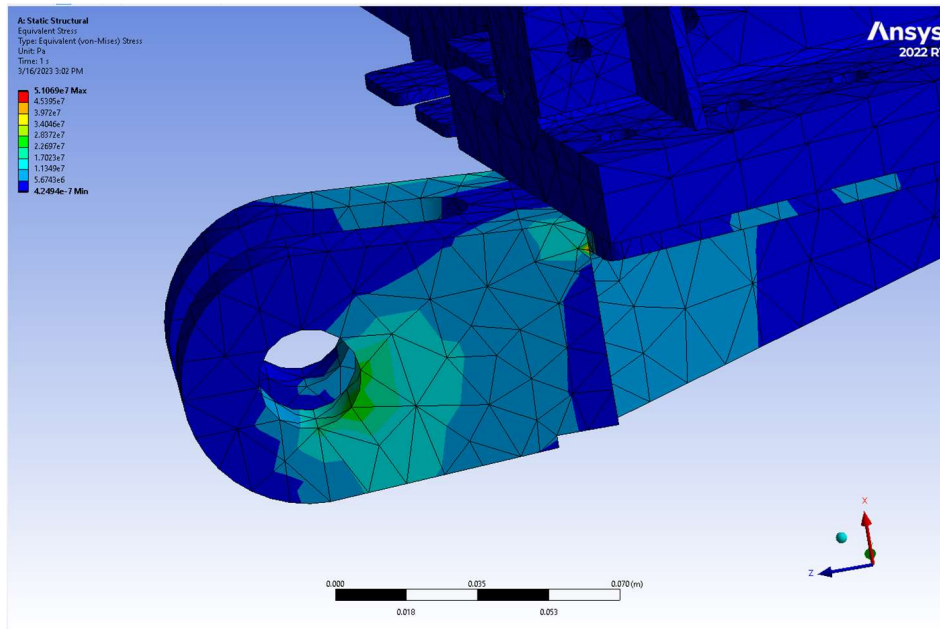


Figure 75: Leading Edge Bottom Bracket Close Up View 1

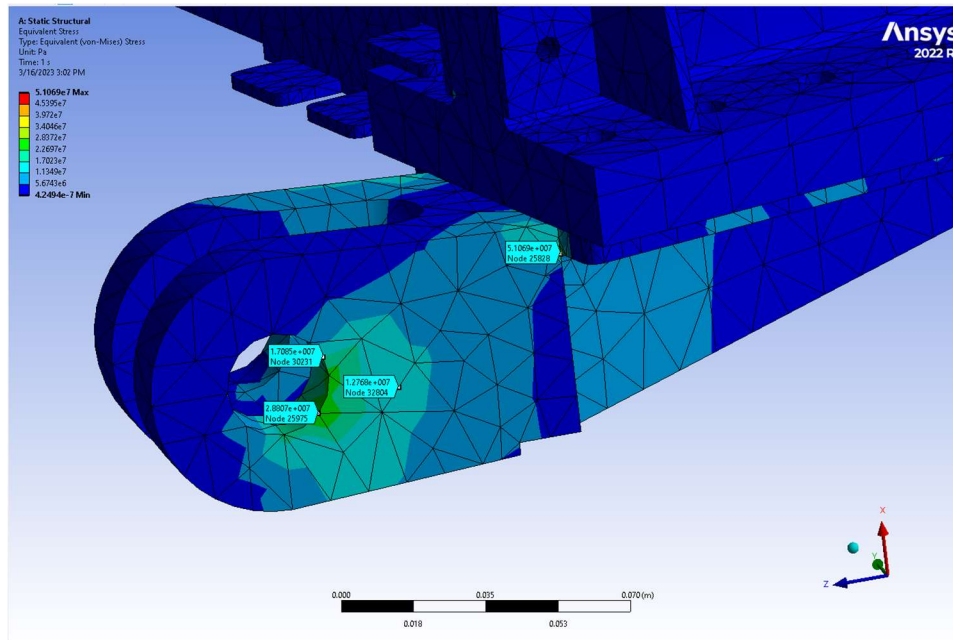


Figure 76: Leading Edge Bottom Bracket Close Up View 1 with Probe Values

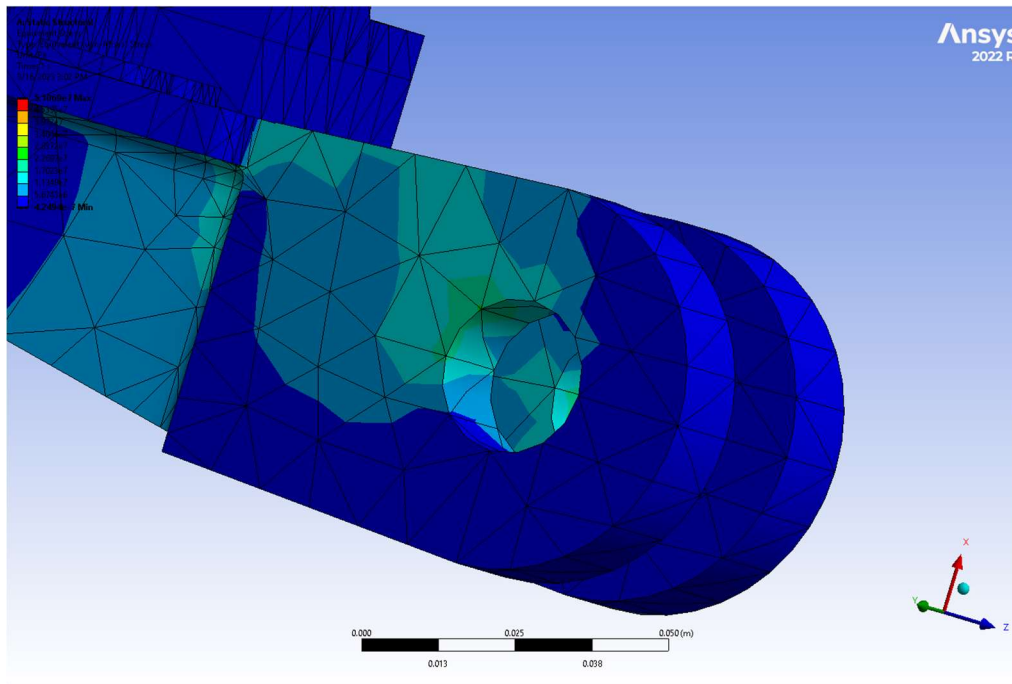


Figure 77: Leading Edge Bottom Bracket Close Up View 2

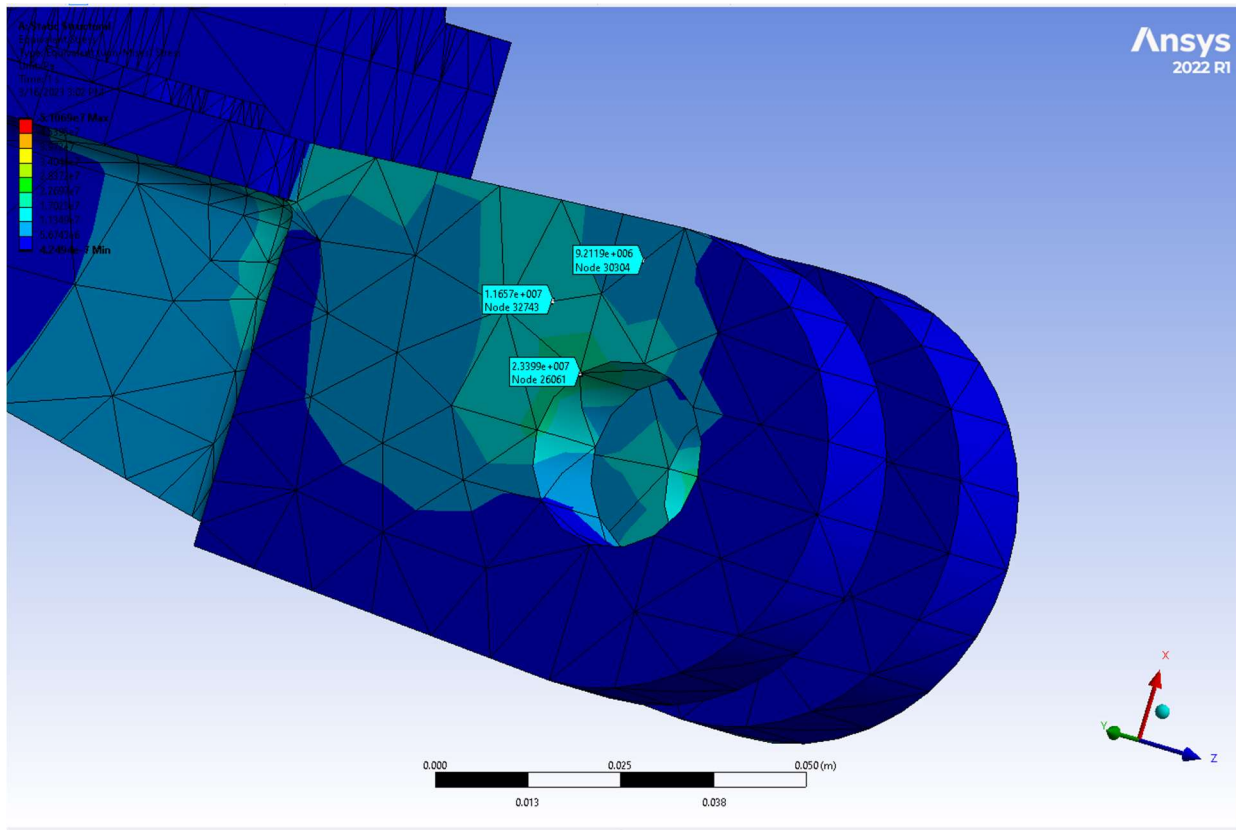


Figure 78: Leading Edge Bottom Bracket Close Up View 2 with Probe Values

Figures 80 and 81 are tables from Ansys Mechanical that show the material properties of the structural steel and aluminum alloy in the rear bracket analysis. From these tables, the team utilized the tensile ultimate strength in our results discussion. These numbers were used in a comparison of the von-mises stress from the simulation.

Structural Steel



Fatigue Data at zero mean stress comes from 1998 ASME BPV Code, Section 8, Div 2, Table 5-110.1

Density	7850 kg/m ³
Structural	
▼ Isotropic Elasticity	
Derive from	Young's Modulus and Poisson's Ratio
Young's Modulus	2e+11 Pa
Poisson's Ratio	0.3
Bulk Modulus	1.6667e+11 Pa
Shear Modulus	7.6923e+10 Pa
Isotropic Secant Coefficient of Thermal Expansion	1.2e-05 1/°C
Compressive Ultimate Strength	0 Pa
Compressive Yield Strength	2.5e+08 Pa
Strain-Life Parameters	
S-N Curve	
Tensile Ultimate Strength	4.6e+08 Pa
Tensile Yield Strength	2.5e+08 Pa

Figure 79: Structural Steel Properties on Leading Edge Bracket Pair (C and D)

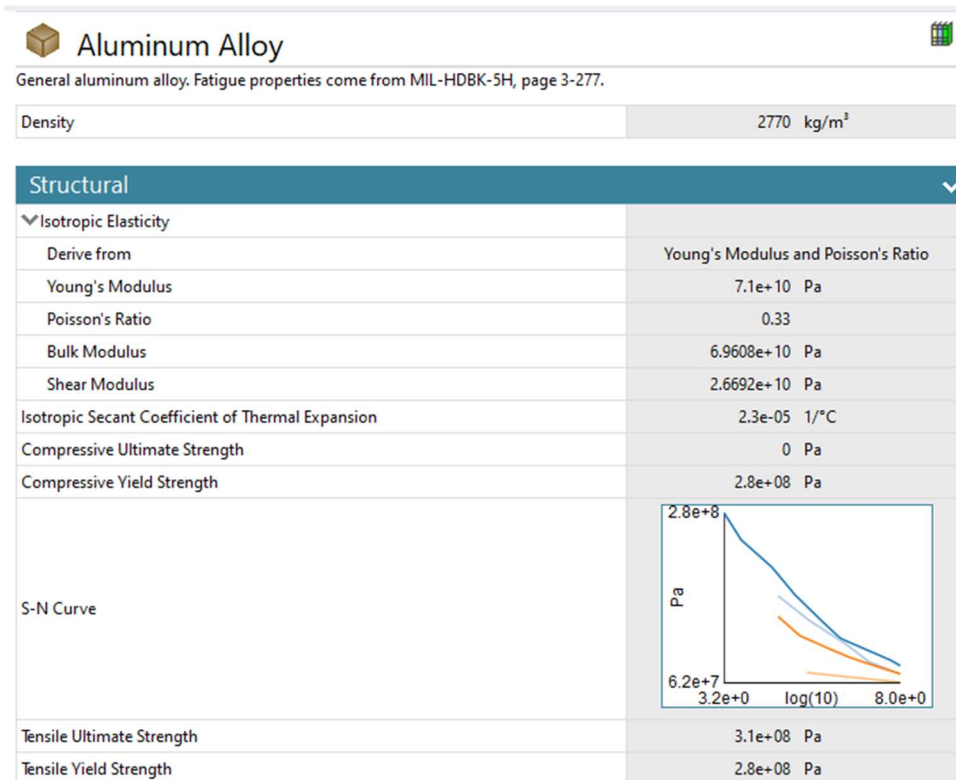


Figure 80: Aluminum Material Properties on Leading Edge Bracket Pair (C and D)

4.4.2 DC-3 Structural Analysis

The team's structural analysis of the DC-3 yielded the stress and deformation maps with the results presented in Figures 82 and 83, and 85 and 86, respectively. Results are displayed through color mapping, using the scale shown in Figure 84 for von Mises stress, and Figure 87 for deformation. Figure 82 shows that the stress on the bracket concentrates in the bolt holes above the ribs of the wing and decreases by more than a factor of three around the rest of the attachment. This is shown in Figure 82, in which stress in the bolt holes above the wing ribs is 72.649 MPa, while the stress only eight bolt holes away from the rib is only 19.995 MPa. Another point of lower stress on the attachment, but away from a wing rib, is shown in Figure 83. Additionally, total stress on the attachment, but away from a wing rib, is shown in Figure 83. Additionally, total

deformation is concentrated not in the brackets, but in the thin plate half a meter away from the attachment point, which deforms by almost a millimeter. Total deformation on the analyzed section is shown in Figure 85. The bolt holes in the attachment above the wing ribs where the stress concentrates do not deform by any significant amount, despite having a high stress value. The bolt holes where stress was concentrated, but deformation was not, are shown in Figure 86.

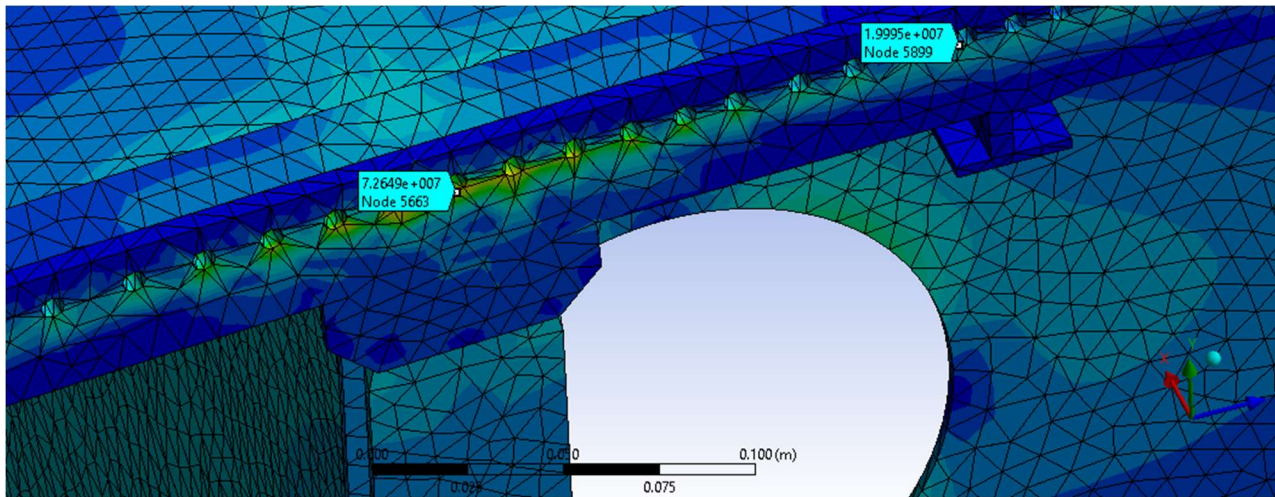


Figure 81: DC-3 wing attachment stress concentration map

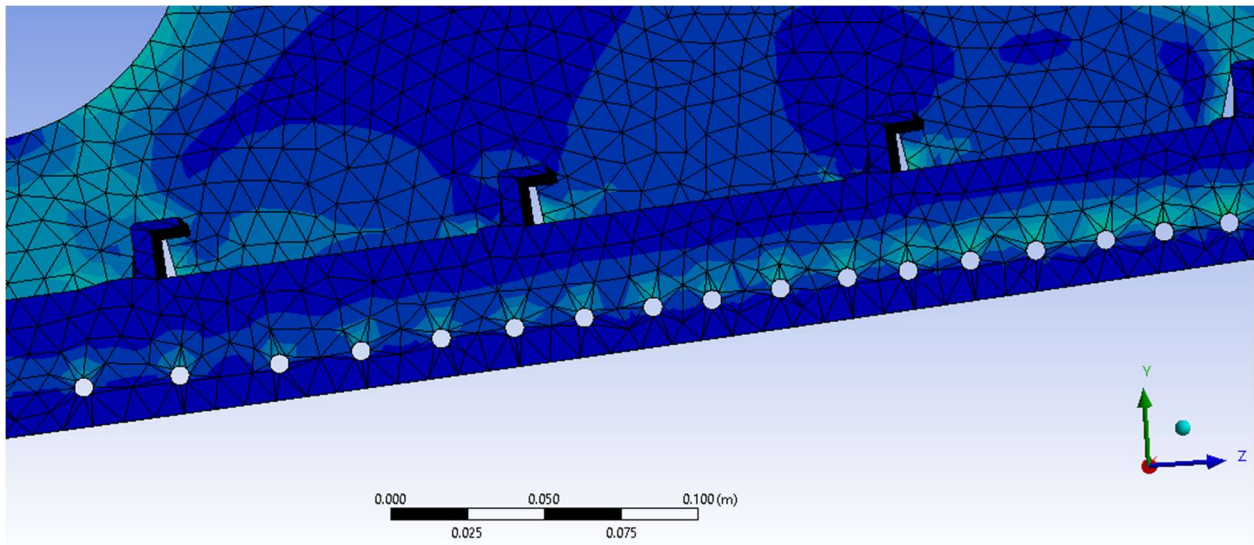


Figure 82: DC-3 Stress Concentration away from the Wing Rib

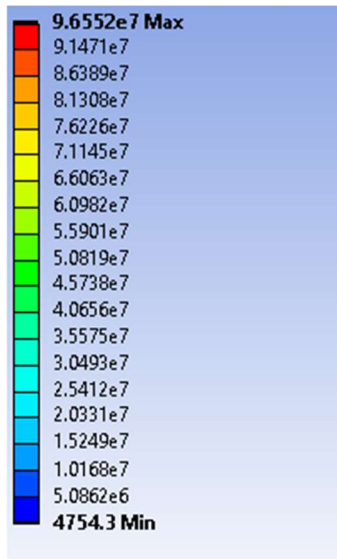


Figure 83: DC-3 Stress Scale showing von Mises stress in units of Pa. This scale is used to interpret results in Figures 82 and 83

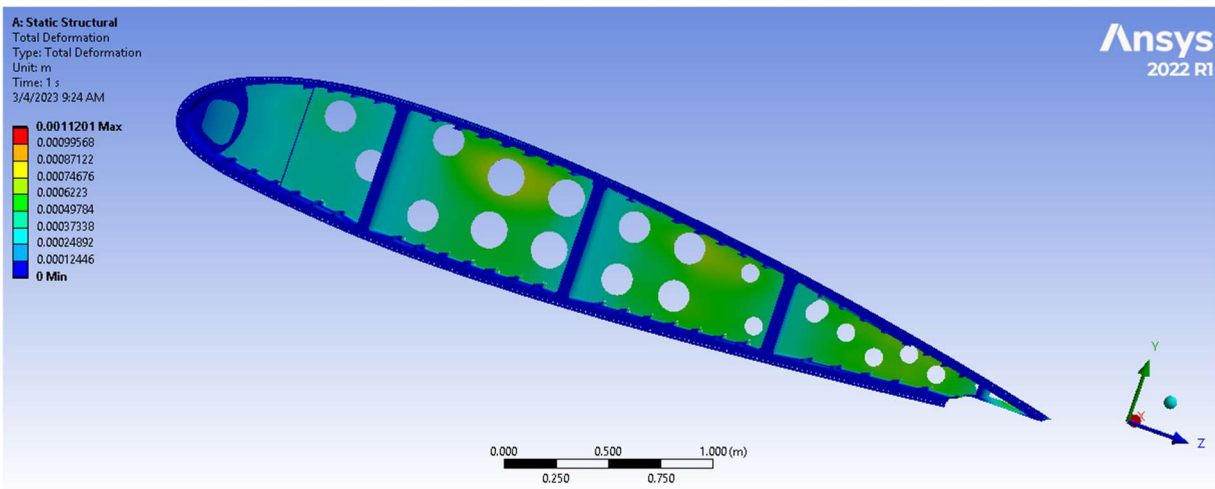


Figure 84: DC-3 Total Deformation

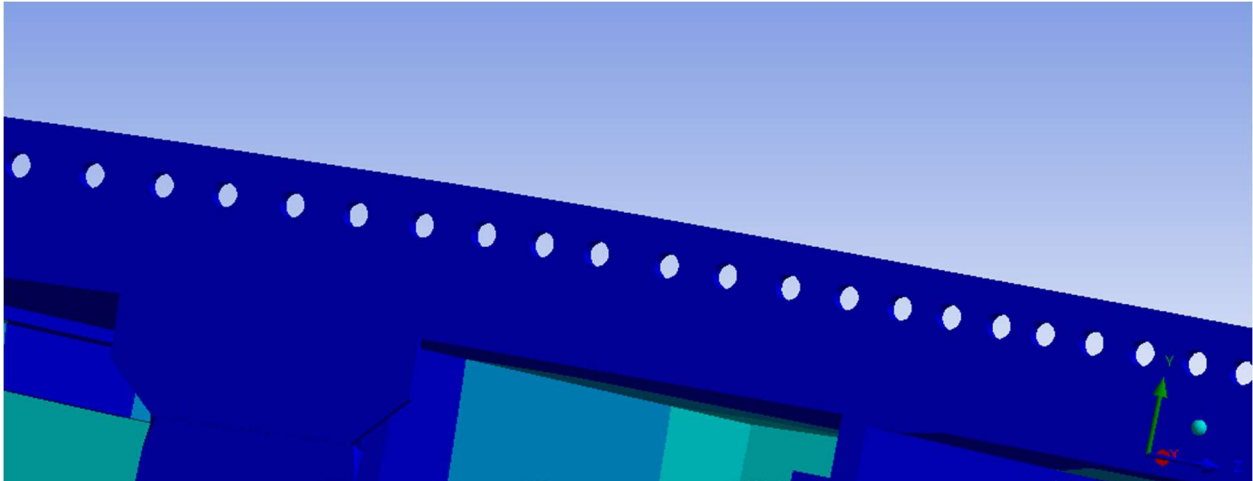


Figure 85: DC-3 Deformation Map at a Point of Stress Concentration

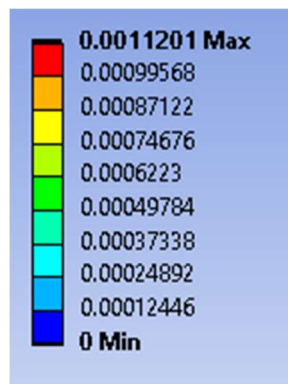


Figure 86: DC-3 Total Deformation Scale showing deformation in units of meters. This scale is used to interpret results in Figures 85 and 86

4.4.3 Discussion of Results

The main point of discussion for the comparison of wing attachments for the DC-3 and CBY-3 is the maximum numerical value for equivalent stress. The maximum equivalent stress can be compared to each material's ultimate tensile strength, providing an estimate of how close each of the wing attachments were to failure. For an aircraft, the dimensionless safety factor is the ratio

between the materials' ultimate tensile strength and the calculated von-Mises stress. This ratio is illustrated in Equation 7.

$$\text{safety factor} = \frac{\sigma_u}{\sigma_c} \quad 7$$

Where:

σ_u = ultimate tensile strength

σ_c = calculated stress

Both stresses are expressed in the same unit, Pa, in the case of the present work. Based on the safety factor calculated from the Ansys Mechanical results, the team determined that the aircraft with the higher safety factor would likely be the safer aircraft just from the standpoint of the wing attachment investigated in this work.

For the CBY-3, the results indicated that the wing attachments would not be close to the ultimate tensile strength. Shown in the close-up views of both pair of brackets (Figures 61-68 and Figures 72-79), the maximum stress experienced by the trailing pair was 26.5 MPa. The maximum stress experienced by the leading pair was 51.07 MPa. These locations are both in brackets that are made of structural steel with an ultimate tensile strength of 460 MPa. For both pairs the maximum stress was concentrated at a corner, these high values of equivalent stress were determined to be an anomaly by the team because the corners at these locations in the model had a radius of curvature of 3.175 mm, which is much smaller than would have likely been produced in during the manufacturing process. After ruling out these two locations as areas of concern, the focus was placed on the stresses that occurred near the bolt hole in the bracket. The maximum equivalent stresses in these two locations were found to be between 1 and 3 MPa, which is well under the 480 MPa ultimate tensile strength of structural steel. At the points of maximum stress,

at cruise conditions, and using the ultimate strength of aluminum alloy of 310 MPa wing attachment would have a safety factor of 17.3 at the trailing edge and 9.0 at the leading edge.

The stress on the DC-3 wing attachment was primarily concentrated within the bolt holes that were located above the wing ribs. This can be seen in Figure 82, where the maximum stresses were found to be 72.64 MPa, which is lower than both the ultimate tensile strength (310 MPa) and the tensile yield strength (280 MPa) of the chosen aluminum alloy. The stress decreases in the bolt holes the further they are located from these ribs. Therefore, anywhere, it would be within or near these holes that experience the highest stress. The maximum value, shown in 82, is 72.64 MPa. This would mean that at those points of maximum stress, at cruise conditions, and using the ultimate strength of aluminum of 280 MPa, the wing attachment would have a safety factor of 4.26. There is a significant safety factor indicating it is unlikely the material would exceed its ultimate tensile stress and experience failure. This value was calculated using Equation 7. Additionally, this stress is 207.36 MPa below the tensile yield strength of the chosen aluminum alloy, meaning that the wing attachment is unlikely to experience plastic deformation in any flight condition that the aircraft is likely to encounter. Additionally, the deformation maps found for the DC-3 wing attachment, shown in Figures 85, and 86, indicate that while the section of the wing would experience deformation under the assumed flight conditions, the bolt holes in which stress is the most concentrated would not experience significant deformation under these conditions. The safety factor of the DC-3 wing attachment was lower than the team had anticipated and was lower than the CBY-3 wing attachment safety factor.

While the simulation results suggest that neither the DC-3 and CBY-3 would fail or experience plastic deformation, they both had different safety factors, which indicate that with a safety factor of 17.3 in the trailing edge and 9.0 in the leading edge before failure, the CBY-3 wing

attachment would be safer than the DC-3 wing attachment, which had a safety factor of 4.26. Furthermore, as these values were found from cruise conditions, rather than maximum likely load that the aircraft could experience, both aircraft would remain safe as neither aircraft is likely to surpass the ultimate yield strength. Additionally, since the load of the wing is spread out over 328 bolt holes in the DC-3 attachment that if one bolt, or surrounding structure, experiences plastic deformation or is otherwise damaged, the risk to the wing would be low, as there are 327 other bolts that would continue to hold the wing to the fuselage. Conversely, in the unlikely event that one of the brackets of the CBY-3 wing attachment was damaged or failed, one fourth of the connection between the wing and the fuselage would be compromised, with potentially catastrophic results for the aircraft. Despite this difference in the design of the two wing attachments, the minimum safety factor of the CBY-3 is 2.11 times the safety factor of the DC-3, indicating that the CBY-3 wing connection is, by that metric at least, safer.

5 Methodology for Assessment of Restoration Workflow

5.1 Interviews

To complete Goal 3, the team decided questionnaires would be the best method to understand NEAM's current restoration workflow and use of rapid prototyping. These questions would also be used to identify any potential gaps in both areas that the museum believed needed improvement. Once the interview(s) with NEAM were conducted it was important to reach out to other museums that specialized in aircraft restoration and interview them with the same set of questions so that we could compare our findings. This approach would allow the team to use museum testimonials to create a list of recommendations to upgrade NEAM's restoration

workflow and rapid prototyping use. The list of interview questions given to the museums is shown below:

1. How often during a historical aircraft restoration do you encounter trouble finding all the components needed to bring the aircraft back to its “original” state (for display, not for flight worthiness)?
2. When you encounter the need to replace a missing part, how do you typically go about recreating that part? How is this process different when you have at least one copy of the missing part as compared to when you may only have a photograph to work with?
3. Have there been instances when you used 3D printed parts to “replace” these missing pieces? If you have, could you talk a little about the process of how you went about that?
4. Could you describe to us the workflow the team uses from when you acquire an aircraft all the way to it being fully restored on the floor of the museum? For example, how do you decide what projects to prioritize? How do you decide what needs to be disassembled, repaired, painted, and how is the order of these steps determined?
5. What are the best functioning parts of this workflow?
6. What areas of the workflow do you believe need the most improvement?
7. Are there any approaches to the restoration workflow that have been adopted over the years but have been found to NOT work out well? If so, can you describe these?

To begin the interview process, the team reached out to Mr. Bob Vozzola, the Restoration Coordinator at NEAM. He was sent the questions provided above so that we could understand NEAM’s restoration workflow, the pros and cons of this procedure, and instances of rapid

prototyping use. Once these answers were received the team identified areas that might improve their workflow and rapid prototyping use. These improvements became the main driving points in queries to other museums; by focusing on these weaker areas, the team would ask more targeted questions in future interviews.

Interviews were conducted with three other museums to gather feedback about their restoration workflow and rapid prototyping. The same list was used as a base for the conversation, with interviews conducted over video call having more targeted questions depending on their responses and the gaps that were previously identified in NEAM's workflow. From these responses the team was able to compile a list of recommendations to strengthen NEAM's workflow.

5.2 Project Management Software

In the context of streamlining the processes of restoration projects, the use of project management software could serve as a helpful tool. Software that is developed specifically to accommodate the organizational needs of a project puts things that are difficult to keep track of into one place, eliminating inefficiencies pertaining to the communication and organization of the project. The New England Air Museum could utilize such software for keeping track of tools and equipment across multiple projects and for communicating issues between volunteers, crew chiefs, committee members and whoever else may be involved with each project. When conducting the research on available software these functions were the main criteria in consideration, along with ease of use, cost, and functionality.

5.3 Rapid Prototyping

Once the use of rapid prototyping at different museums was understood from interview responses, the team assessed what recommendations to present to NEAM. Using a combination of personal knowledge and research of rapid prototyping companies, the team was able to recommend NEAM new ways to approach rapid prototyping, as presented in Section 6.3.

6 Results and Recommendations Regarding Restoration Workflow

6.1 NEAM Interview Results

The interview questions listed in Section 5.1 were answered by Mr. Bob Vozzolla (personal communication, Email from B. Vozzolla to Amaya Massari, January 27, 2023) on behalf of NEAM. His answers gave the team insight into how much effort, time and attention are needed in a project as well as allowing the team to conduct the proper research on what software and rapid prototyping recommendations we would make. His answer to Question 4, asking him to describe the restoration workflow, is paraphrased as a procedure and is listed below:

1. The pros and cons list for each of the projects available to the museum is made by the Restoration Coordinator.
2. For each project, a plan is made that identifies the level of repair maintenance, and restoration that will be carried out over the coming year.
3. Once a project is ready to be executed, the restoration coordinator appoints the Crew Chief, and a schedule is created.
4. A thorough inspection of the aircraft is performed and a draft restoration plan with lists of options for the work are prepared.

5. Vendors are contacted to get quotes in order to develop an estimate of the funding needed for the project.
6. Requests for funding to support the project are submitted to outside organizations as appropriate.
7. Based on the level of funding received (or committed), the extent of restoration that can be undertaken is decided and a restoration project plan is completed.
8. A team of volunteers is set up to execute the project.
9. Technical documents needed for the work are acquired, and research is started.
10. The Crew Chief prepares an ordered list of tasks and assigns these tasks to volunteers based on their skills (This is subject to change throughout the project as issues come up.)
11. If equipment or fixtures needed are not already available, these will be specially designed for the project.
12. The Crew Chief supervises the team of volunteers that completes the final assembly of all components and any finishing touches on the aircraft.
13. The Restoration Coordinator consults with the Museum Coordinator and Executive Director on where and when the project should be displayed.
14. The aircraft to be displayed will then have informational signage prepared and be taken to its dedicated place in the museum where other final touches can be added if needed.
15. Lastly, the display is made available to the public.

Many of these steps depend on what the outcome of previous steps are, resulting in variations in the process from project to project. Throughout the execution of the restoration plan for a project, there can be many modifications to the original task plan as problems or issues arise. The day-to-day issues are addressed by the Crew Chief and any strategic decisions are addressed

by the Restoration Coordinator. Both work together to consult and refine the project plan around problems related to space, equipment and budget. When decisions need to be made regarding changes to the project scope, the NEAM Executive Director will make a final decision in consultation with the Restoration Planning Committee.

In his responses to the other questions in the interview, Mr. Vozzola's explained that the museum strives to prioritize projects that benefit the museum's interest rather than someone's individual interest, in order to conserve resources and time. The team also learned that in the context of the use of rapid prototyping and software, NEAM has only 3D printed a few minor parts and could benefit from expanding their knowledge and use of this technology to streamline their restoration workflow.

6.2 Museum Interview Results

To find museums to contact, the team conducted multiple internet searches looking for local museums that specialized in historic aircraft restoration. The team also spoke with NEAM to see if they had any contacts at other museums that they believed would be good candidates for interviews. After contacting seven museums, two gave responses over emails and one interview was conducted over video call. The three museums and their contacts that responded were:

- National Air and Space Museum, Washington D.C: Peter Torraca, Manager of Aircraft Restoration and Interpretation (ptorraca@intrepidmuseum.org)
- Intrepid Museum, New York, NY: Luke A. Jones, Restoration Shop Supervisor (JonesL@si.edu)
- Cradle of Aviation Museum, Long Island, NY: Peter Trusdell, Restoration Manager and Exhibit Designer (icepjt@yahoo.com)

The team was able to collect information regarding each of these museum’s restoration workflow in addition to NEAM’s. This information is paraphrased and summarized in Table 11 below.

Table 11: Information Collected from Museum Interviews

1. How often during a historical aircraft restoration do you encounter trouble finding all the components needed to bring the aircraft back to its “original” state (for display, not for flight worthiness)?

Museum	Paraphrased Response
National Air and Space Museum	<p>Responded through email to Amaya Massari, received on 2/22/2023:</p> <p>This depends on the rarity of the aircraft, most of the time finding these pieces comes down to being in the right place at the right time.</p>
Intrepid Museum	<p>Responded through Zoom videochat with Amaya Massari, conducted on 2/21/2023:</p> <ul style="list-style-type: none"> - It tends to be a 50/50 for finding the pieces that they need. It usually relates to the rarity of the aircraft they are working with. - Much of the time they know that some pieces that are missing from the aircraft would not fare well in the harsh conditions that come with storing the planes outside in New York all year long, so they do not look to replace them.
Cradle of Aviation	<p>Responded through email to Gabrielle Tims, received on 2/27/2023:</p> <p>It occurs very often that they need to search for missing or damaged parts.</p>

2. When you encounter the need to replace a missing part, how do you typically go about recreating that part? How is this process different when you have at least one copy of the missing part as compared to when you may only have a photograph to work with?

Museum	Paraphrased Response
National Air and Space Museum	<p>Responded through email to Amaya Massari, received on 2/22/2023</p> <p>The first option is to search the internet for the piece. Some aircraft have small communities out there, they have tons of parts that can be used. The last resort is to make the piece in-house. The museum has tools such as “3d scanners, 3d printers, waterjet cutters, CAD software, GelSight (3D tactile sensing technology for surface characterization) tech, laser etchers, laser welders and many others” along with lots of modeling software that can be used to fabricate the missing part(s). They typically try to scale as best they can if they only have a drawing.</p>
Intrepid Museum	<p>Responded through Zoom videochat with Amaya Massari, conducted on 2/21/2023</p> <p>The museum has had a lot of success finding missing parts on eBay. If eBay is not successful, they would usually have an in-house machinist, make the piece.</p>
Cradle of Aviation	<p>Responded through email to Gabrielle Tims, received on 2/27/2023:</p> <p>Typically, they will search for drawings of that part and then if any information is missing, they will try to find it within pictures of that piece. If none of this information is available, they will make educated guesses on how to recreate it based on similar aircraft and materials.</p>

3. Have there been instances when you used 3D printed parts to “replace” these missing pieces? If you have, could you talk a little about the process of how you went about that?

Museum	Paraphrased Response
National Air and Space Museum	<p>Responded through email to Amaya Massari, received on 2/22/2023</p> <p>Refer to response from previous question.</p>
Intrepid Museum	<p>Responded through Zoom videochat with Amaya Massari, conducted on 2/21/2023</p> <p>There have been a few instances of 3D printing, but typically the plastic filament that is used is not suitable for outdoor storage.</p>
Cradle of Aviation	<p>Responded through email to Gabrielle Tims, received on 2/27/2023:</p> <p>3D printing has not yet been utilized, but they have done research on this method and would like to look to it as an option for future projects.</p>

4. Could you describe to us the workflow the team uses from when you acquire an aircraft all the way to it being fully restored on the floor of the museum? For example, how do you decide what projects to prioritize? How do you decide what needs to be disassembled, repaired, painted, and how is the order of these steps determined?

Museum	Paraphrased Response
National Air and Space Museum	<p>Responded through email to Amaya Massari, received on 2/22/2023</p> <p>Once a project has been chosen it will be evaluated by the Preservation Restoration Unit and Conservation. This evaluation is documented in a Condition Assessment Treatment (C.A.T) report that lists a short history of the aircraft, its current condition</p>

	<p>and structural integrity, and finally the proposed treatment. The “treatment proposal” is looked over by the collections department and curators to make sure it is a well-rounded group effort and will then approve it. Once the treatment is approved, the process begins and is well-documented for recordkeeping. The treatment is “intentionally reversible to ensure ease of removal in case someday it is decided a different method of treatment is needed.”</p>
<p>Intrepid Museum</p>	<p>Responded through Zoom videochat with Amaya Massari, conducted on 2/21/2023</p> <ul style="list-style-type: none"> - When a project first arrives, Peter and his boss give it a thorough inspection, they remove all removable panels and see the condition. After this a cleaning of the aircraft occurs since most of them have lived outdoors prior to this. The plane is then treated with a spray on corrosion deterrent. - The restoration team then starts working on the exterior of the aircraft. The paint and sometimes the primer is first sanded down. They stencil on original marking before painting. These markings sometimes come from original pictures, but if these are not pictures provided, they look to eBay for pictures of small “children's models” and some different marking for these small model airplanes also on eBay. - Then they apply finishing coatings that prep the aircraft for outdoor storage, it's an acrylic based spray paint that is extremely fade resistant. After painting, the aircraft is moved to the outdoor flight deck.
<p>Cradle of Aviation</p>	<p>Responded through email to Gabrielle Tims, received on 2/27/2023:</p>

	<p>General features of their workflow:</p> <ul style="list-style-type: none"> - No deadlines are set for any projects. - Volunteer teams work once a week and need time to learn what to do. - The main goal is to preserve the aircraft and conserve the history of it as closely as possible, however there are financial and spatial limitations that get in the way of this. This means that occasionally aircraft are only repaired partly so that aspects of the aircraft's history are not covered up through the restoration process. For example, if the original paint is in good enough condition, it could be left alone instead of undergoing repair to preserve history.
--	---

5. What are the best functioning parts of this workflow?

Museum	Paraphrased Response
National Air and Space Museum	<p>Responded through email to Amaya Massari, received on 2/22/2023</p> <p>No specified response.</p>
Intrepid Museum	<p>Responded through Zoom videochat with Amaya Massari, conducted on 2/21/2023</p> <ul style="list-style-type: none"> - Given the restraints under which they work, specifically budgets, their restorations are done well. - They can usually come up with workable answers for issues. - They are proficient at keeping the structural integrity for the safety of the aircraft. - They excel at having historically accurate markings on their aircraft. - The use of the paint technique, backmasking, to create their markings.

Cradle of Aviation	<p>Responded through email to Gabrielle Tims, received on 2/27/23:</p> <p>The organization of small teams of people into specific parts of the project that caters to their specific set of skills (that they either already had or can be taught) rather than having a large group of people work on the whole project together.</p>
--------------------	---

6. What areas of the workflow do you believe need the most improvement?

Museum	Paraphrased Response
National Air and Space Museum	<p>Responded through email to Amaya Massari, received on 2/22/2023</p> <p>The main method of communication in the restoration process is email. Using email to communicate is very slow and sometimes causes miscommunication.</p>
Intrepid Museum	<p>Responded through Zoom videochat with Amaya Massari, conducted on 2/21/2023</p> <p>The lack of formal recordkeeping for restations projects. It can be hard for new people to be integrated into restoration because they do not have records of how previous projects were completed.</p>
Cradle of Aviation	<p>Responded through email to Gabrielle Tims, received on 2/27/23:</p> <p>They do not utilize any software programs that could assist with project management or tool tracking.</p>

7. Are there any approaches to the restoration workflow that have been adopted over the years but have been found to NOT work out well? If so, can you describe these?

Museum	Paraphrased Response
National Air and Space Museum	<p>Responded through email to Amaya Massari, received on 2/22/2023</p> <p>No.</p>
Intrepid Museum	<p>Responded through Zoom videochat with Amaya Massari, conducted on 2/21/2023</p> <p>There was an instance of a paint change for one of the aircraft using a polyethylene two-part paint. This paint has a lifetime of about 30 years compared to the 7-12 years that their typical acrylic paint lasts before wearing. This polyethylene paint is very hazardous, so it was painted on using a roller, but it dries very quickly so once the aircraft was finished being painted it was not a clean layer. The aircraft was repainted with typically acrylic paint afterwards.</p>
Cradle of Aviation	<p>Responded through email to Gabrielle Tims, received on 2/27/23:</p> <p>Sometimes the crew will try to get ahead of themselves to finish things quickly and then not complete tasks with the best quality.</p>

Once all the interviews were conducted the team found some common themes in their responses. All the museums take multiple factors into account when completing their restoration these are mainly: the state of the aircraft when it is acquired by the museum, importance of the project, budget, storage and display location, time, and skills of the staff/volunteers. These factors are the basis for how, why, and when the project gets completed. The second theme is the importance of historical preservation. These museums complete a significant amount of research to find historically accurate paint colors and markings so that when the aircraft are on display, they

are representative of the time when they were flown. Lastly, all the museums noted that their restoration workflow is an iterative process, where each step depends on the previous one and there is cycling back and forth between each step. This is the result of having many groups working on one project together. Many of the museums also noted that they do not use project management software to help facilitate communication and organize between the teams and within the project. This lack of software usage is also seen at NEAM where they have stated that they do not take advantage of digital software to enhance project completion.

6.3 Team Recommendations

6.3.1 Software Recommendations

After conducting research on software that could help improve NEAM's restoration workflow as described in Section 5.2.2, there were a few suggestions to be made. We found that there are numerous software options available to assist in tool and asset tracking, with costs usually based on a monthly subscription fee. For example, *EZ Office Inventory* by EZO is an asset tracking software that companies use to keep track of all their assets across many locations and projects including computers, tools, equipment and more. It allows the user to organize them by value, if they're being used, where it's located, essentially allowing the user to organize assets in any way that is desired. This software also allows you to display this information through charts, graphs and lists based on preference as shown in Figure 86 and Figure 87 [32].

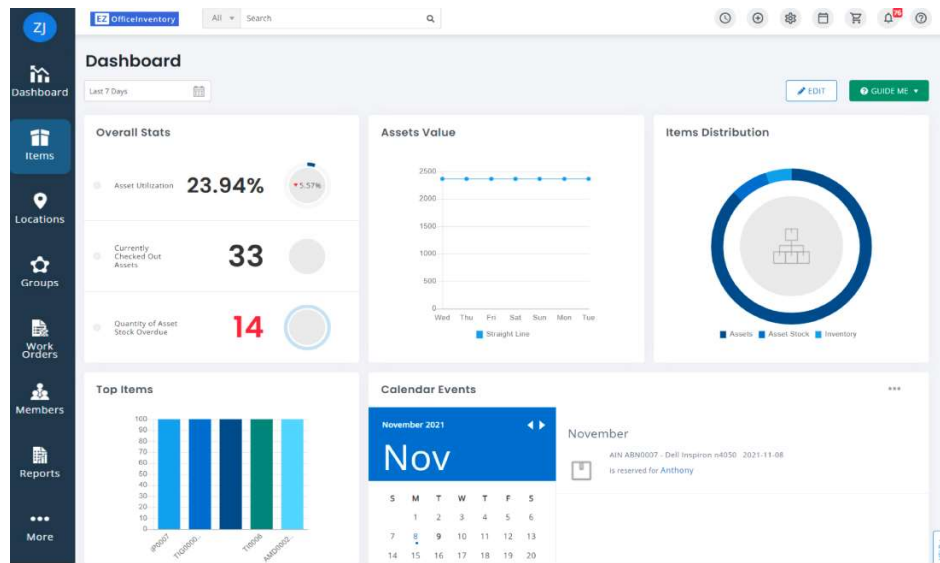


Figure 87: Picture of the user interface for EZ Office Inventory showing the differing ways to organize assets [32], Copyright 2006-2023, Software Advice, Inc.

The Assets page includes the following elements:

- Navigation:** Dashboard, Items, Locations, Groups, Members, Reports, More.
- Actions:** IMPORT ASSETS, + ADD ASSET, EXPORT TO CSV.
- Search and Filter:** Search Assets, Select View.
- Asset List:**

ASSET #	NAME	DISPLAY PICTURE	LOCATION
11	Apple iMac		San Francisco
3	Camera		New York
8	Chromebook		San Francisco
10	Dell Alienware		New York
9	Guitar		New York
1	HP Probook		San Francisco

Figure 88: Picture of the user interface for EZ Office Inventory showing an example of a list of assets [32] Copyright 2006-2023, Software Advice, Inc.

Therefore, this software is very customizable and simple, making it easy and accessible for the user to find any asset based on their needs. NEAM could possibly benefit from using *EZ Office Inventory* for keeping track of tools and equipment across multiple projects. As explained in

Section 6.1, there is much consideration that goes into formulating the budget for these projects and adding this expense for this purpose may simply not be necessary. However, it is still an option.

Since the Microsoft Office suite of software is already available to the NEAM staff, the team searched for free Excel templates that could be downloaded from the internet and imported into Excel that would allow for NEAM restoration staff to track the use of tools and parts, as well as managing different restoration projects taking place at the same time. Several easily available Excel templates were found that were designed to track inventory but could easily be repurposed by NEAM staff to track the location and use of parts and tools during different restoration projects. An example of a template that could be used for this purpose is shown in Figure 91 from reference 31. Additionally, the team found several templates that could be useful for restoration team leaders that need to track multiple projects taking place concurrently, each with many smaller tasks, and different timelines and personal working on them. Many of these templates take the form of Gantt charts and similar spreadsheets that allow for multiple different projects and timelines to be easily tracked, and which display this information in a way that is easy to understand. An example of an Excel template that could be used to help in project workflow management is shown in Figure 92. These Excel templates combine relative ease of use, and a low cost with near infinite variety. If a template does not fulfill NEAMs needs, then there are many other possibilities. Based on the responses that NEAM provided to the interview questions, the Team recommend several Microsoft Excel templates, either those we suggest above or others that are available online, to improve and computerize both part and tool tracking and project workflow management.

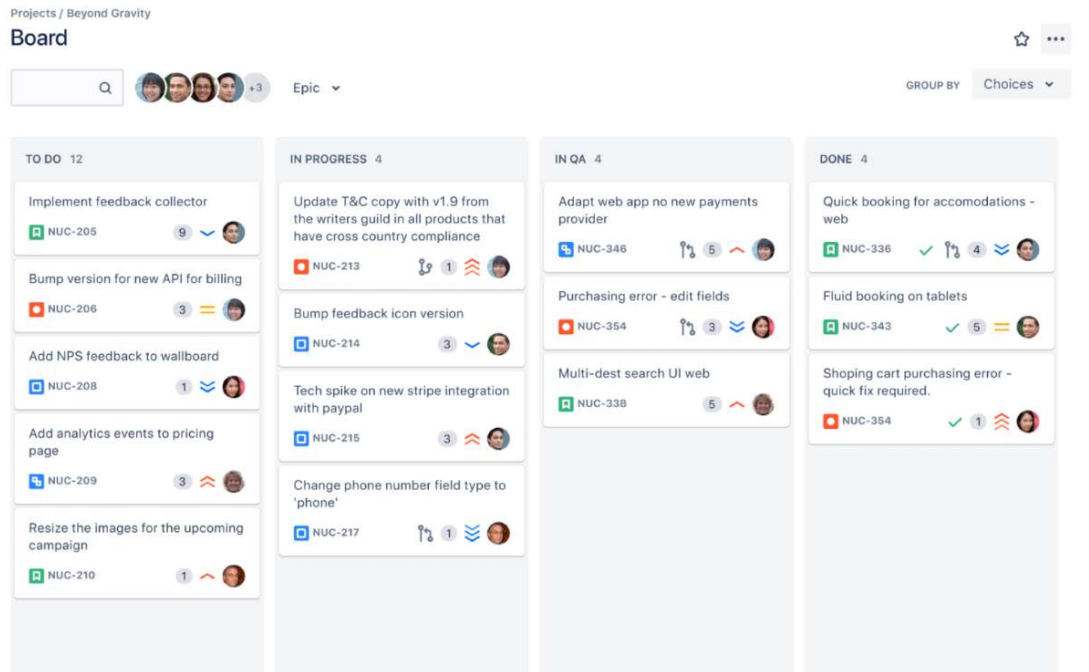


Figure 91: Picture of the user interface of Jira [42], Copyright 2023 Atlassian

Jira would allow NEAM to keep track of issues or send reminders across multiple projects in one place. This would avoid confusion and eliminate the need for sending too many emails or having to track anyone down.

6.3.2 3D Printing Recommendations

NEAM reported two instances of rapid prototyping having been used in their restoration process. The first instance was part of the CBY-3 restoration. The landing gear of the aircraft was missing small hubs that covered it. These hubs were not provided when the aircraft was donated, so from pictures a machinist who previously volunteered at the museum used his own knowledge and 3D printer to fabricate these missing pieces. The second instance occurred when the fuse and lock of a Merlin engine needed to be recreated. This effort was led by an intern with CAD modeling skills who created a digital model of the missing parts, which were both nonstructural. Once these

digital models were created, the 3D printing needed to be outsourced. However, there was no established vendor for this, and the pieces were machined in-house instead.

The main takeaway from these two examples is that NEAM does not have a formal process for 3D printing and additive manufacturing. Based on numerous conversations with the volunteers on site the team determined that most members have little to no CAD and solid modeling experience. Having rapid prototyping performed outside of the typical machining done in restoration museums seems to be a feasible option for large scale museums such as the National Air and Space Museum but may not be for those with a more limited budget, as the 3D printing would need to be outsourced. Due to these factors the team believes that the best way to work around this would be to have a designated company the museum uses to outsource solid modeling, 3D printing and additive manufacturing.

Below is a list of companies that the team believes NEAM may be able to use for 3D printing needs that arise during the restoration process.

TriMech Advanced Manufacturing Services (Deep River, CT)

Link: <https://mfg.trimech.com/aerospace-industry/>

- This company has experience performing Additive Manufacturing for the aerospace industry.
- They also offer 3D scanning and reverse engineering services, that may be useful for replacing broken and damaged parts.

Oxford Performance Materials (South Windsor, CT)

Link: <https://oxfordpm.com/our-company/about-us>

- Perform 3D printing for a wide variety of companies, including experience with aerospace applications.

Kris’s 3D Printing (Tolland, CT)

Link: <https://krisfarley.org/>

- This is a much smaller company, that may require an already existing CAD model before a part can be printed.

7 Project Conclusions and Broader Impacts

7.1 Conclusions

Our findings allow us to conclude that the CBY-3 has a higher safety factor than the DC-3 with respect to the wing attachment. At the beginning of the project the team assumed that the DC-3's safety factor would be much higher since it was the “blueprint” for modern commercial aircraft, but that theory, at for the wing attachment, was disproven through FEA. These results are summarized in Table 12 below.

Table 12: Summary of Structural Analysis Results

Aircraft	Max. Equivalent Stress (MPa)	Location of Max. Equivalent Stress	Figure showing Max Equivalent Stress	Material	Safety Factor
CBY-3 (Front Bracket Pair)	51.07	Corner between bolt end of bracket and wing end of bracket	Figure 71	Structural Steel	9
CBY-3 (Rear Bracket Pair)	26.5	Corner between bolt end of bracket and wing end of bracket	Figure 61	Structural Steel	17.3

DC-3	72.64	Inside of a bolt hole above the furthest forward rib	Figure 81	Aluminum Alloy	4.26
------	-------	--	-----------	----------------	------

The team also found that rapid prototyping techniques were regularly used in historical aircraft restoration only at one of the four museums contacted. However, these methods would be of great benefit to restoration efforts since the lack of original parts is a common problem in historical aircraft restoration.

Finally, we identified several options with respect to software that can be used for project management in the restoration workflow. In addition to task management, several software tools can be used to facilitate tracking of tools, parts, and materials being used in multiple concurrent restoration projects. These tools would aim to streamline practices that are already in place and make the entire process more efficient.

7.2 Broader Impacts

The impacts of this project extend beyond simply determining whether the wing attachment design of the CBY-3 is safer than the DC-3. This project demonstrates why engineers and scientists are constantly creating new technology, because conventional designs are not always the safest or most reliable. Just as shown in this project, it is important to consider all available options when determining the solution to any engineering problem.

Additionally, this project worked to bridge the gap between historical and modern engineering. The numerous software tools and technologies used in this project allowed the team to create CAD models of the historical aircraft, as well as create an archive of the historic

documents and blueprints that include detailed information on the aircraft's design. Using this same approach to generate digital models from archival print sources, future investigators will be able to perform analyses and document information on other historical aircraft, vehicles, and structures. The overall methodology adopted in this work can be used to settle historical debates and solve engineering mysteries. To the best of the author's knowledge, this project also pioneered the use of modern numerical analysis, such as FEA on specific components of a historical aircraft. There is a lack of literature surrounding applications of modern analytical tools to historical aircraft.

Continuing Relationship with NEAM

Based on our experience with this project, the team recommends a continued relationship with the NEAM. Throughout this project, the team had multiple opportunities to speak with museum staff and volunteers that were more than happy to share their knowledge of engineering and historical aircraft. These interactions and the friendships formed were very meaningful to the team and we recommended the continuation of this collaboration between WPI and NEAM for future projects.

8 References

- [1] Wood, Richard. The Contributions of Vincent Justus Burnelli - NASA Technical Reports Server (NTRS). 1 Jan. 2003, ntrs.nasa.gov/citations/20030004233. Accessed 23 Sept. 2022.
- [2] Frederick, John H., and Charles A. Wolverton. Safety in Air Navigation. U.S. Govt. Print. Off., 1947. Accessed 26 Sept. 2022.
- [3] Noland , David. “The Burnelli Controversy.” *Smithsonian Magazine*, 1 Nov. 1989, www.smithsonianmag.com/air-space-magazine/the-burnelli-controversy-15233082/#:~:text=Around%201930%20the%20U.S.%20government,Burnelli%20refused. Accessed 20 Sept. 2022.
- [4] Dept. of the Air Force. United States: U.S. Government Printing Office, 1948.
- [5] Holden, Henry M., and Henry M. Holden. “DC-3 Specifications.” *Douglas DC-3/Dakota History*, 8 Nov. 2013, <http://www.dc3dakotahistory.org/specs-stats/dc-3-specifications/>. Accessed 15 Sept. 2022.
- [6] Assadourian, A. & Harper, J.A. (1953). Technical Note 3088: Determination of the Flying Qualities of the Douglas DC-3 Airplane. NACA
- [7] Bardehle, Peter. (1985). *THE DC-3 STORY – A Plane that Changed the World*. Retrieved from <https://www.youtube.com/watch?v=bkXHx0i2vHs>. Accessed 17 Sept. 2022.
- [8] “C-47A Skytrain.” ” *Air Mobility Command Museum*, <http://amcmuseum.org/at-the-museum/aircraft/c-47a-skytrain/>. Accessed 23 Feb. 2023.
- [9] “Understanding the Need to Fully Constrain the Model - Lesson 2.” *Ansys Innovation Courses*, <https://courses.ansys.com/index.php/courses/structural-boundary-conditions/lessons/understanding-the-need-to-fully-constrain-the-model-lesson-2/>. Accessed 3 Jan. 2023
- [10] Glenn Research Center. *The Lift Equation*. <https://www.grc.nasa.gov/WWW/k-12/VirtualAero/BottleRocket/airplane/lifteq.html>. Accessed 12 Oct. 2022.
- [11] Glenn Research Center. *Factors That Affect Lift*. <https://www.grc.nasa.gov/WWW/k-12/VirtualAero/BottleRocket/airplane/factors.html>. Accessed 12 Oct. 2022.
- [12] Glenn Research Center. *The Drag Equation*. <https://www1.grc.nasa.gov/beginners-guide-to-aeronautics/drag-equation/><https://www1.grc.nasa.gov/beginners-guide-to-aeronautics/drag-equation/> Accessed 12 Oct. 2022. Accessed 15 Oct. 2022.
- [13] *Historical Snapshot: DC-3 Commercial Transport*. <https://www.boeing.com/history/products/dc-3.page>. Accessed 28 Feb. 2023.

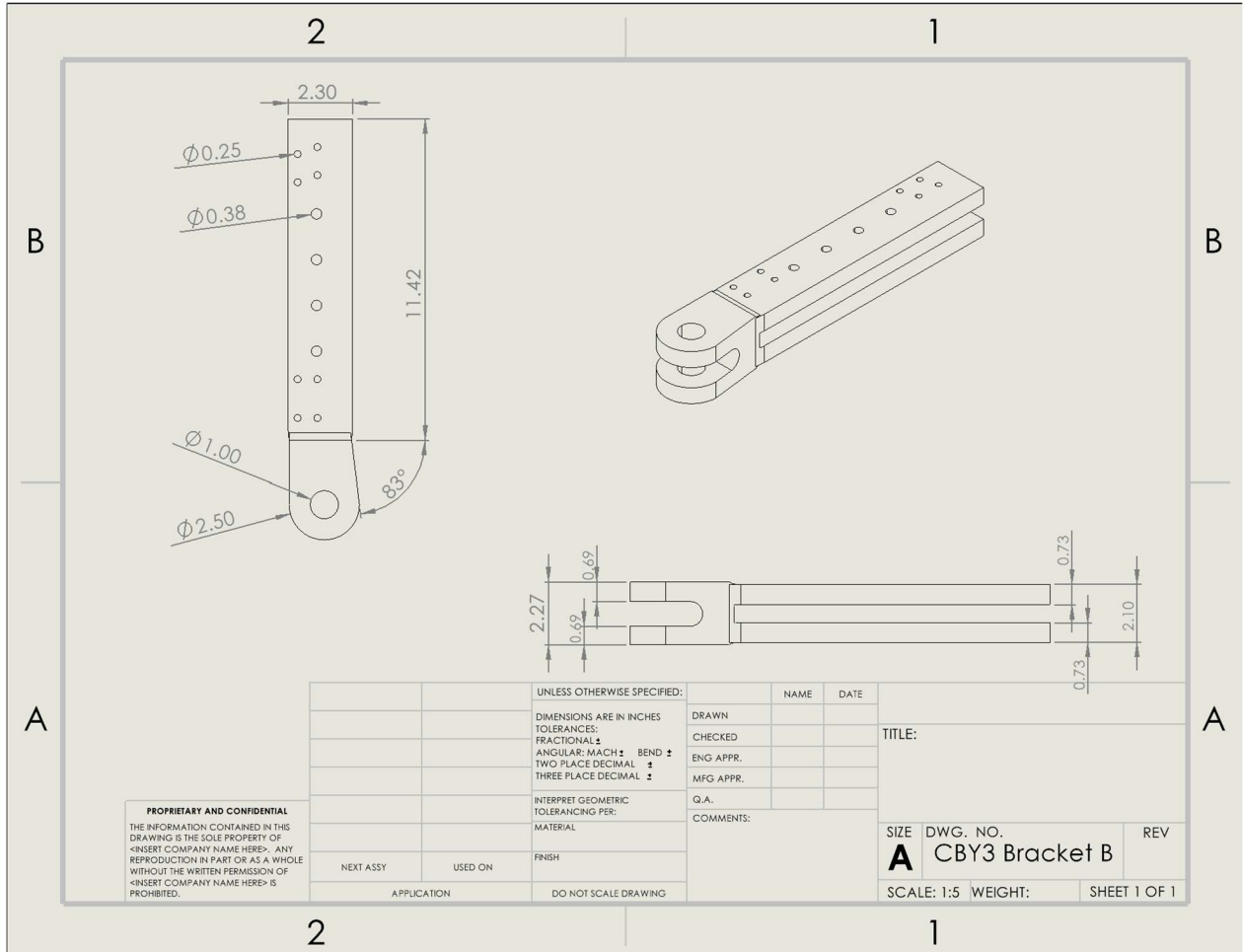
- [14] *Historical Snapshot: DC-2 Commercial Transport*. <https://www.boeing.com/history/products/dc-2.page>. Accessed 28 Feb. 2023.
- [15] "About Us." *New England Air Museum*, <https://neam.org/pages/about-us>. Accessed 12 Oct. 2022.
- [16] "Top Project Management Excel Templates." *Smartsheet*, www.smartsheet.com/top-project-management-excel-templates. Accessed 28 Feb. 2023.
- [17] Mouritz, Adrian P. *Introduction to Aerospace Materials*. American Institute of Aeronautics and Astronautics, 2012.
- [18] Helmons, Rudy. "Excavation of Hard Deposits and Rocks, on the Cutting of Saturated Rock." *Research Gate*, Delft University of Technology, May 2017, www.researchgate.net/publication/316285043_Excavation_of_Hard_Deposits_and_Rocks_on_the_Cutting_of_Saturated_Rock. Accessed 2 Feb. 2023
- [19] *Douglas DC-3 | National Air and Space Museum*. https://airandspace.si.edu/collection-objects/douglas-dc-3/nasm_A19530075000. Accessed 12 Oct. 2022.
- [20] Kellari, Demetrios, et al. "Architectural Decisions in Commercial Aircraft from the DC-3 to the 787." *Journal of Aircraft*, vol. 55, no. 2, 2018, pp. 792–804, <https://doi.org/10.2514/1.C034130>. Accessed 10 Dec. 2022
- [21] Parnell, Duncan. "What Is 3D Laser Scanning Technology?" *Duncan Parnell*, 3 Sept. 2018 <https://www.duncan-parnell.com/blog/what-is-3d-laser-scanning-technology#:~:text=A%203D%20laser%20scanner%20is,of%20a%20three%2Ddimensional%20object> Accessed 14 Dec. 2022
- [22] "Restoration Diary Burnelli CBY-3." *New England Air Museum*, neam.org/pages/restoration-diary-burnelli-cby-3. Accessed 20 Dec. 2022
- [23] Orlovsky, N., Wojciechowski M., "Computational Fluid Dynamics (CFD) Analysis of the Burnelli CBY-3 Loadmaster," WPI Major Qualifying Project (MQP) Report 32651, Advisor: J. Blandino, 2022
- [24] Pham, D.T. , et al. "A Comparison of Rapid Prototyping Technologies." *International Journal of Machine Tools and Manufacture*, Pergamon, 17 June 1999, https://www.sciencedirect.com/science/article/abs/pii/S0890695597001375?casa_token=brJ-L7zJ1tsAAAAA%3AqgXmb1EB9fLZlzmqiEIGBK1a_sv6fb_i7c9IcUOQF33bxUqXewthWwgj_KfPGYyEoTlBons.
- [25] "Lifting Body." *Wikipedia*, Wikimedia Foundation, 20 Feb. 2023, en.wikipedia.org/wiki/Lifting_body#:~:text=The%20lifting%20body%20was%20conceived,a%20patent%20by%20Roy%20Scroggs. Accessed 23 Feb. 2023

- [26] Michael Gregor. CBY-3., Central Aircraft Corporation, 1945, *Wing Root Hinge Fittings*. [Archival Source from NEAM]
- [27] “Aerodynamics and Performance.” *CFI Notebook: "Higher" Education*, www.cfinotebook.net/notebook/aerodynamics-and-performance/aircraft-components-and-structure. Accessed 10 Oct. 2022.
- [28] “Pop 2 3D Scanner (Infrared Light | Precision 0.05mm) .” *Revopoint 3D US*, [Revopoint, us.revopoint3d.com/products/pop2-3d-scanner](http://Revopoint.us.revopoint3d.com/products/pop2-3d-scanner). Accessed 14 Dec. 2022.
- [29] eFunda, Inc. “Rapid Prototyping: An Overview.” *Efunda*, www.efunda.com/processes/rapid_prototyping/intro.cfm. Accessed 5 Jan. 2023.
- [30] “3D Printing vs Additive Manufacturing: What's the Difference?: Blog Posts.” *Monroe Engineering*, 27 Oct. 2021, monroeengineering.com/blog/3d-printing-vs-additive-manufacturing-whats-the-difference/. Accessed 12 Dec. 2022.
- [31] “Excel Asset Tracking Template.” *General Blue Corporation*, www.generalblue.com/asset-tracking-template/p/ttv1wv5bw. Accessed 28 Feb. 2023.
- [32] “EZOfficeInventory Software Reviews, Demo & Pricing - 2023.” *Software Advice*, www.softwareadvice.com/cafm/ezofficeinventory-profile/. Accessed 28 Feb. 2023.
- [33] “What Is Laser Triangulation?” *MoviMED*, 4 Apr. 2018, www.movimed.com/knowledgebase/what-is-laser-triangulation/. Accessed 28 Feb. 2023.
- [34] Liu, Qianchu & Sun, Shi & Walker, Kevin & Choi, Yi rye & Brandt, Milan. (2017). Repair and manufacturing of military aircraft components by additive manufacturing technology.
- [35] “NTS300 Pro Inspection Camera with 5-Inch HD Screen.” *Teslong*, teslong.com/collections/industrial-endoscopes/products/nts300-industrial-endoscope. Accessed 3 March 2023.
- [36] Central Aircraft Company, New York, NY, 1945, pp. 4–5, *Static Test - Wing Root Fitting, Lower Rear Prototype CBY-3*. [Archival Source from NEAM]
- [37] “Inventor: Powerful Mechanical Design Software for Your Most Ambitious Ideas.” *Autodesk*, 1 Oct. 2022, www.autodesk.com/products/inventor/overview?term=1-YEAR&tab=subscription. Accessed 3 March 2023.
- [38] “XFLR5” 21 Jan. 2021, <http://www.xflr5.tech/xflr5.htm>. Accessed 3 March. 2023
- [39] “What Is Structured Light.” *IGI Global*, www.igi-global.com/dictionary/structured-light/45961. Accessed 28 Feb. 2023. Accessed 5 March 2023.

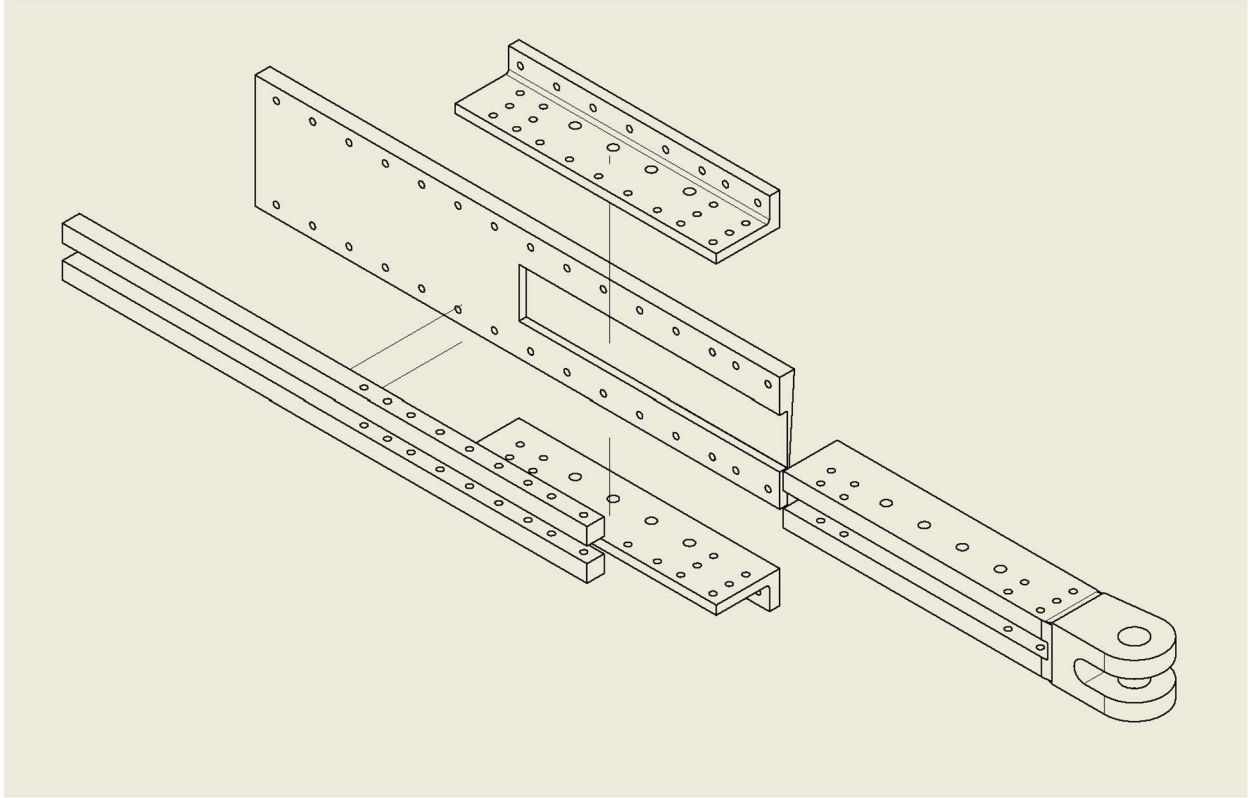
- [40] “Z-BOLT Infrared Training Lasers .” *Z-BOLT* , www.z-bolt.com/infrared-eye-safe-training-lasers#:~:text=Class%20%26%20Class%203R,-Lasers%20vs%20Military&text=Class%20%20infrared%20lasers%20are,target%20marketing%20at%20%20C000%20meters. Accessed 28 Feb. 2023.
- [41] D. Aircraft, *Douglas DC-3 Assembly Line, 1930s*. Boeing, 1937, <https://secure.boeingimages.com/archive/Douglas%20DC-3%20Assembly%20Line,%201930s-2JRSXLJ8L1G2.html>. Accessed 20 Nov. 2023.
- [42] Atlassian. “Jira: Issue & Project Tracking Software.” *Atlassian*, www.atlassian.com/software/jira?&aceid=&adposition=&adgroup=136973856930&campaign=18440774103&creative=647869050229&device=c&keyword=jira&matchtype=e&network=g&placement=&ds_kids=p73335831609&ds_e=GOOGLE&ds_eid=700000001558501&ds_e1=GOOGLE&gclid=CjwKCAjwiOCgBhAgEiwAjv5whGhGnniV67CNr8oAHMrhl-PimsCfltHgqykDH50CPbXklo32j08HgRoCe5QQA vD_BwE&gclsrc=aw.ds. Accessed 28 Feb. 2023.

9 Appendices

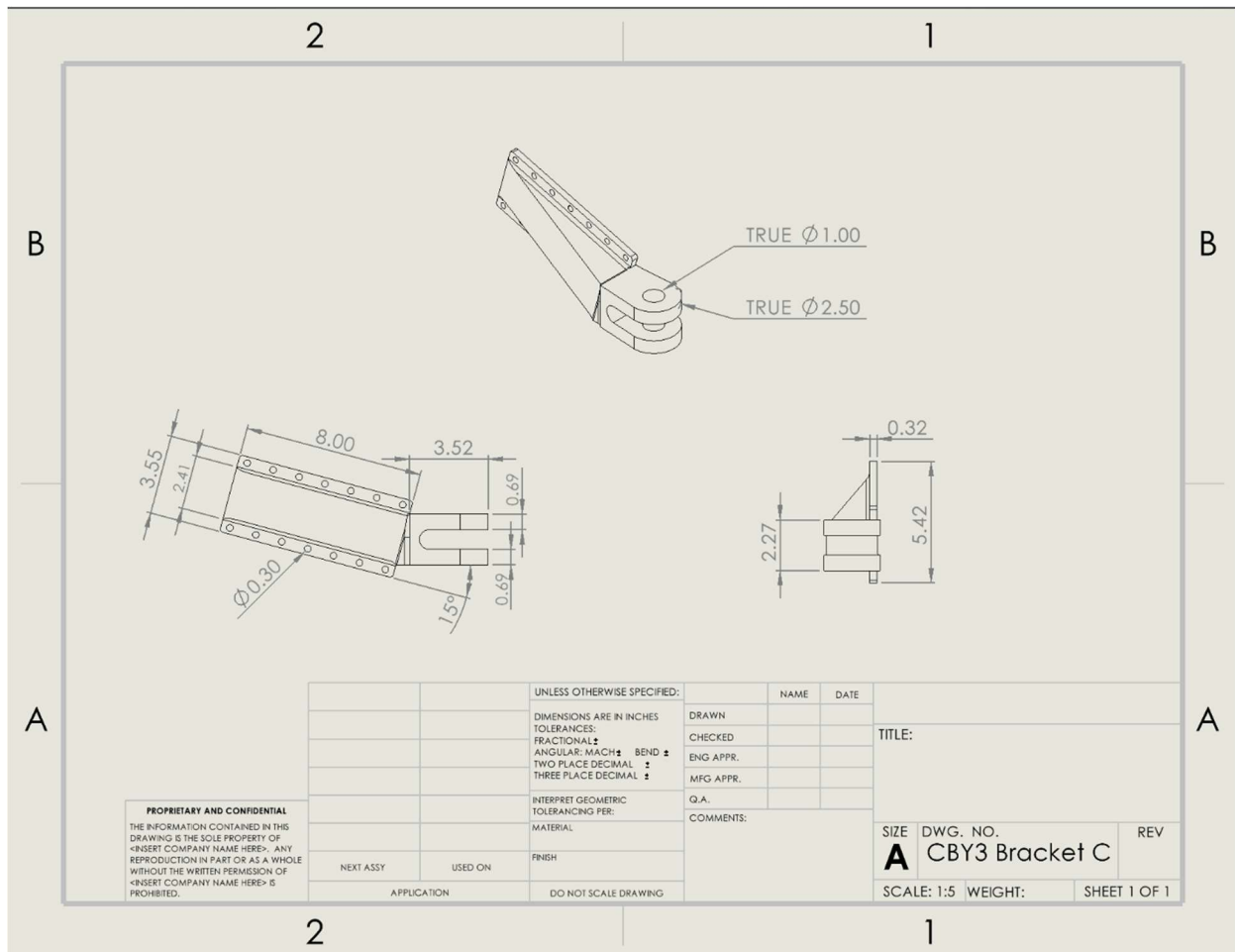
9.1 Appendix A: Additional Drawings of CBY-3 Internal Wing Structure



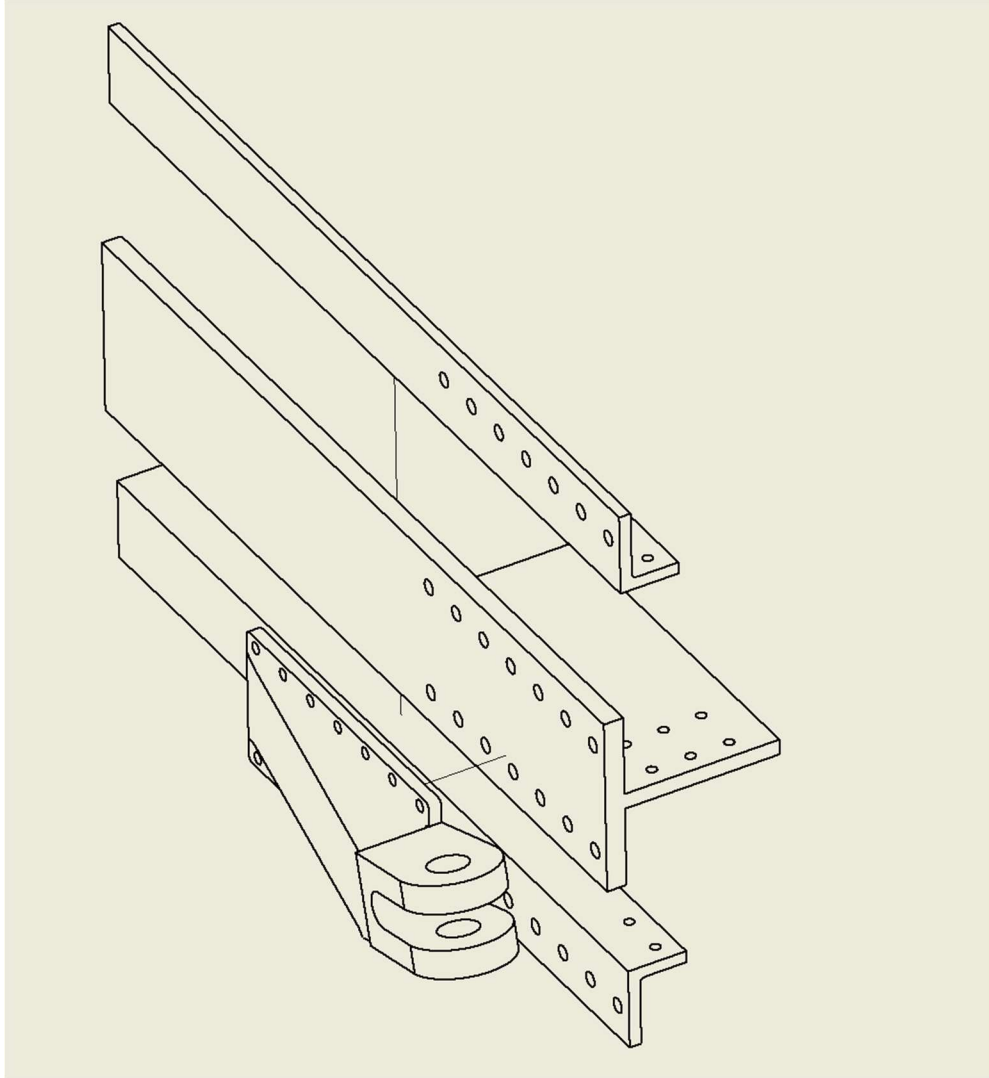
CAD model drawing of bracket B (lower rear bracket of wing)



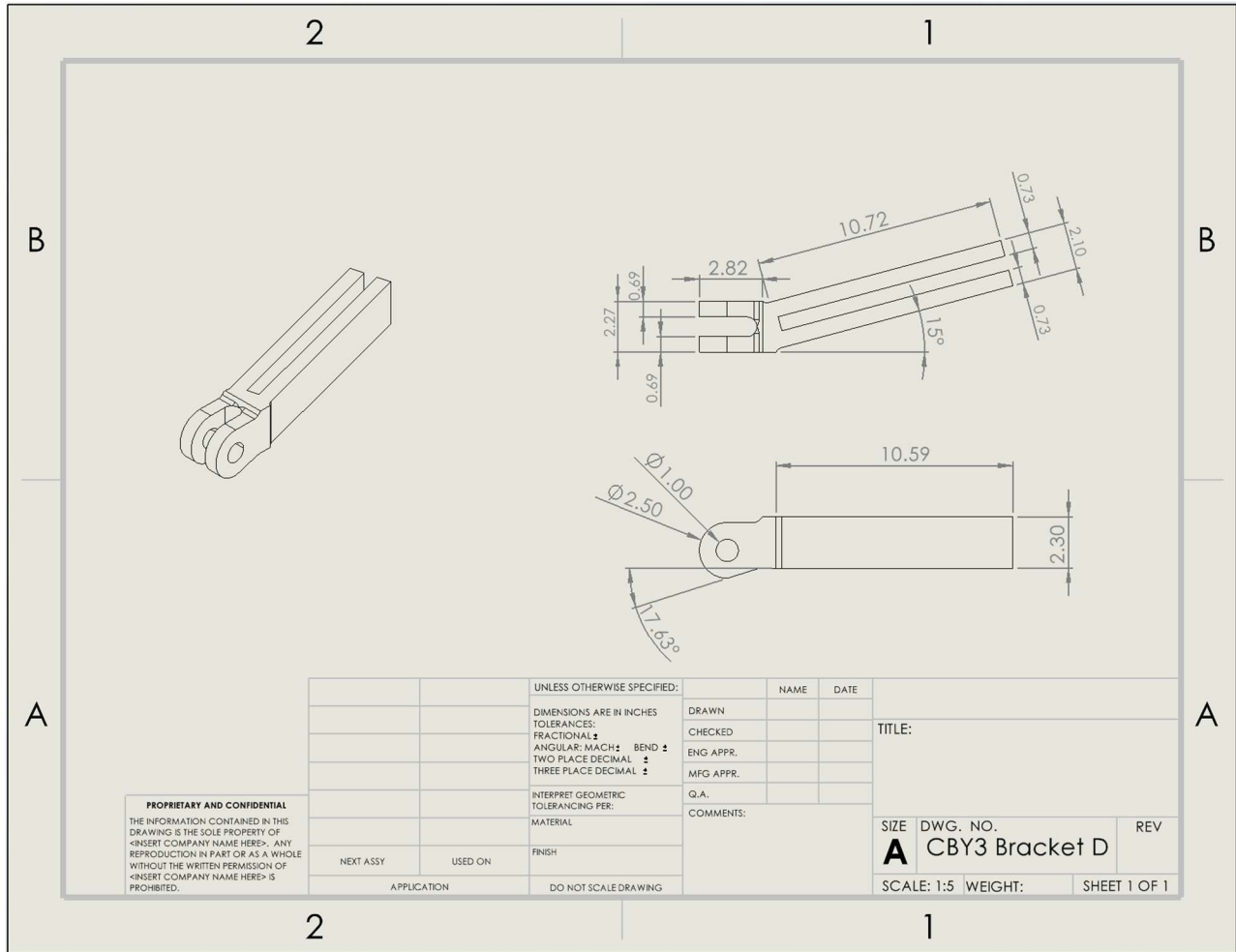
Exploded view of box structure surrounding bracket B



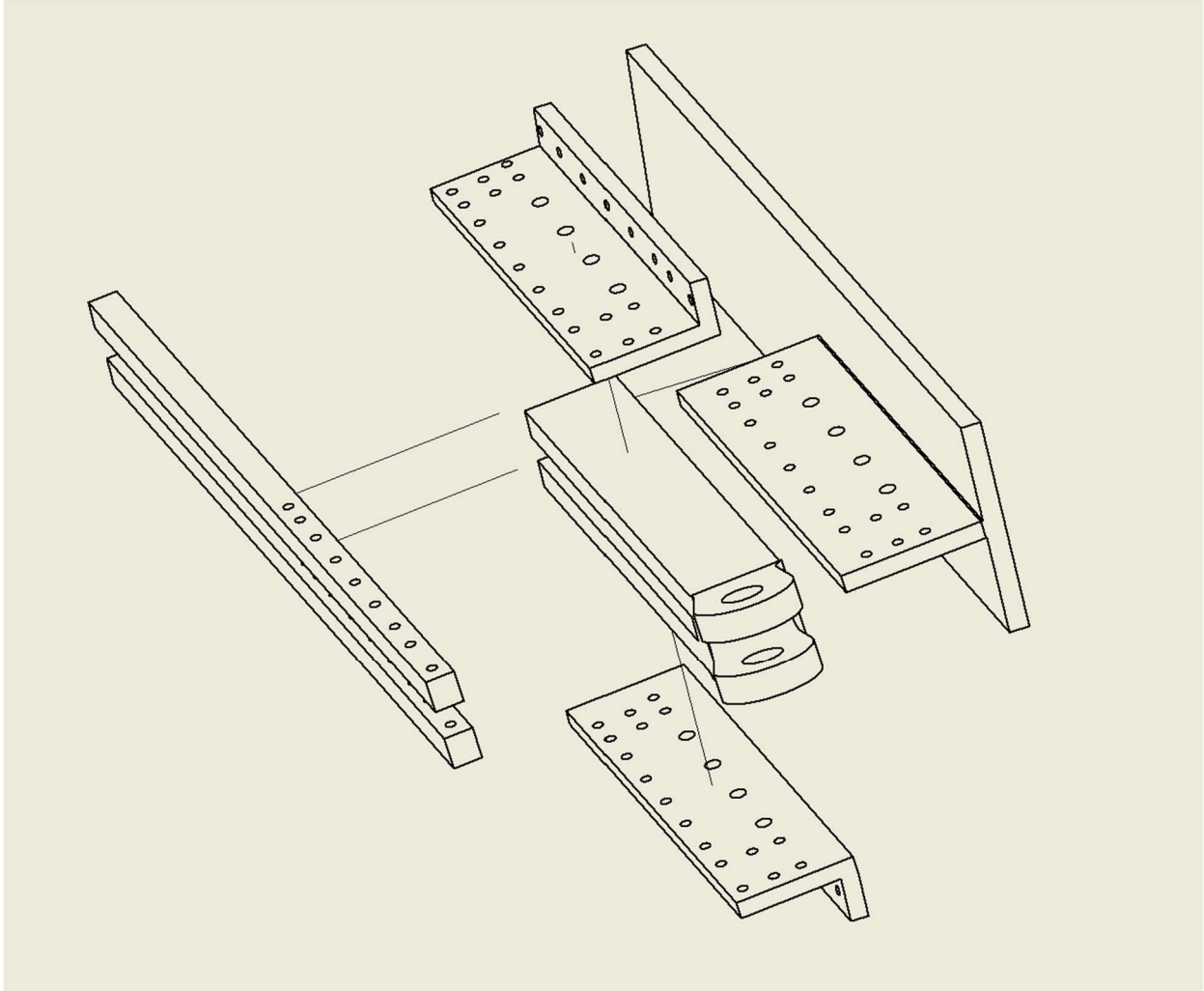
A CAD model drawing of bracket C (lower rear bracket of wing)



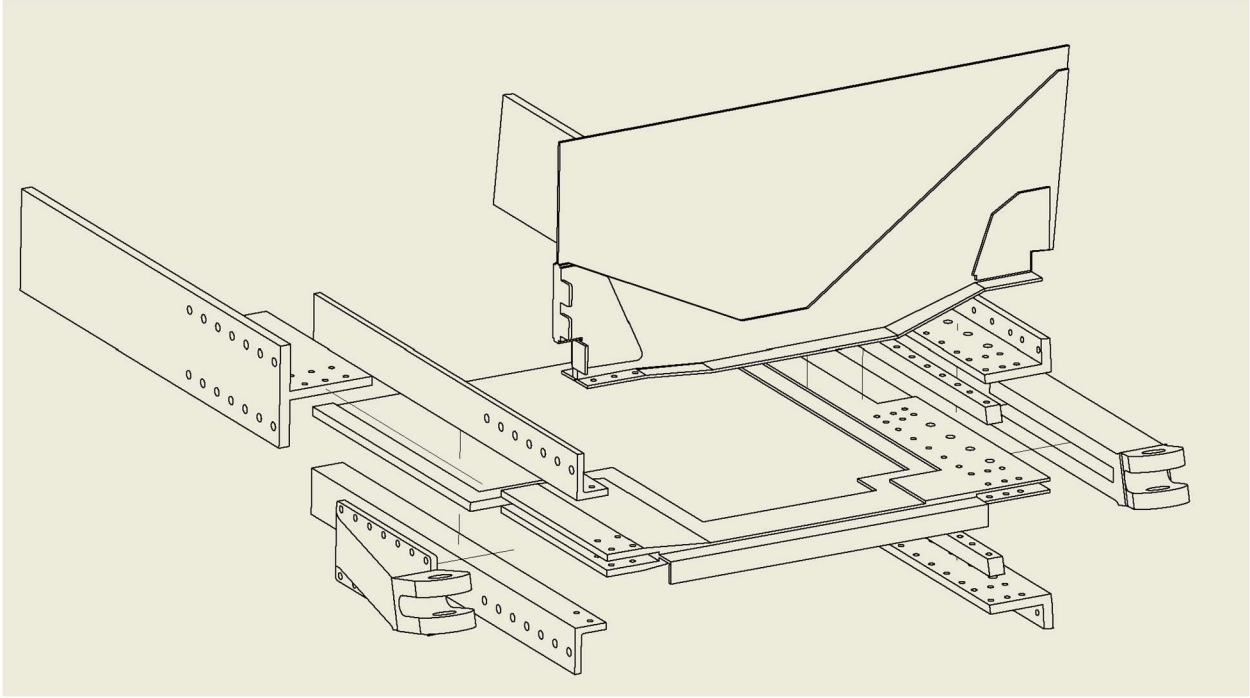
Exploded view of box structure surrounding bracket C



A CAD model drawing of bracket D (lower rear bracket of wing)

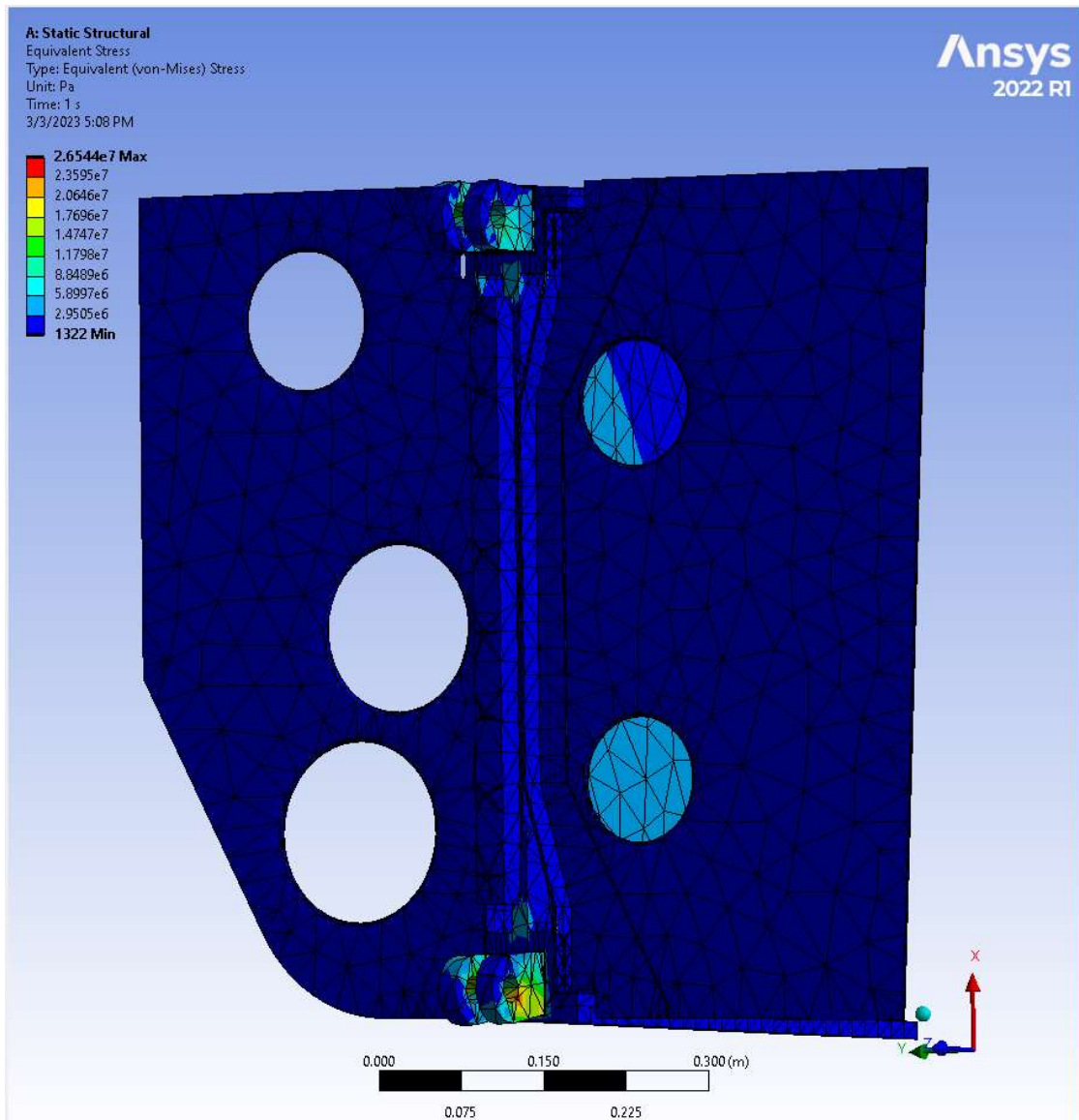


Exploded view of box structure surrounding bracket D

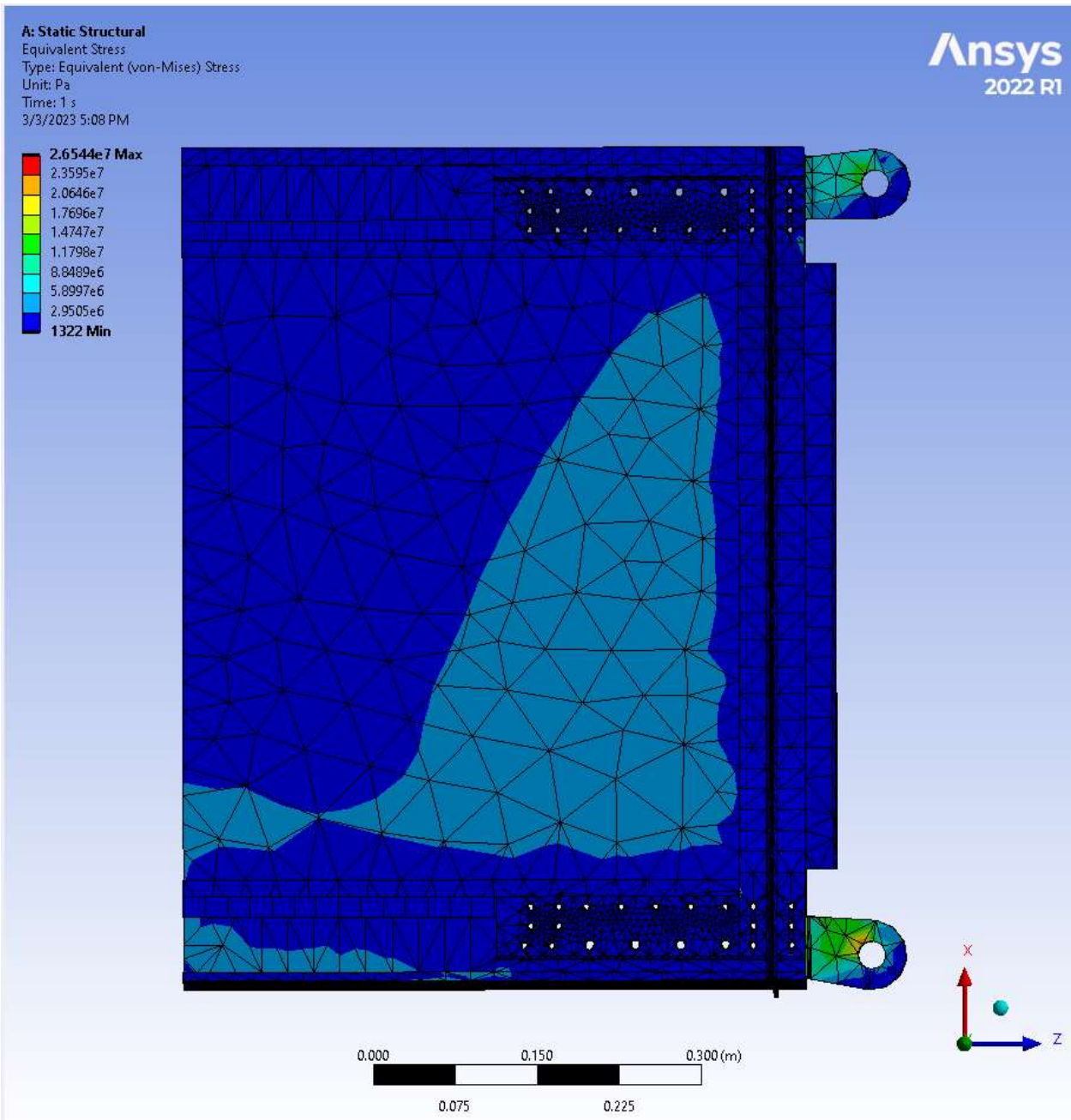


Exploded view of the trailing edge comprised of brackets C and D

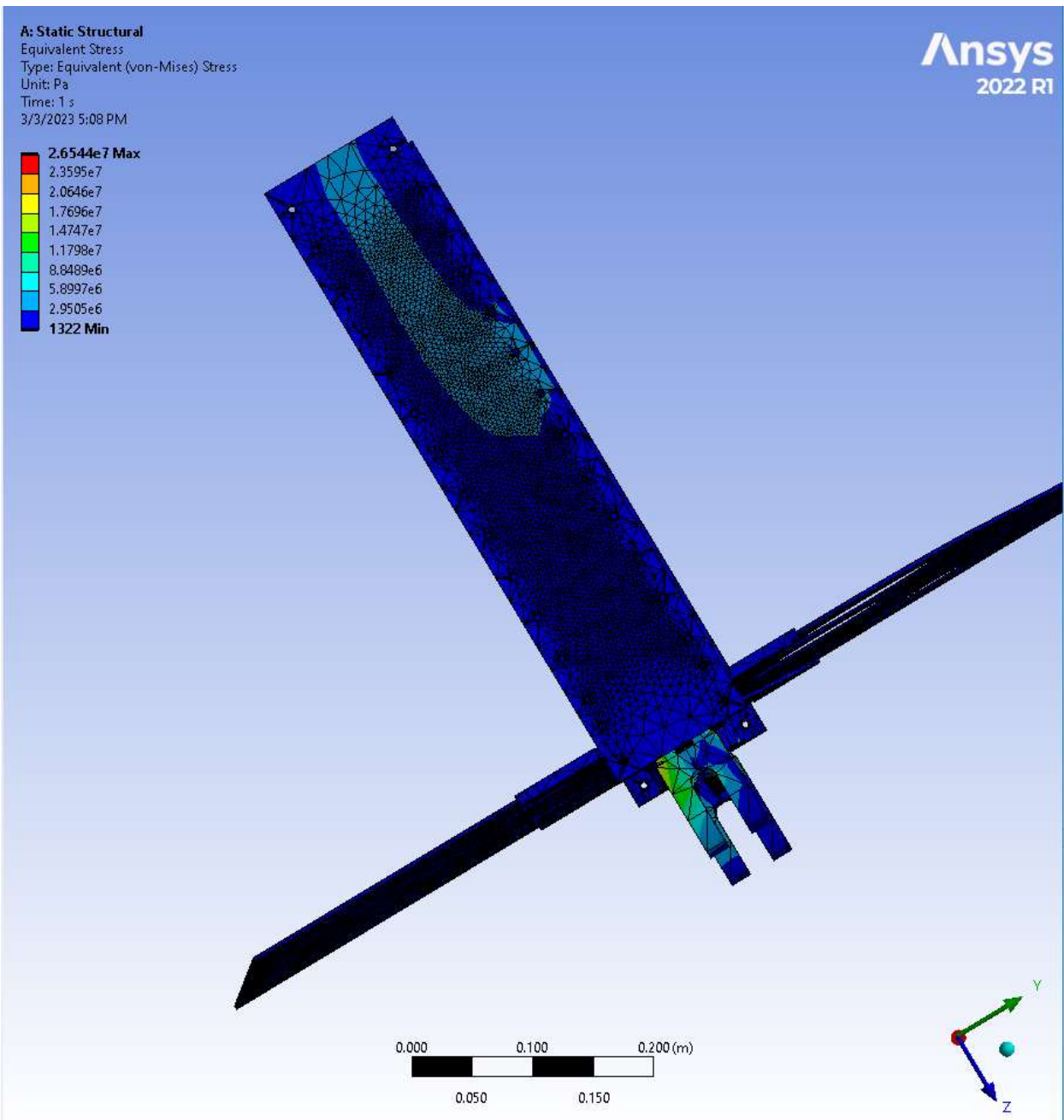
9.2 Appendix B: Additional Results of CBY-3 Ansys Mechanical Stress Map



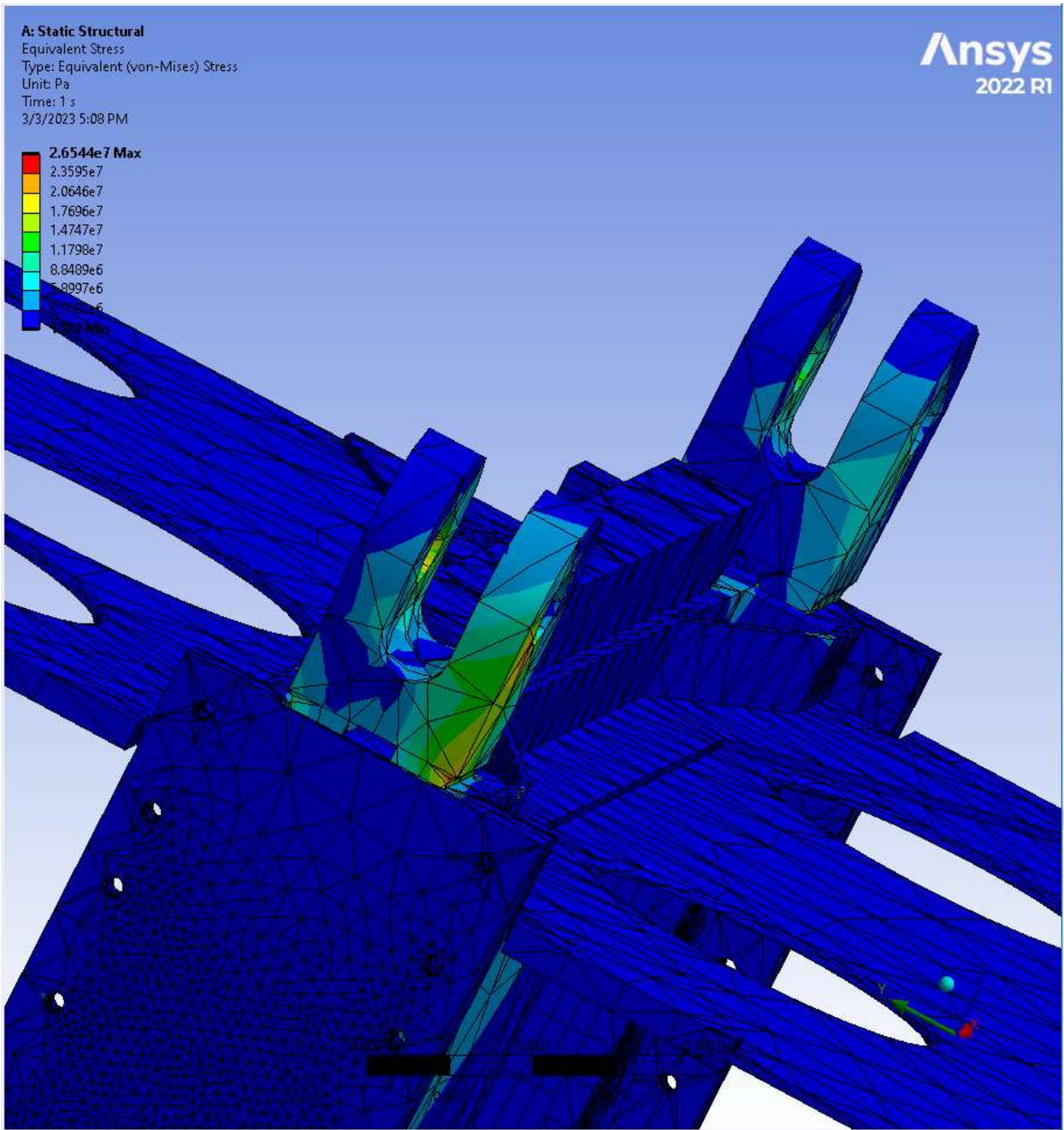
Trailing Edge Bracket Pair Stress Map View



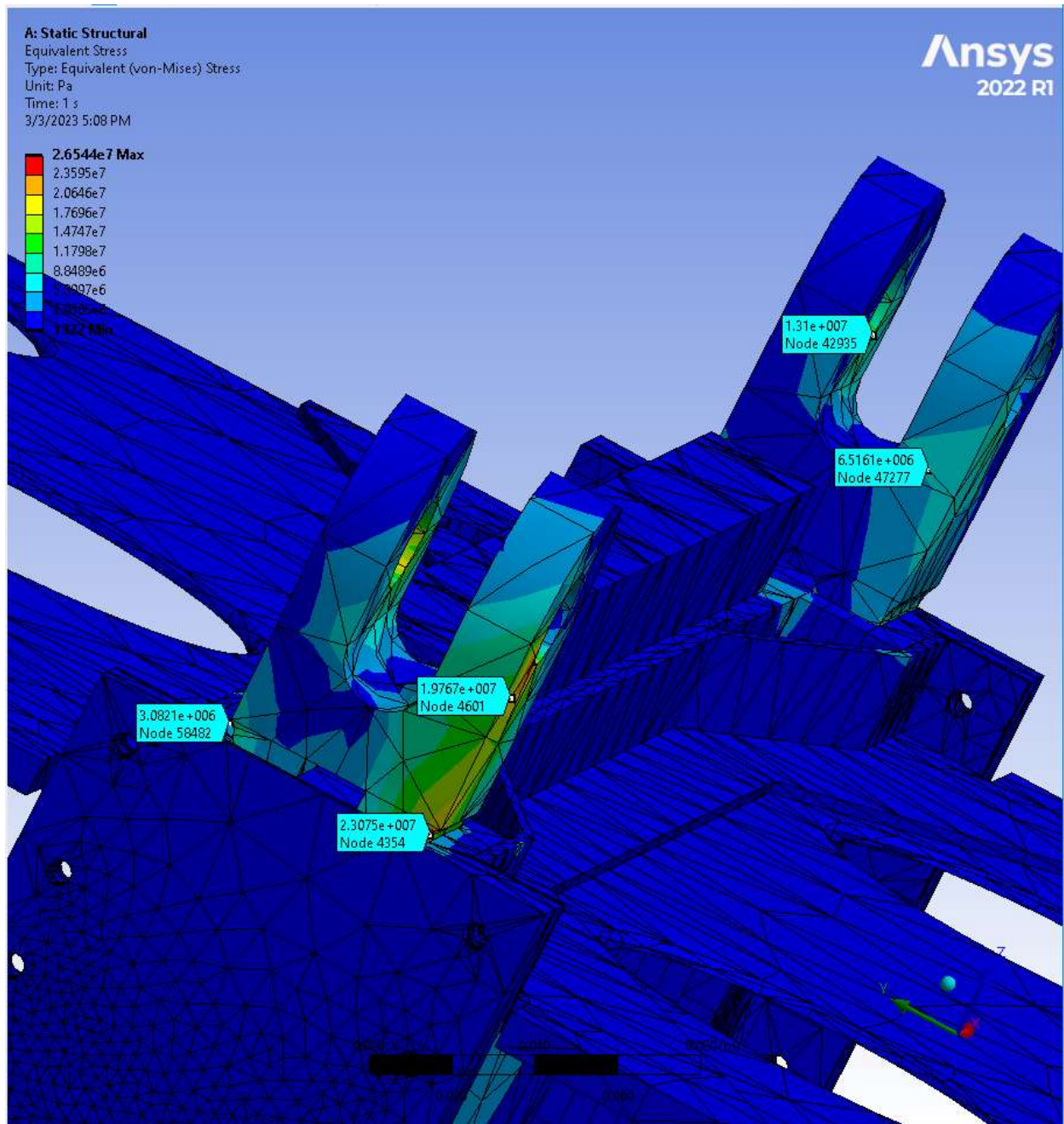
Trailing Edge Bracket Pair Stress Map View



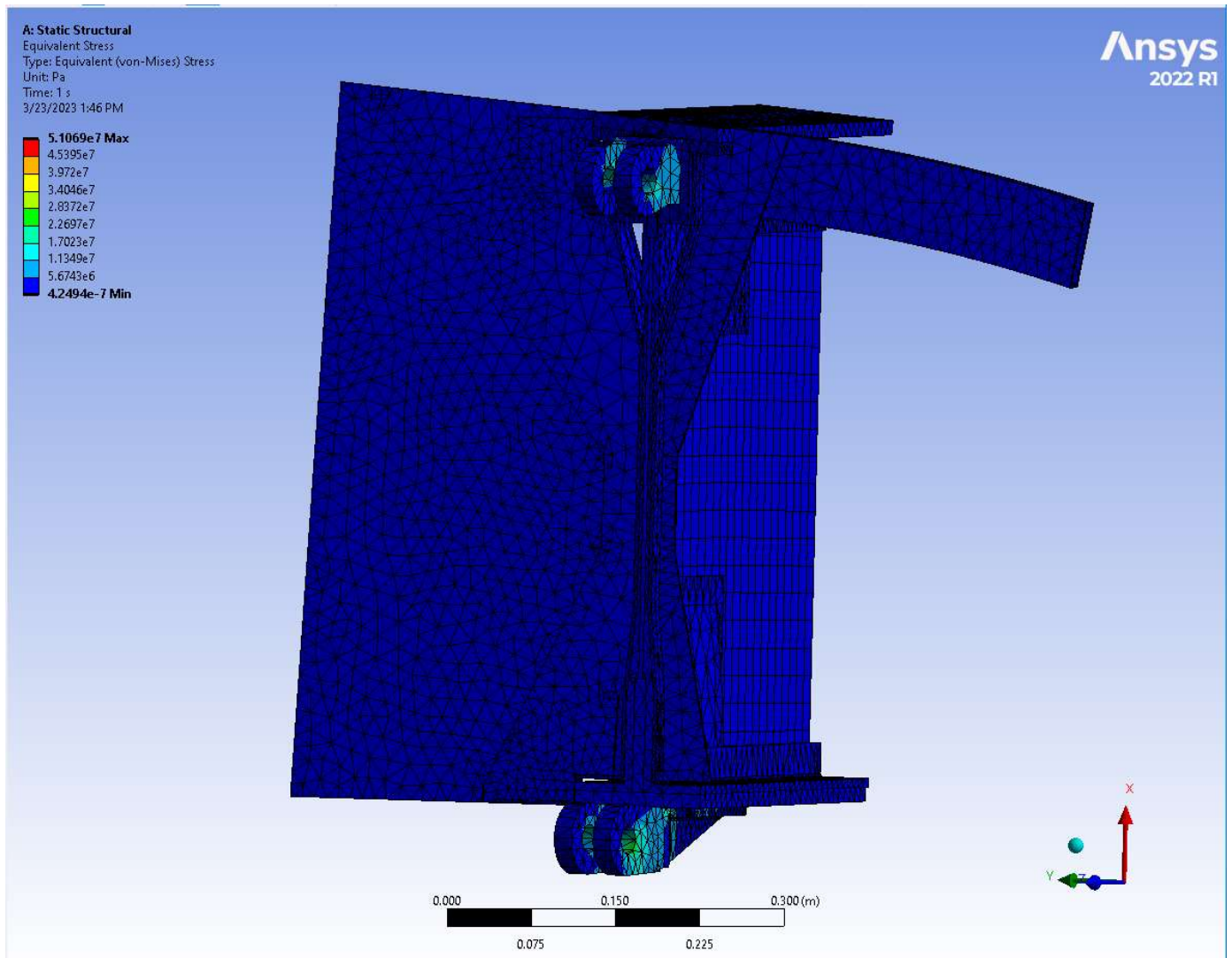
Trailing Edge Bracket Pair Stress Map View



Underside View of Trailing Edge Brackets

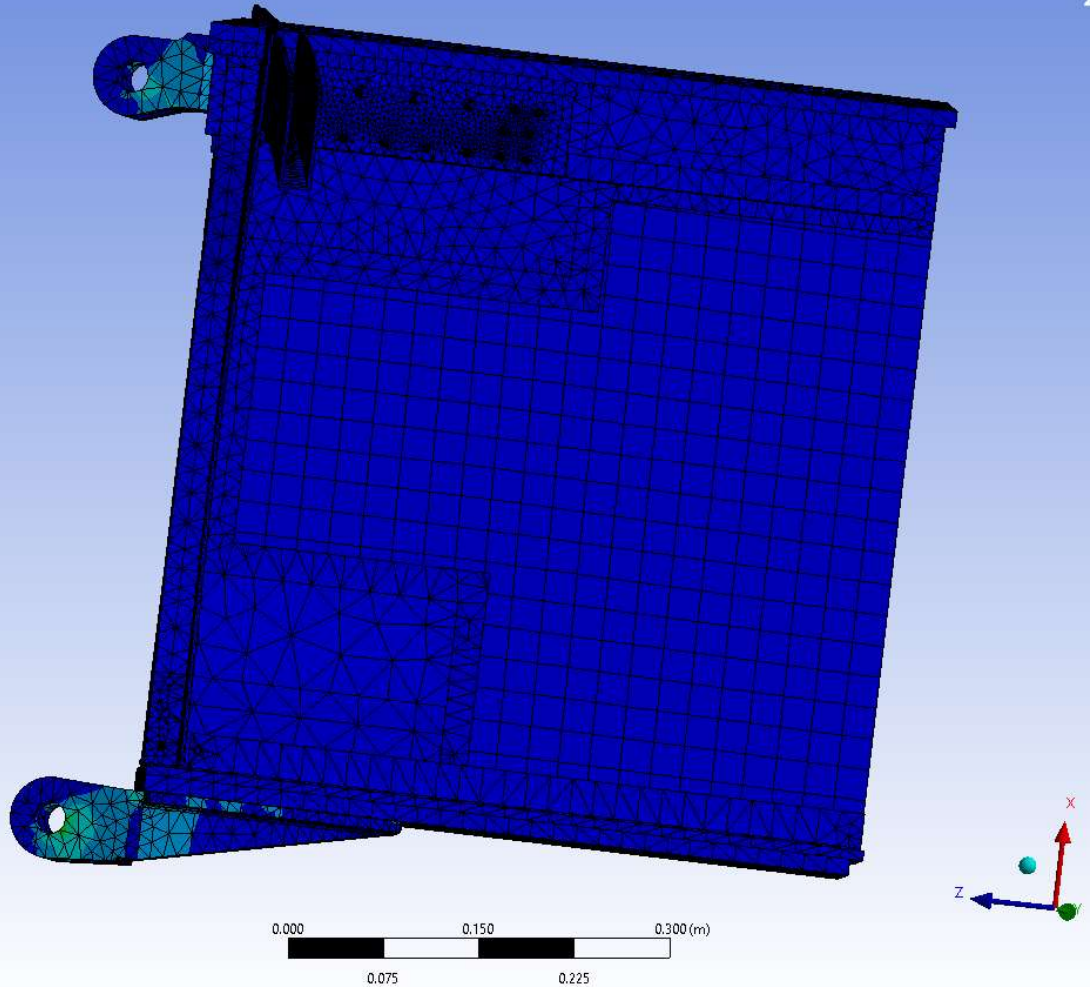
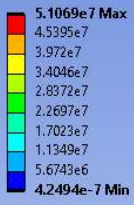


Underside View of Trailing Edge Brackets with Probe Values



Leading Edge Bracket Pair Stress Map View

A: Static Structural
Equivalent Stress
Type: Equivalent (von-Mises) Stress
Unit: Pa
Time: 1 s
3/23/2023 1:46 PM

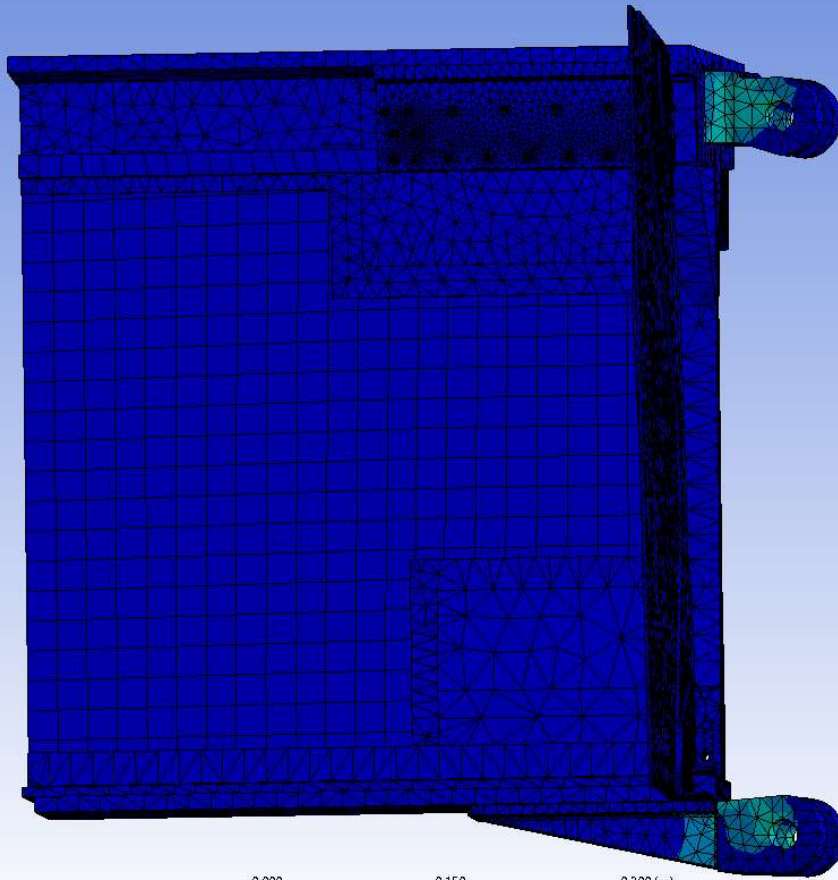


Leading Edge Bracket Pair Stress Map View

A: Static Structural
Equivalent Stress
Type: Equivalent (von-Mises) Stress
Unit: Pa
Time: 1 s
3/23/2023 1:46 PM

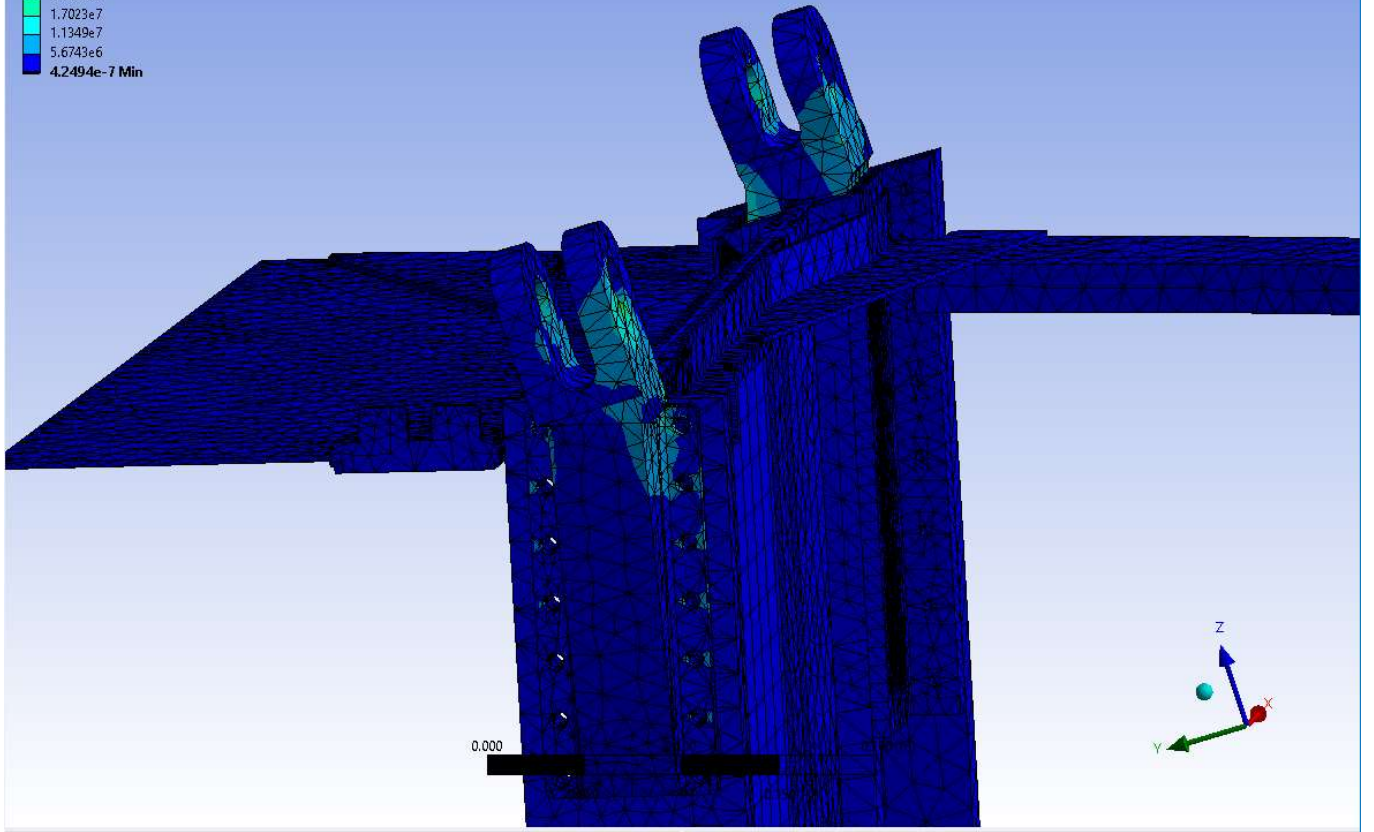
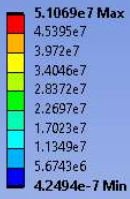
Ansys
2022 R1

5.1069e7 Max
4.5395e7
3.972e7
3.4046e7
2.8372e7
2.2697e7
1.7023e7
1.1349e7
5.6743e6
4.2494e-7 Min

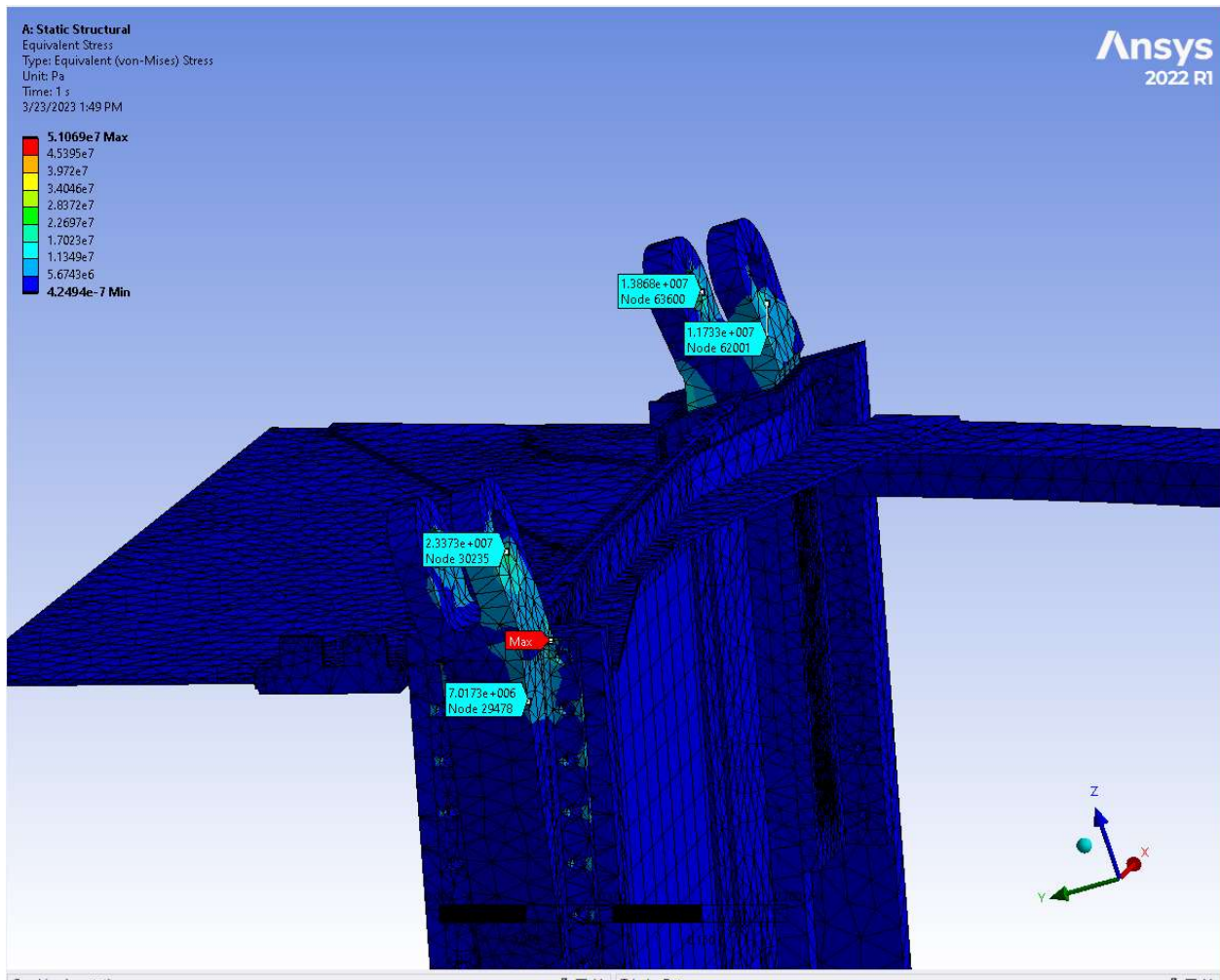


Leading Edge Bracket Pair Stress Map View

A: Static Structural
Equivalent Stress
Type: Equivalent (von-Mises) Stress
Unit: Pa
Time: 1 s
3/23/2023 1:46 PM



Underside View of Leading Edge Brackets



Underside View of Leading Edge Brackets with Probe Values